U.S. Department of Energy • Office of Fossil Energy
National Energy Technology Laboratory

Journal of Energy & Environmental Research

3610 Collins Ferry Road
P.O. Box 880
Morgantown, WV 26507-0880

626 Cochrans Mill Road
P.O. Box 10940
Pittsburgh, PA 15236-0949

National Petroleum
Technology Office
Williams Center Tower 1
One West Third Street
Tulsa, OK 74103-3519

www.netl.doe.gov

Vol. 2, No. 1
February 2002

Carbon Sequestration II

Journal Papers—Modeling

Journal Papers—Ocean Sequestration

About This Issue

This is the second issue of the *Journal of Energy & Environmental Research*. The Journal highlights work being conducted by U.S. Department of Energy, National Energy Technology Laboratory (NETL) researchers, in collaboration with investigators from industry, academia, and other national laboratories. This issue focuses on carbon sequestration, as did Volume 1, Number 1. The papers included in these first two issues were presented at the First National Conference on Carbon Sequestration, May 14 to 17, 2001 in Washington, D.C.

NETL's programs assist in providing the United States with acceptable, affordable, and available energy. They also provide the quality science that contributes to the development of sound energy policies. The challenge we face in addressing our Nation's energy issues is formidable. Our academic, scientific, and technological communities must continue to share information to develop solutions to this challenge. We hope that this technical journal facilitates information sharing among these communities.

Your comments, questions, and suggestions for future issues are welcome. We look forward to hearing from you. Please feel free to contact the Editor in Chief, Edward J. (Jerry) Boyle, at edward.boyle@netl.doe.gov or 304-285-4000.

Engineering and Economic Assessment of Carbon Dioxide Sequestration in Saline Formations

Lawrence A. Smith (smithla@battelle.org; 614-424-3169)
Neeraj Gupta (gupta@battelle.org; 614-424-3820)*
Bruce M. Sass and Thomas A. Bubenik
Battelle Memorial Institute, 505 King Avenue, Columbus, OH 43201
*Corresponding Author

Charles Byrer [(a)] and Perry Bergman [(b)]
National Energy Technology Laboratory
(a) P.O. Box 880, Morgantown, WV, 26507-0880
(b) P.O. Box 10940, Pittsburgh, PA, 15236-0940

ABSTRACT

Concern over the potential effects of greenhouse gases such as carbon dioxide (CO_2) on global climate has triggered research about ways to mitigate the release of these gases to the atmosphere. A project to study the engineering feasibility and costs of sequestering CO_2 in deep, saline reservoirs was completed as part of a U.S. Department of Energy (DOE) program supporting research on novel technologies to mitigate greenhouse gas emissions. Study activities included a review of the status of existing technologies that could be used for CO_2 sequestration, development of a preliminary engineering concept for accomplishing the required operations, and estimation of costs for sequestration systems. The primary components of the CO_2 sequestration system considered are:

Capture of the CO_2 from the flue gas
Preparation of the CO_2 for transportation (compression and drying)
Transportation of the CO_2 through a pipeline
Injection of the CO_2 into a suitable aquifer.

Costs are estimated for sequestration of CO_2 from two types of power plants: pulverized coal with flue gas desulphurization (PC/FGD) and integrated coal gasification combined cycle (IGCC). The sensitivity of cost to a variety of transportation and injection scenarios was also studied. The results show that the engineering aspects of the major components of CO_2 capture and geologic storage are well understood through experience in related industries such as CO_2 production, pipeline transport, and subsurface injection of liquids and gases for gas storage, waste disposal, and enhanced oil recovery. Capital costs for capture and compression and the operational cost for compression are the largest cost components.

INTRODUCTION

The U.S. Department of Energy (DOE) is supporting research on fast-breaking technologies to mitigate greenhouse gas emissions. Concern over the potential effects of greenhouse gases such as carbon dioxide (CO_2) on global climate has triggered extensive studies of ways to reduce emissions of these gases. One method to help control greenhouse gas emissions is to capture and sequester CO_2 in the flue gas from coal fired power plants. Battelle was funded by DOE to study sequestration of CO_2 in deep saline reservoirs. This project included a task to perform an engineering and economic (EEA) which resulted in the research reported in this paper.

Related DOE-funded work on geologic storage of CO_2 in saline formations conducted at Battelle includes compositional reservoir simulations (Gupta et al., 2001), evaluation of geochemical aspects through

modeling and experiments (Sass et al., 2001a and Sass et al., 2001b), and assessment of seismic aspects (Sminchak el al., 2001).

OBJECTIVE

The objective of the EEA was to review the status of existing technologies for handling CO_2, develop a preliminary engineering concept for accomplishing the required operations, and estimate capital and operating costs for sequestration systems under various design conditions. The primary components of the CO_2 sequestration system studied in the EEA are as follows (see Figure 1):

Capture of the CO_2 from the flue gas
Preparation of the CO_2 for transmission as a supercritical liquid (compression and dehydration)
Transmission of the CO_2 through a pipeline
Injection of the CO_2 into a suitable aquifer.

Electrical generating plants using existing technologies or plants that could be brought into service in the near future were considered as possible CO_2 sources for this study. The CO_2 source was assumed to be located in the eastern United States with CO_2 injection occurring close to the source using a regionally extensive formation such as the Mt. Simon Sandstone. Conceptual piping and instrument diagrams were developed for compression, pipeline transmission, and injection systems. These diagrams served as the basis for a preliminary budget estimate of capital and operating costs (+50% to –30% accuracy).

APPROACH

Costs are estimated for sequestration of CO_2 from the following two types of power plants:

Pulverized Coal with Flue Gas Desulphurization (PC/FGD)
Intergrated Coal Gasification Combined Cycle (IGCC).

The PC/FGD plant is used as the base case because it is the most common type of coal fired power generation system. Costs are estimated for the IGCC plant to provide information about possible economies provide by an innovative technology that has been developed and tested at the commercial scale. The PC/FGD plant is assumed to use a high performance SO_2 removal system such that the flue gas is compatible with a conventional CO_2 capture system such as amine absorption. Sulfur removal at the IGCC is assumed to be accomplished using wet oxidation to remove H_2S with CO_2 capture at elevated pressure using physical absorption. Cost results are presented on an annual basis with the capital costs being converted to yearly costs using a capital recovery factor calculated using an effective interest rate of 4.1% for a useful life of 25 years. The input data for the cost calculations are summarized in Table 1.

The sensitivity of cost to pipeline length, terrain, and injection depth was studied. The minimum pipeline length was assumed to be 15 km (9.3 mi). Increasing pipeline length in the cost estimation model allows examination of the cost increases that would occur if a suitable injection zone cannot be located near the power plant. The maximum transmission distance was assumed to be 400 km (249 mi) based on the assumption that the wide extent of the Mt. Simon formation would allow location of a suitable injection site within a reasonable distance. Analysis of scenarios involving pipeline construction in difficult (i.e., hilly and rocky) terrain or an urban area was done to quantify the cost sensitivity of the transmission system. The depth of the Mt. Simon formation ranges from about 1,000 to 3,000 m (3,281 to 9,843 ft) in the area of interest, so the cost effect of this range of injection depths was evaluated.

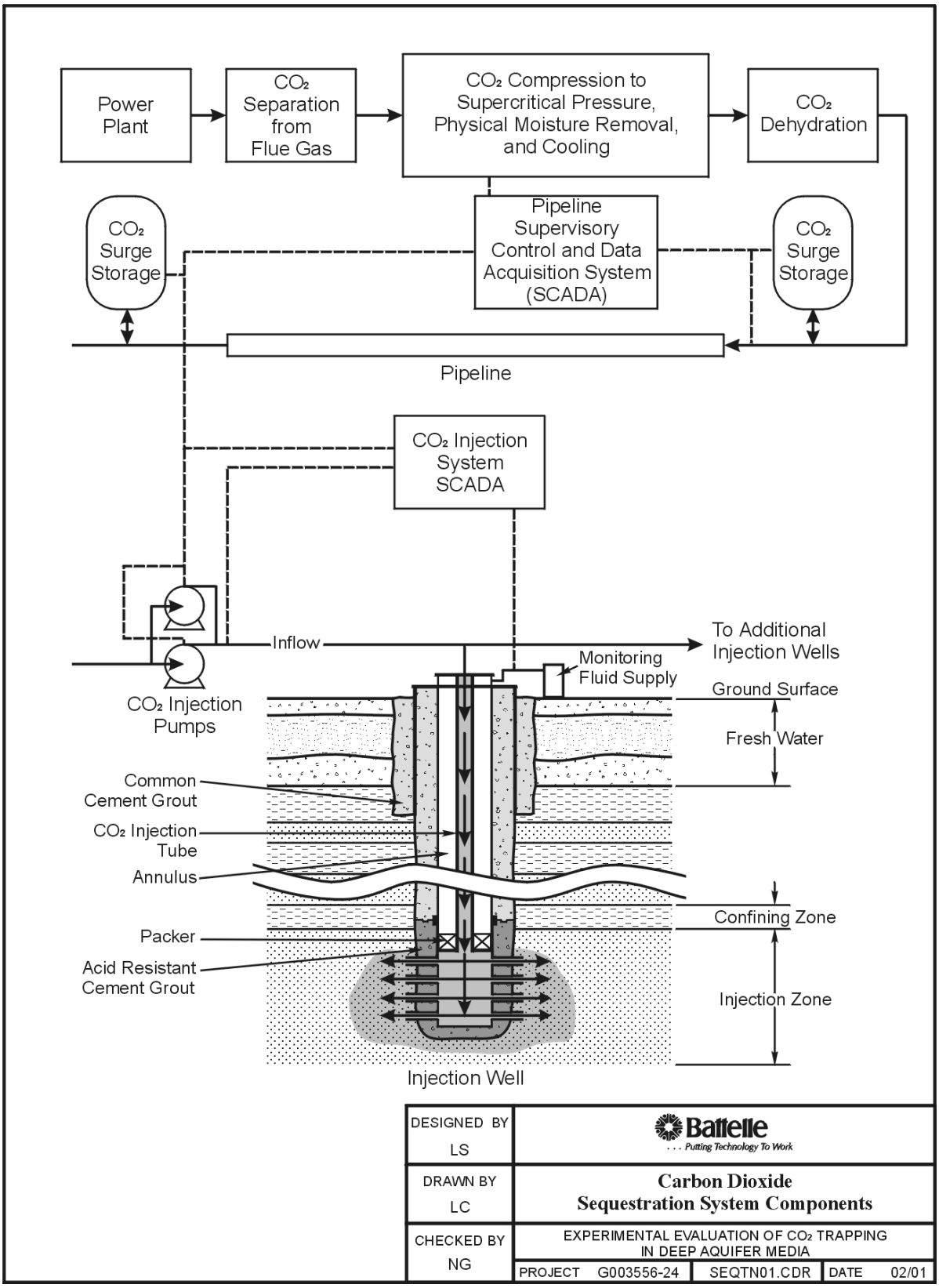

Figure 1. Carbon Dioxide Sequestration System Components

Table 1. Summary of Basis for Cost Estimation

	PC/FGD and CO_2 Capture by Amine Absorption	IGCC and CO_2 Capture by Physical Absorption
System Power Output		
Power without CO_2 capture (MW)	500	500
Power with CO_2 capture (MW)	362	428
System Cost		
Electricity price without capture (bus bar) ($/kWh)	4.9	5.3
Electricity price with capture (bus bar) ($/kWh)	7.4	6.3
CO_2 Capture Output		
CO_2 released without capture (kgs/kWh)	0.828	0.756
CO_2 released with capture (kgs/kWh)	0.083	0.136
CO_2 to pipeline (metric ton/yr)	3,360,000	2,800,000
CO_2 to pipeline (standard ft^3/hr)	6,860,000	5,710,000
CO_2 supply pressure	170 kPa (25 psig[a])	170 kPa (25 psig[a])
Pipeline operating pressure	10,340 kPa (1500 psig[a])	10,340 kPa (1500 psig[a])

(a) psig = pounds per square inch gauge (i.e., absolute pressure – atmospheric pressure)

The sensitivity of cost to pipeline length, terrain, and injection depth was studied. The minimum pipeline length was assumed to be 15 km (9.3 mi). Increasing pipeline length in the cost estimation model allows examination of the cost increases that would occur if a suitable injection zone cannot be located near the power plant. The maximum transmission distance was assumed to be 400 km (249 mi) based on the assumption that the wide extent of the Mt. Simon formation would allow location of a suitable injection site within a reasonable distance. Analysis of scenarios involving pipeline construction in difficult (i.e., hilly and rocky) terrain or an urban area was done to quantify the cost sensitivity of the transmission system. The depth of the Mt. Simon formation ranges from about 1,000 to 3,000 m (3,281 to 9,843 ft) in the area of interest, so the cost effect of this range of injection depths was evaluated.

Capital cost data for compression and pipeline were taken from the annual pipeline economic issue of the Oil and Gas Journal (2000). Capital cost for dehydration equipment was estimated using data from Ormerod (1994) and Holt and Lindeberg (1993). Costs for other transmission equipment such as surge storage tanks and booster pumps were estimated using standard sources such as Richardson (1999), Peters and Timmerhaus (1991), and Page (1996). Injection well capacity of 1,500 metric tons CO_2 per day was estimated using data from Doherty and Harrison (1996), Hendriks and Blok (1993), and Van der Meer (1993) and well installation costs were derived from Ormerod (1994). All costs were adjusted to the year 2000 using Nelson-Farrar refinery cost indexes.

The estimate for the compressor capital cost is based on using 3 parallel 13.0 MW (17,400 hp) four-stage centrifugal compressors with diesel engine drives costing $18,400,000 each. Interstage cooling for the compressors is assumed to be provided using cooling water from the power plant. The capital cost for a dehydration plant is estimated as $5.1 million/metric ton of CO_2 processed per year. Dehydration of the compressed CO_2 stream is assumed to be done using adsorption in a packed particle bed.

The estimated cost for installing the pipeline was $710/m ($220/ft) based on a buried 20 in-diameter carbon steel pipe. The evaluation includes consideration of the sensitivity of the cost of pipeline installation in different types of terrain. Pipeline installation cost is estimated for hilly/rocky or urban terrain as well as for the base case of normal terrain. The pipeline installation costs for hilly/rocky terrain is assumed to be 5% higher than the cost for normal terrain over the entire length of the pipeline. The pipeline length that occurs in urban areas in the urban terrain scenario is assumed to be the greater of 10 km or 20% or the pipeline length, because it is unlikely that a long pipeline would be installed entirely in an urban area. The installation cost in urban terrain is assumed to be 20% higher than the cost in normal terrain. Cost for acquiring the right-of-way (ROW) in urban terrain is assumed to be 5 times has high as the ROW cost in normal terrain.

Fuel for the diesel engine that powers the compressor is the largest operating cost for the transmission system. Fuel cost was estimated by assuming that the engine is 40% efficient, diesel fuel provides a net energy output of 129,000 Btu/gal, and diesel fuel cost $1.00 per gallon. The unit cost for disposal of the water removed from the compressed CO_2 by physical separation is assumed to be $0.15/1,000 gal. The energy cost for regenerating the CO_2 adsorbent dryer was estimated by using a cost of $4.20/1,000 lbs for steam at 4,140 kPa (600 psi) assuming that the heating process to regenerate the adsorbent is 50% efficient. The cost for cooling water for the compressor is estimated assuming the cooling water is supplied at 27°C (80°F) and returned at 35°C (95°F) and costs $0.19/1,000 ga. Maintenance materials are assumed to be 4% of the initial material cost. Labor requirements for compressor and pipeline operations are assumed to be 5 maintenance workers, 5 operators, 2 pipeline inspectors, 0.5 full-time equivalent each for quality assurance (QA) and health and safety (H&S) support, and 1 supervisor. This assumes that there will be one QA and one H&S support person for the overall system who split their work time about equally between the transmission system and the injection system. The labor rates are assumed as $30/hr for the maintenance workers and operators, $50/hr for the QA and H&S support personnel, and $70/hr for the supervisor.

A capital costs estimate for preliminary site screening and candidate evaluation was prepared by determining the cost for primary site selection activities. The activities included in the capital cost estimate for preliminary site screening are as follows:

Definition of screening factors
Collection of documents describing candidate areas
Evaluation of candidates with respect to screening factors
Prepare report identifying and ranking candidate sites.

The activities included in the capital cost estimate for candidate evaluation are as follows:

Install 10 groundwater sampling wells in USDW associated with the site
Collect and analyze water samples from the USDW
Install one test well in the saline aquifer
Log the test well
Collect and analyze liquid samples from the injection zone
Collect and analyze mineral samples from the injection zone
Perform an injectivity test in the injection zone
Perform surface geophysical (e.g., seismic) testing of the area
Install geophones and perform seismic monitoring
Perform site modeling
Perform site seismic evaluation
Prepare candidate evaluation report.

Costs for preliminary site screening and candidate evaluation were estimated as $330,000 and $1,355,000, respectively.

The estimated cost for drilling an injection well into a deep saline aquifer was $645/m ($197/ft). Annual operating costs for the injection system are determined by estimating the utility consumption, analytical needs, and labor amounts expected to be needed to operate and maintain the system. Electricity is provided for the injection pumps (if needed) plus 0.20 MW of additional power consumption for other loads such as smaller pumps, instruments, lighting. An electrical cost of $0.065/kW-hr is used. Maintenance materials are assumed to be 4% of the initial material cost. Labor requirements are assumed to be 2 maintenance workers, 11 operators, 0.5 full-time equivalent each for quality assurance (QA) and health and safety (H&S) support, and 1 supervisor. The labor rates are assumed as $30/hr for the maintenance workers and operators, $50/hr for the QA and H&S support personnel, and $70/hr for the supervisor. Analytical requirements are estimated based on CO_2 samples collected from 3 points weekly at a cost of $200 per analysis and USDW samples from 20 wells quarterly at a cost of $300 per analysis.

TECHNOLOGY DESCRIPTION

The following types of fossil fueled power plant initially considered in the EEA as possible CO_2 sources were:

Pulverized Coal with Flue Gas Desulfurization (PC/FGD)
Coal Combustion with Oxygen and Recycled CO_2 (PC/O_2)
Integrated Coal Gasification Combined Cycle (IGCC)
Natural Gas Combined Cycle (NGCC).

The main components in these four types of power plants are illustrated in Figure 2. A variety of processes have been studied for capture of CO_2 from the flue gas of these plants as summarized in Table 2.

Carbon dioxide produced by combustion at a power plant and concentrated and purified by a capture system must then be compressed, dehydrated, and moved to the injection site. The main components of the CO_2 compression and dehydration system are shown in Figure 3. Transporting carbon dioxide to a remote site for injection will be done with a high-pressure large-diameter pipeline. Hundreds of thousands of miles of pipelines carry hazardous liquids and gases throughout the United States, operating safely for many years. In addition, high-pressure carbon dioxide pipelines have been used heavily in the oil-recovery business, especially in the last 20 to 30 years. Carbon dioxide pipelines are designed in similar fashion as natural gas or hazardous liquid pipelines, and are regulated by 49 CFR 195, the same code used for hazardous liquid pipelines. Design standards for hazardous liquid pipelines are described in the American Society of Mechanical Engineer's (ASME) code B31.4, *Pipeline Transportation Systems for Liquid Hydrocarbons and Other Liquids*.

Systems for pipeline transmission of CO_2 are in many ways similar to the pipelines used for natural gas. However, there are some differences in the properties of CO_2 compared to natural gas that must be accounted for in the design of the transmission system. These property differences raise the following potential concerns:

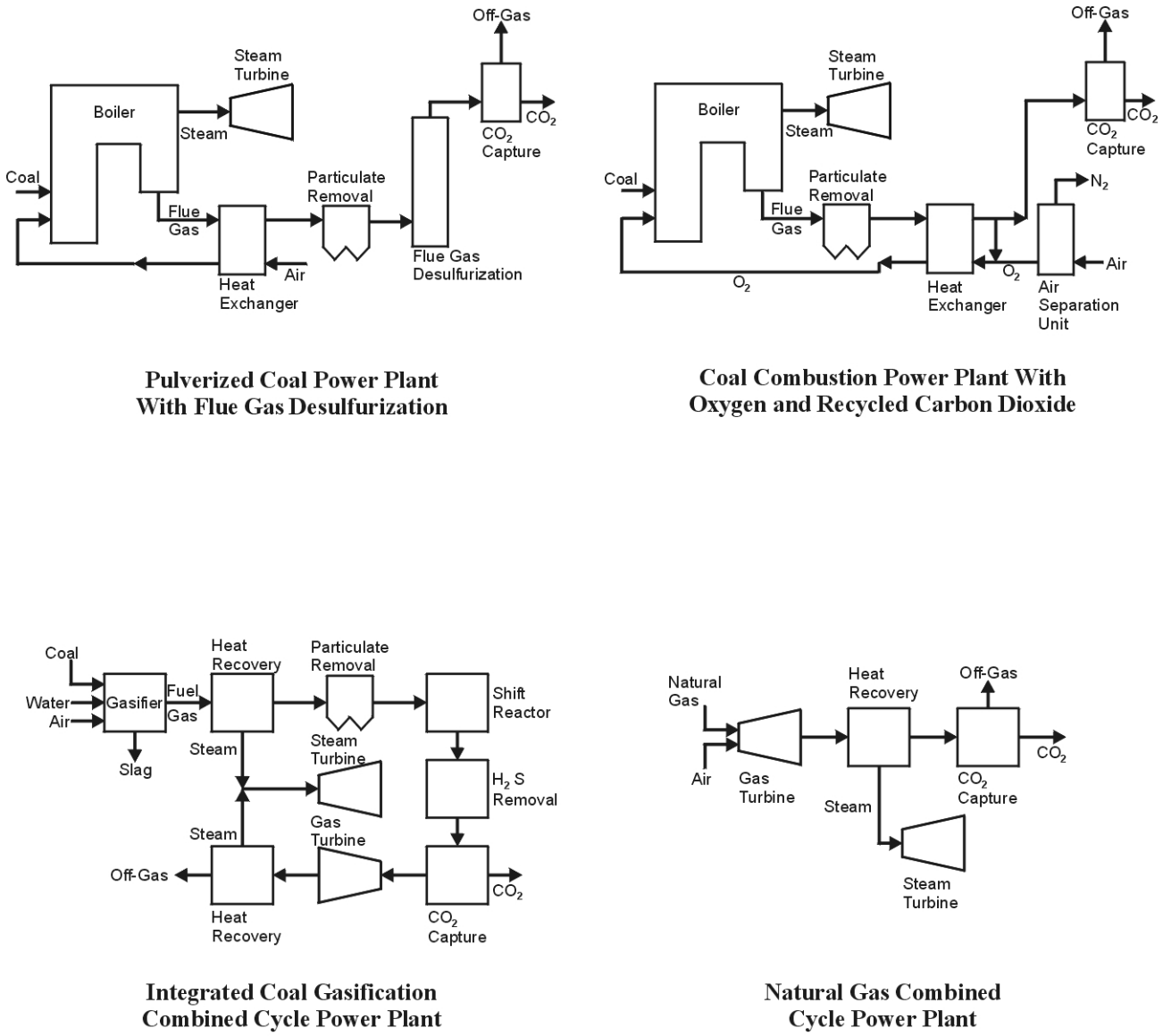

Figure 2. Illustrations of Four Types of Fossil Fuel Power Plants

Compressibility and density of CO_2 show strong, nonlinear dependence on the system pressure and temperature.

Condensation of liquid water in the presence of compressed CO_2 allows the formation of carbonic acid of sufficient strength to corrode carbon steel.

Supercritical CO_2 damages many elastomer sealing materials.

Petroleum-based and many synthetic lubricants can harden and become ineffective in the presence of supercritical CO_2.

Careful design and installation of joints, seals and packing is required to prevent CO_2 leakage.

Compressed CO_2 cools dramatically during decompression.

Dry supercritical CO_2 has poor lubricating characteristics requiring special design features for compressors, pumps, and pipeline pigging equipment.

Unlike flow in compressed gas pipelines, CO_2 pipeline flow can experience transients similar to "water hammer" that can occur during flow changes in liquid piping systems.

Table 2. Summary of CO_2 Capture Methods

Capture Process	Description	Comments
Chemical absorption	CO_2 captured using a reversible reaction between CO_2 and an aqueous solution of an amine or alkaline salt. The solution is regenerated and recirculated.	Used at the commercial scale to remove low concentrations of acid gases (e.g., CO_2) from natural gas. Solution tends to saturate with high CO_2 loading, so the process is more efficient for lower CO_2 concentrations
Physical absorption	CO_2 captured using physical dissolution in an absorption fluid. The fluid is regenerated and recirculated.	Used at the commercial scale to remove high concentrations of acid gases (e.g., CO_2) from natural gas. More efficient for high CO_2 partial pressure (i.e., concentration and/or pressure) Does not typically remove acid gases as completely as chemical or hybrid absorption
Hybrid absorption	CO_2 captured using a combination of chemical absorption and physical dissolution. The fluid is regenerated and recirculated.	Used at the commercial scale to remove intermediate concentrations of acid gases (e.g., CO_2) from natural gas.
Pressure swing adsorption	CO_2 captured on solid sorbent. The sorbent is loaded at high pressure and regenerated by pressure reduction and, in some cases, heating.	Used at the commercial scale to remove CO_2 and other impurities from H_2. Some H_2 cleanup processes also produce high purity CO_2.
Gas separation membrane	CO_2 captured by preferential permeation through a membrane. CO_2 is collected near atmospheric pressure as a permeate.	Used at the commercial scale to recover CO_2 used for enhanced oil recovery (EOR) (i.e., high CO2 concentration) Requires two or more separation stages to reach a CO_2 removal of 90% and purity of 99%, so the process typically is used for gas with high CO_2 content (e.g., PC/O_2 plants). Membranes are very sensitive to particulate fouling
Gas absorption membrane	The process involves using a microporuous membrane between the flue gas and an absorption fluid. CO_2 is preferentially removed from the gas stream by selective absorption in the fluid.	Innovative process Membrane separation unit is more compact than the tall towers needed for chemical or physical absorption due to high surface area allowed by membrane. Membranes are very sensitive to particulate fouling
Cryogenic separation	Flue gas is cooled and compressed to condense CO_2 which can then be captured and purified by distillation.	Used at the commercial scale to recover CO_2 used for EOR (i.e., high CO2 concentration) Gas fed to the cryogenic separation unit must be dehydrated to prevent formation of solids (e.g., ice and CO_2 clathrates) Due to energy needed to reach cryogenic conditions, cryogenic separation typically is used for gas with high CO_2 content (e.g., PC/O_2 plants)

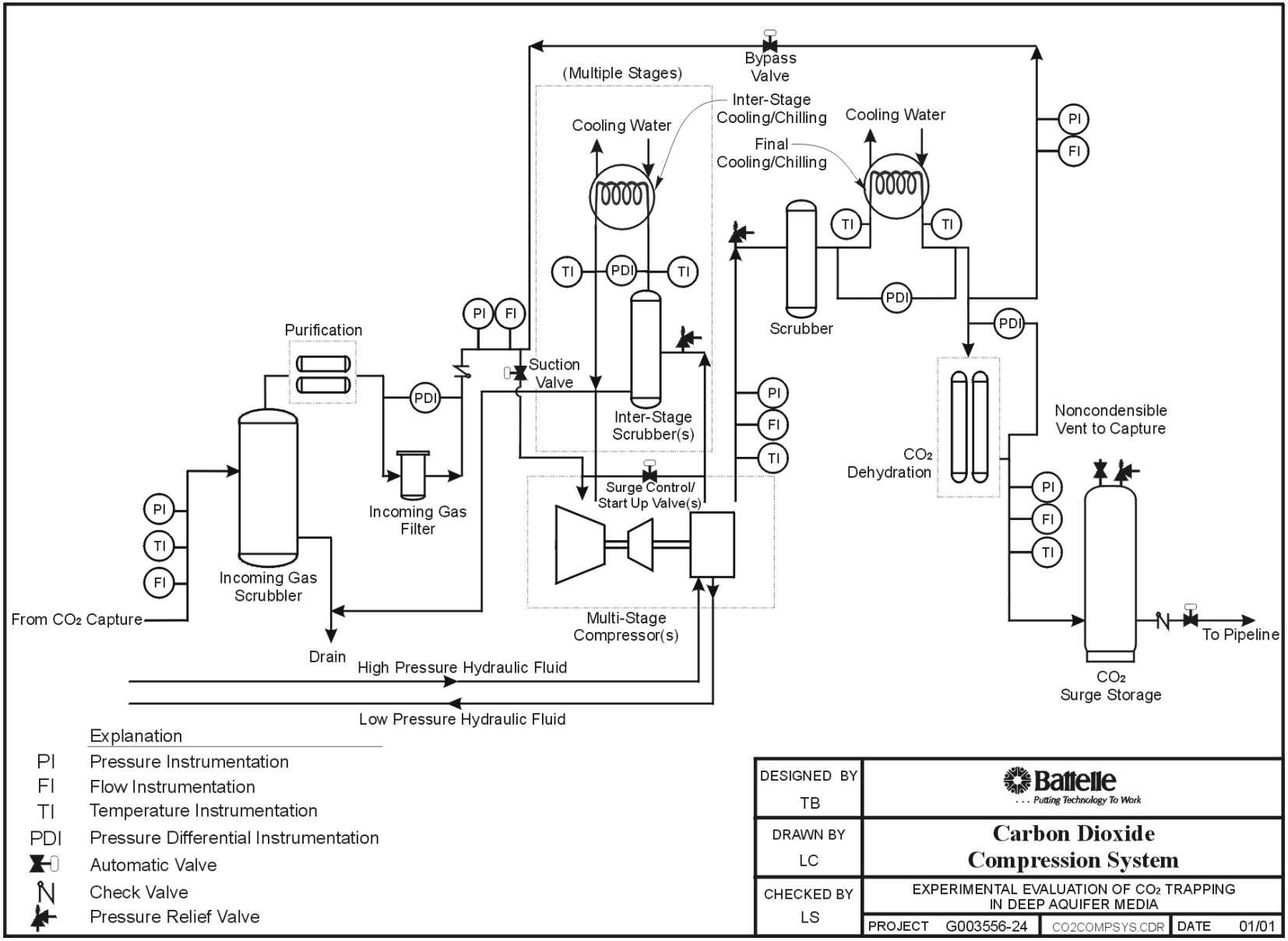

Figure 3. Carbon Dioxide Compression System

Methods to overcome these concerns have been developed during design and operation of pipelines used to move supercritical CO_2 for EOR projects (Mohitpour et al., 2000).

Equipment must be available at the injection site to accept pressurized CO_2 from the pipeline and transfer it to the injection well at the flow rate and pressure required for injection. The primary components are a pressurized surge storage tank, injection pumps (if needed), piping to distribute CO_2 to the injection wells, CO_2 flow control equipment, and equipment to monitor well condition. The need for injection pumps at the site depends on the depth to the injection zone. For sites shallower than about 1,500 m (4,920 ft), pipeline pressure should be adequate to allow injection. The conceptual arrangement of these components is shown in Figure 4.

The injection wells function as conduits for moving supercritical CO_2 fluid from the surface down into the deep saline aquifer. The well consists of three or more concentric casings (Figure 5) extending to various depths as follows:

Exterior surface casing
Intermediate protective (long-string) casing(s)
Injection tubing (hang down tube).

The exterior surface casing is designed to protect underground sources of drinking water (USDWs) in surface aquifers that the well passes through and to reduce corrosion potential by preventing water contact with the intermediate protective casing. The exterior surface casing extends from the surface into the first competent aquitard below the deepest USDW and is cemented along is full length. The intermediate protective casing extends from the surface into the injection zone and is cemented along is full length. The injection tubing extends from the surface into the top of the injection zone. The injection tubing should be designed so as to be removable to facilitate well maintenance, if needed. The discharge end of the injection tubing is equipped with a backflow preventer to prevent CO_2 escape in the event of a well casing failure. Carbon dioxide injection wells will be regulated under the provisions of the Underground Injection Control (UIC) program under the Federal Safe Drinking Water Act (SDWA) as either Class I or Class V wells.

Determining the operating pressure at the top of the well requires consideration of the pressure required at the bottom of the well to force CO_2 into the injection zone, the pressure increase in the pipe due to the height of the CO_2 column, and the pressure loss due to flow in the pipe. The reported rate of pressure rise with depth in most reservoirs ranges from 0.105 to 0.124 bar/m (0.464 to 0.548 psi/ft) with a few sites having gradients as high as 0.23 bar/m (1.02 psi/ft) (Hendriks and Blok, 1993). Moving the CO_2 into the aquifer requires raising the CO_2 sufficiently above the in situ pressure to provide a driving force but not so high as to risk hydrofracturing the injection interval. Typically the CO_2 injection pressure is about 9 to 18% above the in situ pressure (Hendriks and Blok, 1993). Pressure caused by the weight of the column of CO_2 in the injection tubing provides some of the required pressure. This pressure contribution is a function of the density of the CO_2 at the pressure and temperature conditions in the injection tubing. The results of calculations to determine the well head pressure for various depths are shown in Table 3.

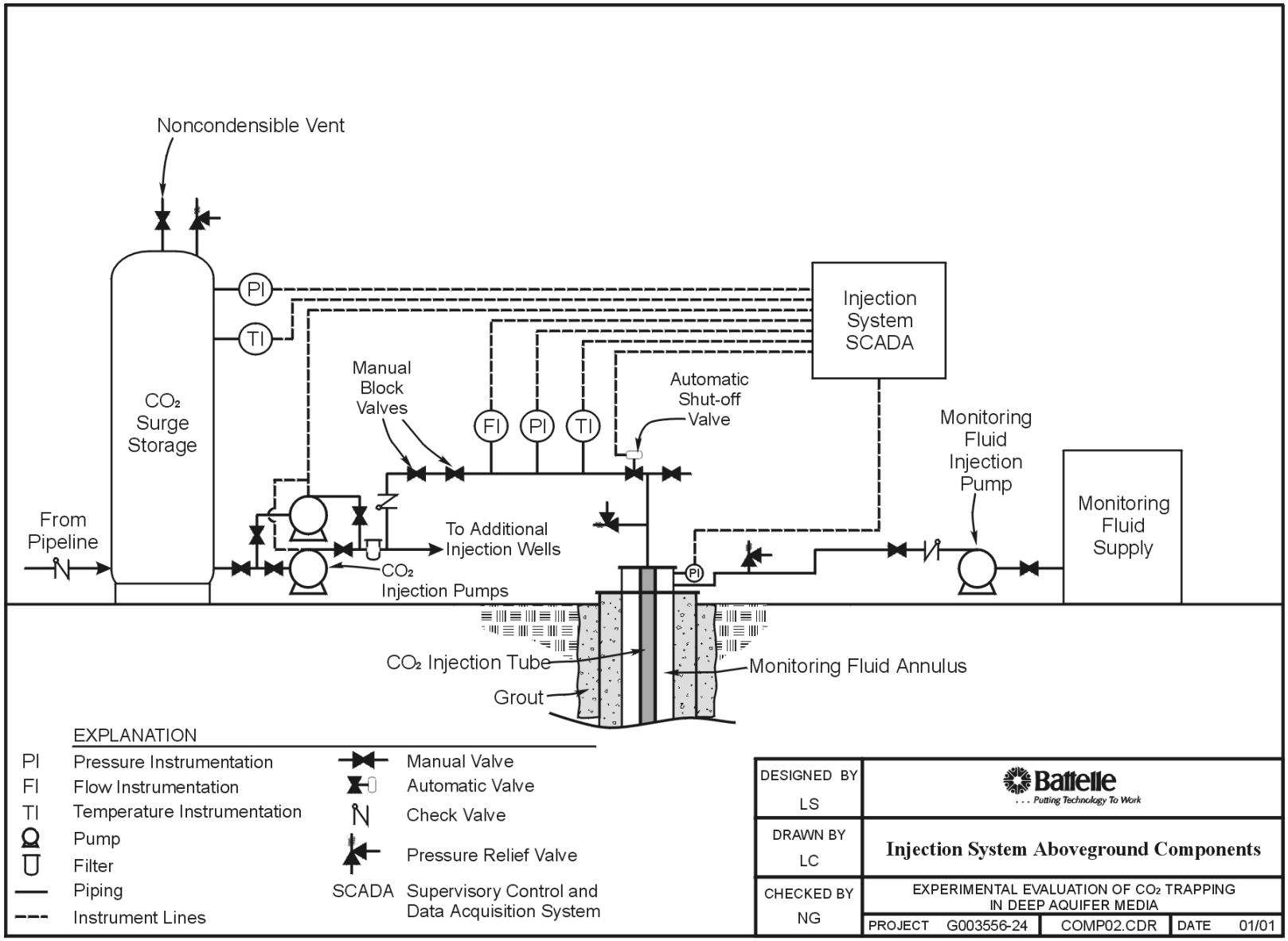

Figure 4. Injection System Aboveground Components

Table 3. Estimated Injection Tubing Pressure

Depth (m [ft])	CO_2 pressure at well head (MPa [psi])	CO_2 specific gravity at well head	CO_2 pressure at injection point (MPa [psi])	CO_2 specific gravity at injection point
1000 (3,281)	7.50 (1,090)	0.71	14.7 (2,140)	0.77
2,000 (6,562)	12.8 (1,860)	0.83	29.5 (4,278)	0.87
3,000 (9,843)	18.7 (2,710)	0.83	44.2 (6,417)	0.91

COST RESULTS

The EEA was conducted to review the status of existing technologies that could be used for CO_2 sequestration, develop a preliminary engineering concept for accomplishing the required operations, and estimate capital and operating costs for sequestration systems under various design condition. This review did not identify any technical obstacles to implementing CO_2 sequestration. Although injecting CO_2 into a deep saline aquifer is an emerging technology with limited application history, design, construction, operation, and maintenance of such a system can draw on a significant body of existing experience. Carbon dioxide injection into oil bearing formations to stimulate production has been done at the commercial scale in since the mid-1980's. These EOR operations use compression, dehydration, pipeline transmission, and deep well injection equipment that is, in many ways, directly analogous to the systems that will be needed for CO_2 sequestration.

The costs estimated for the scenarios analyzed for PC/FGD and IGCC plant in this EEA, reported as cost per metric ton of CO_2 avoided, are summarized in Table 4. The total cost for capture, compression, pipeline transmission, and injection (including capital and present worth of operating cost for 25 years at 4.1% interest) is $1.00 billion for a PC/FGD plant assuming a 15-km pipeline and 2,000-m injection depth. The total cost of sequestration for an IGCC plant is estimated as $0.583 billion. As indicated in the comparison shown in Table 5 and Figure 6, capture and compression is the most expensive portions of the sequestration system, with the greatest contribution coming from the capital and operating cost for the compressor and associated cooling and dehydration equipment. The cost to construct and operate injection wells contributes only a small portion of the total cost for the system. However, it is important to note that efficient injection requires that the CO_2 be in the form of a supercritical fluid so compression, cooling, and dehydration are required prior to injection and to overcome the in situ pressure of the formation. Therefore, even if the injection zone is directly under the power plant, the cost of the compression system must be incurred to allow injection.

The costs calculated in this study can be compared to the costs reported in the literature for CO_2 capture and compression. Costs from a variety of studies range from $33 to $72/metric ton of CO_2 avoided for PC/FGD plants and $21 to $62/metric ton of CO_2 avoided for IGCC plants (Gottlicher and Pruschek, 1999; Herzog, 1999). To directly compare the costs calculated for the EEA with the literature results the costs for transmission and injection would need to be deleted. However, capture and compression are the main contributors to cost, particularly for the shortest pipeline and shallowest injection case, so the adjustment is small. Even without adjustment, the EEA values are well within the range reported in the literature. With a small reduction to convert the estimates to a common basis, the EEA values would shift somewhat nearer the middle of the reported range.

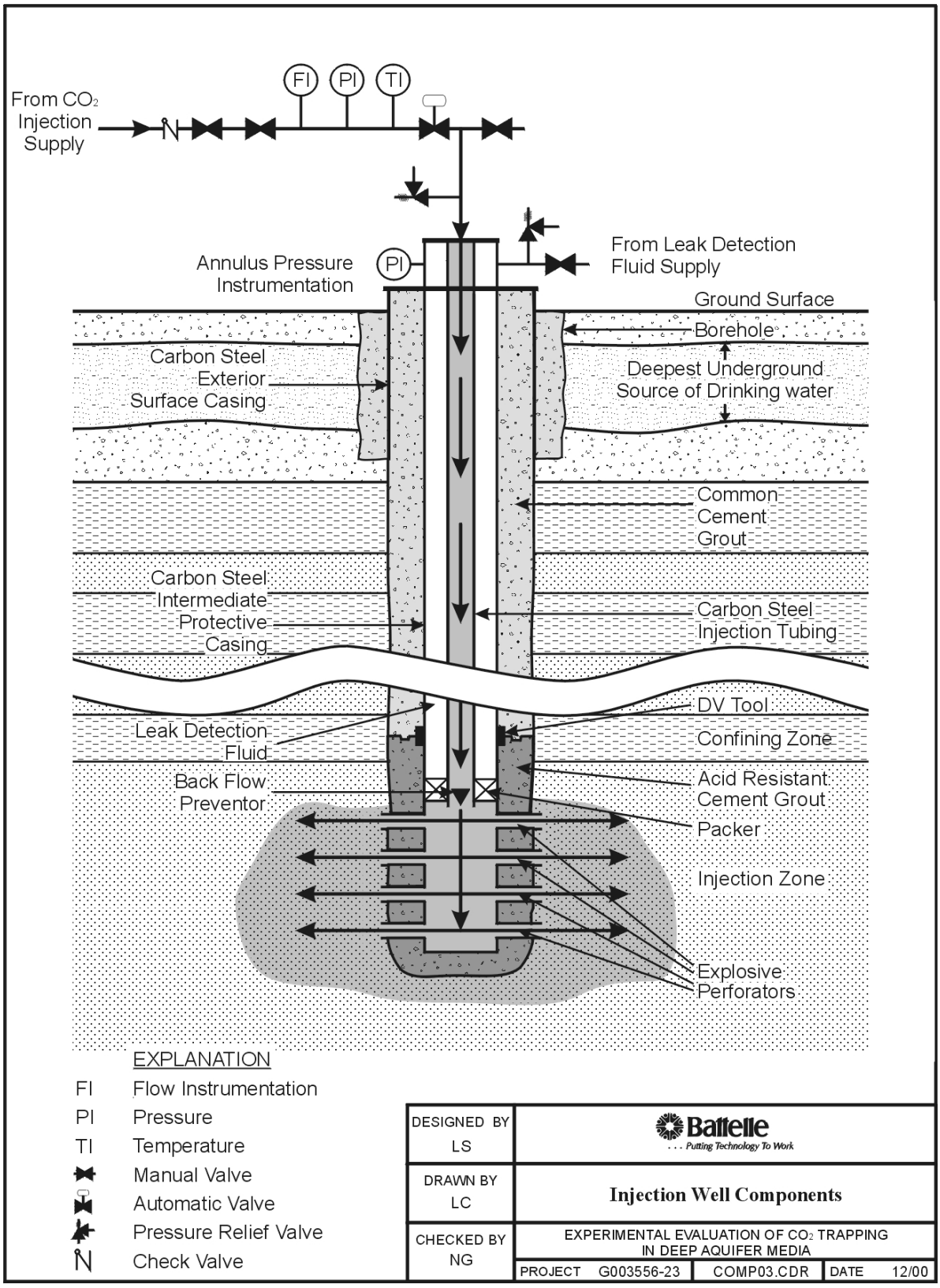

Figure 5. Injection Well Components

Table 4. Summary of Costs for Transmission/Sequestration Scenarios[(a)]

Well Depth (m/ft)	Cost of CO_2 Avoided for Various Scenarios ($/metric ton)				
	15 km (9.3 mi) and Normal Terrain	100 km (62.1 mi) and Normal Terrain	400 km (249 mi) and Normal Terrain	15 km (9.3 mi) and Rocky/Hilly Terrain	15 km (9.3 mi) and Urban Terrain
PC/FGD Plants[(b)]					
1,000/3,281	62.48	NA	NA	NA	NA
2,000/6,562	63.26	66.05	76.49	63.56	63.45
3,000/9,843	65.40	NA	NA	NA	NA
IGCC Plants[(c)]					
2,000/6,562	39.77	NA	NA	NA	NA

(a) NA indicates a cost estimate was not prepared for this case.
(b) Sequestration cases estimated for a 500 MWe plant burning pulverized coal with flue gas desulfurization and CO_2 capture by amine absorption
(c) Sequestration cases estimated for a 500 MWe IGCC plant and CO_2 capture by physical absorption

APPLICATION

The information collected during this project can serve as a starting point for the conceptual design of a CO_2 injection system. Reported experience with industrial handling and injection of CO_2 for commercial application (e.g., enhanced oil recovery [EOR]) did not indicate any technical obstacles to implementing CO_2 sequestration. Although injecting CO_2 into a deep saline aquifer is an emerging technology with limited application history, design, construction, operation, and maintenance of such a system can draw on a significant body of existing experience. Carbon dioxide injection into oil bearing formations to stimulate production has been done at the commercial scale in since the mid-1980's. These EOR operations use compression, dehydration, pipeline transmission, and deep well injection equipment that is, in many ways, directly analogous to the systems that will be needed for CO_2 sequestration.

Procedures for design and operation of CO_2 handling systems can, for the most part, be based on accepted practices used for hazardous liquids and gases in the oil and gas industry. However, some special properties of CO_2 require special design features for a sequestration system. Methods to account for these properties are well documented in the design of existing CO_2 pipeline and injection projects literature. Appropriate materials and methods have been developed to account for the special properties of CO_2.

The cost estimates developed for this project provide a preliminary budget evaluation (+50% to –30% accuracy) of the costs of sequestration of CO_2 from coal-fired power generation stations and a basis for assessing the effects of different storage conditions. For example, the tradeoff of increasing pipeline length (which increases transmission cost) to reach as shallower aquifer (which decrease injection cost) can be evaluated.

Table 5. Summary of Cost Contributions for CO_2 Sequestration[a,b]

Plant Type	Depth (m)	Pipeline Length (km)	Terrain Type	Cost for Capture ($mil/yr) A	Cost for Compression ($mil/yr) B	Cost for Capture and Compression ($mil/yr) C[c]	Cost for Pipeline ($mil/yr) D	Cost for Injection ($mil/yr) E	Total Cost ($mil/yr) F[d]
PC/FGD[e,f]	2,000	15	Normal	20.04	33.39		1.79	3.88	
Scenario totals						53.43			59.10
PC/FGD	2,000	100	Normal	20.04	33.39		7.66	3.88	
Scenario totals						53.43			64.97
PC/FGD	2,000	400	Normal	20.04	33.39		28.89	3.88	
Scenario totals						53.43			86.20
PC/FGD	1,000	15	Normal	20.04	33.39		1.79	2.79	
Scenario totals						53.43			58.01
PC/FGD	3,000	15	Normal	20.04	33.39		1.79	6.11	
Scenario totals						53.43			61.33
PC/FGD	2,000	15	Rocky	20.04	33.39		2.06	3.88	
Scenario totals						53.43			59.37
PC/FGD	2,000	15	Urban	20.04	33.39		2.19	3.88	
Scenario totals						53.43			59.50
IGCC[g]	2,000	15	Normal	4.07	28.28		1.79	3.59	
Scenario totals						32.35			37.73

(a) Capital costs annualized assuming a useful life of 25 yrs and an effective interest rate of 4.1% (capital recover factor = 0.0647)
(b) Totals not exact due to rounding
(c) C = A + B
(d) F = C + D + E
(e) These conditions are used as the base case. Variations from the base case are indicated by shading.
(f) 500 MWe conventional coal fired power plant with CO_2 capture by amine absorption.
(g) 500 MWe IGCC power plant with CO_2 capture by physical absorption.

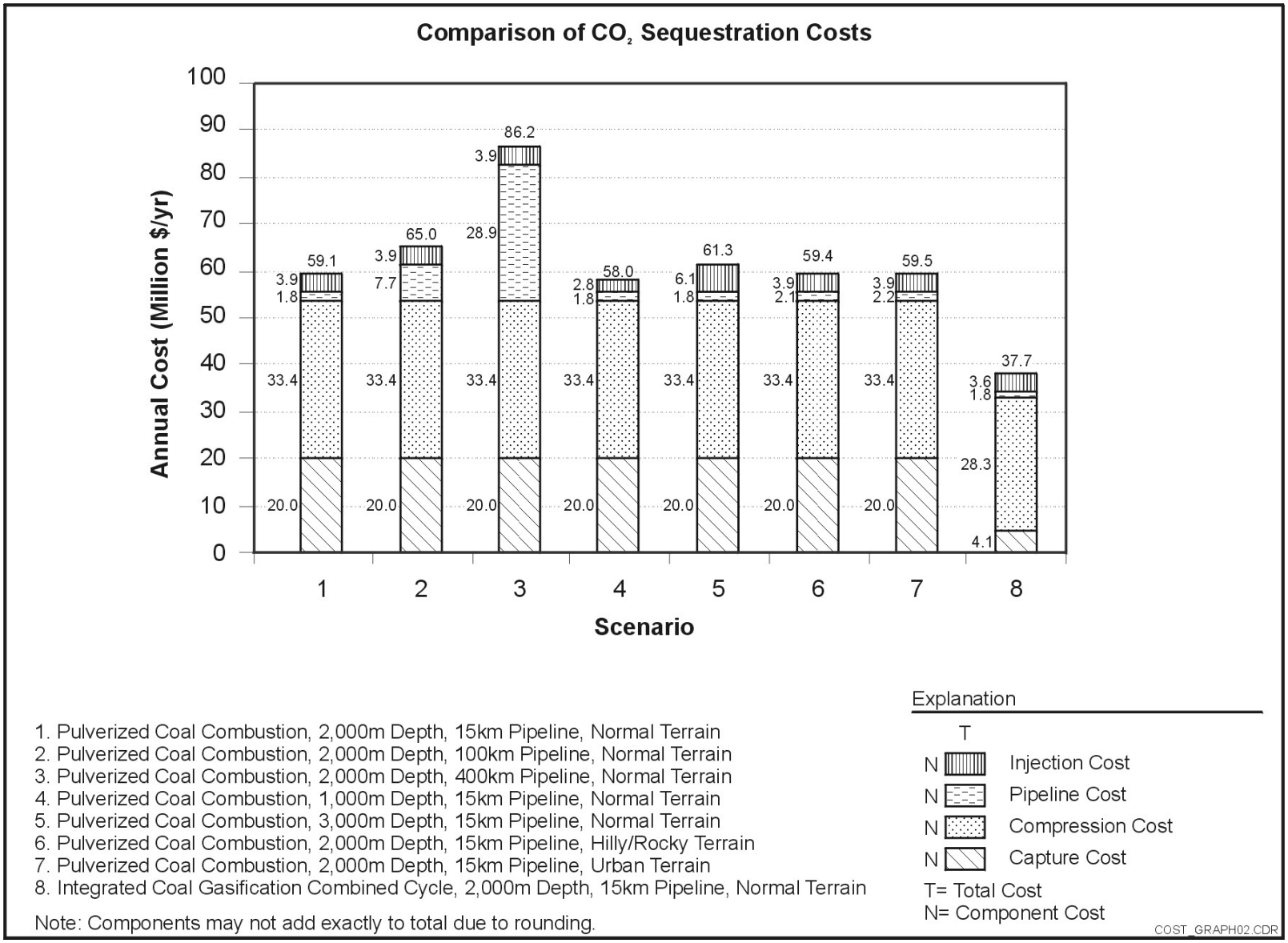

1. Pulverized Coal Combustion, 2,000m Depth, 15km Pipeline, Normal Terrain
2. Pulverized Coal Combustion, 2,000m Depth, 100km Pipeline, Normal Terrain
3. Pulverized Coal Combustion, 2,000m Depth, 400km Pipeline, Normal Terrain
4. Pulverized Coal Combustion, 1,000m Depth, 15km Pipeline, Normal Terrain
5. Pulverized Coal Combustion, 3,000m Depth, 15km Pipeline, Normal Terrain
6. Pulverized Coal Combustion, 2,000m Depth, 15km Pipeline, Hilly/Rocky Terrain
7. Pulverized Coal Combustion, 2,000m Depth, 15km Pipeline, Urban Terrain
8. Integrated Coal Gasification Combined Cycle, 2,000m Depth, 15km Pipeline, Normal Terrain

Note: Components may not add exactly to total due to rounding.

Figure 6. Comparison of Cost Elements in a CO_2 Sequestration System

FUTURE ACTIVITIES

Future activities related to this study will involve efforts to improve the accuracy of cost estimation for system to sequester CO_2 in deep saline aquifers. The review and evaluation of the current status of CO_2 handling and injection methods provides a firm engineering basis for conceptual design of processes and mechanical equipment to implement sequestration in a deep aquifer. More detailed understanding of the system performance requirements and design features will allow development of preliminary specifications to support more accurate cost estimation.

Acknowledgement: The work presented here was conducted with funding from the U.S. Department of Energy's National Energy Technology Laboratory as part of project number DE-AC26-FT40418.

REFERENCES

Doherty, P. and B. Harrison. 1996, "Techno-Economics of Underground Disposal." *The Underground Disposal of Carbon Dioxide*. Pp. 277-300. Final Report of JOULE II Project No. CT92-0031. Ed S. Holloway. British Geological Survey.

Gupta, N., J. Sminchak, C. Byrer, P. Bergman. 2001. *Issues Related to Seismic Activity Induced by the Injection of CO_2 in Deep Saline Aquifers*. Battelle. Columbus, Ohio.

Gupta, N., P. Wang, B. Sass, P. Bergman, and C. Byrer. 2001. "Regional and Site-Specific Hydrogeologic Constraints on CO_2 Sequestration in the Midwestern United States Saline Formations." *Proceedings of Fifth International Conference on Greenhouse Gas Control Technologies, Cairns, Australia, August 14-16, 2000.*

Hendricks, C.A. and K. Blok. 1993. "Underground Storage of Carbon Dioxide." *Energy Conversion Management 34*(9-11):949-957.

Mohitpour, M., H. Golshan, and A. Murray. 2000. *Pipeline Design & Construction: A Practical Approach*. American Society of Mechanical Engineers Press, New York, NY.

Oil and Gas Journal. 2000b. "Pipeline Economics." *Oil and Gas Journal 98*(36):68-86.

Ormerod, B. 1994. *The Disposal of Carbon Dioxide from Fossil Fuel Fired Power Stations*. IEAGHG/SR3. International Energy Agency.

Peters, M.S. and K.D. Timmerhaus. 1991. *Plant Design and Economics for Chemical Engineers*. McGraw-Hill, Inc., New York, NY.

Page, J.S. 1996 *Conceptual Cost Estimating Manual*. Gulf Publishing Corporation, Houston, TX.

Richardson. 1999. *Process Plant Construction Estimating Standards – Volume 4 – Process Equipment*. Richardson Engineering Services, Inc., Mesa, AZ.

Sass, B., N. Gupta, J. Ickes, M. Engelhard, D. Baer, P. Bergman, and C. Byrer. 2001a. "Interaction of Rock Minerals with Carbon Dioxide and Brine: A Hydrothermal Investigation." *First National Conference on Carbon Sequestration, Washington, D.C., May 15-17.*

Sass, B., N. Gupta, J. Ickes, P. Bergman, and C. Byrer. 2001b. “Experimental Evaluation of Chemical Sequestration of Carbon Dioxide in Deep Saline Formations.” *Proceedings of Fifth International Conference on Greenhouse Gas Control Technologies, Cairns, Australia, August 14-16, 2000.*

Sminchak, J., N. Gupta, C. Byrer, and P. Bergman. 2001. “Issues Related to Seismic Activity Induced by the Injection of CO_2 in Deep Saline Aquifers.” *First National Conference on Carbon Sequestration, Washington, D.C. May 15-17.*

van der Meer, L.G.H. 1993. “The Conditions Limiting CO_2 Storage in Aquifers.” *Energy Conversion Management 34*(9-11):959-966

INTERACTION OF ROCK MINERALS WITH CARBON DIOXIDE AND BRINE: A HYDROTHERMAL INVESTIGATION

Bruce M. Sass (sassb@battelle.org; 614-424-6315)
Neeraj Gupta (gupta@battelle.org; 614-424-3820)
Jennifer A. Ickes (ickesj@battelle.org; 614-424-3723)
Battelle Memorial Institute
505 King Avenue
Columbus, Ohio 43201-2693

Mark H. Engelhard (mark.engelhard@pnl.gov; 509-376-1664)
Donald. R. Baer (don.baer@pnl.gov; 509-376-1609)
Pacific Northwest National Laboratory
P.O. Box 999
Richland, WA 99352

Perry Bergman (perry.bergman@netl.doe.gov; 412-386-4890)
National Energy Technology Laboratory
Pittsburgh, PA 15236-0940

Charles Byrer (cbyrer@netl.doe.gov; 304-285-4547)
National Energy Technology Laboratory
P.O. Box 880
Morgantown, WV, 26507-0880

INTRODUCTION

This paper presents interim results of a feasibility study on carbon dioxide (CO_2) sequestration in deep saline formations. The focus of the investigation is to examine factors that may affect chemical sequestration of CO_2 in deep saline formations. Findings of the first phase (Phase I) of this investigation were presented in a topical report (Sass et al., 1999a). Preliminary results of the second phase (Phase II) experiments, now underway, have been reported elsewhere (Sass et al., 1999b; 2001). Evaluations of the suitability of the Mt. Simon formation for sequestering CO_2 and economic issues are reported by Gupta et al. (1999; 2001); Smith et al. (2001). This study is sponsored by the U.S. Department of Energy's (DOE's) National Energy Technology Laboratory (NETL) under a Novel Concepts project grant (Contract No. DE-AC26-98FT40418).

OBJECTIVE

The overall objectives of Phase II experiments were to determine: (1) the potential for long-term sequestration of CO_2 in deep, regional host rock formations; and (2) the effectiveness of overlying caprock as a barrier against upward migration of the injected CO_2. To meet these goals, experiments were conducted using rock samples from different potential host reservoirs and overlying rocks. In addition, pure mineral samples were used in some experimental runs to investigate specific mineralogical reactions. Due to space limitations, the scope of this paper will be limited to two types of equilibration experiments using pure minerals. Implications for more complex natural systems will be discussed in the report for Phase II being finalized at this time.

APPROACH

Experiments were conducted using an apparatus designed to simulate conditions in geologic formations deeper than 800 meters, so that hydrostatic pressure exceeds the critical pressure of CO_2 (7.375 MPa). Samples of anorthite (calcium-rich plagioclase feldspar) and glauconite (iron-rich clay) were obtained from mineral suppliers for use in these tests. Standard hydrothermal techniques were used throughout this study. Pressurized cylinders of carbon dioxide and nitrogen gases were used to control the gas composition and system pressure. Synthetic brine solutions were prepared to simulate regional compositions within the Mt. Simon formation in Ohio and Indiana. At the conclusion of the experiments, samples of the solid, liquid, and gas phases were analyzed to characterize the reactions having taken place.

PROJECT DESCRIPTION

Experimental Setup and Operation

All experiments were conducted in liter-capacity pressure vessels. The vessels were composed of Hasteloy-C material that were fitted with internal PTFE-Teflon™ liners for chemical inertness. Reactants consisted of pure phase solids, brine, and gas. A small amount of sodium sulfite was added immediately before closing each vessel to scavenge residual dissolved oxygen. After closure, the vessels were pressurized with CO_2 or a mixture of CO_2 and N_2. Heating wire was wrapped around each of the vessels, and thermocouple attachments allowed temperature to be controlled automatically. Figure 1 is a schematic drawing of the laboratory setup.

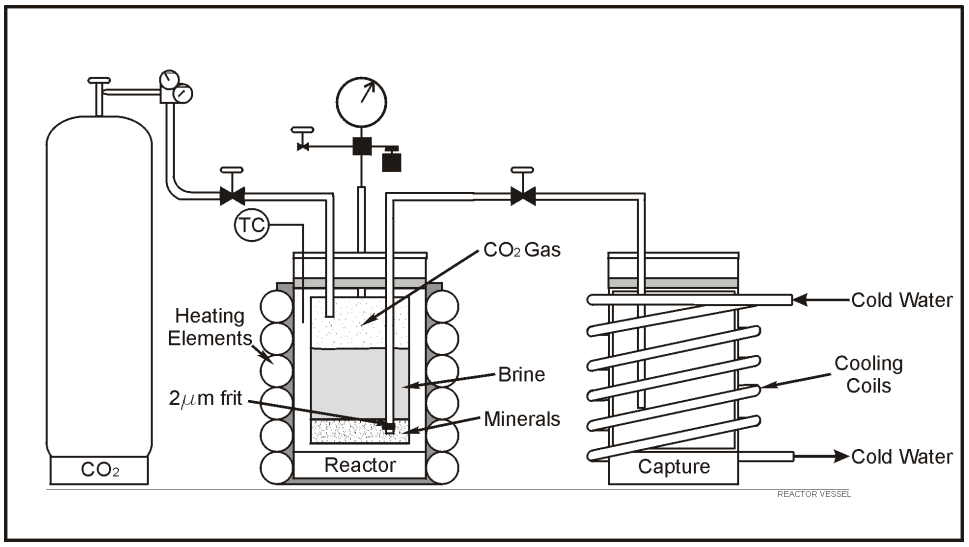

Figure 1. Schematic Drawing of Reaction Vessel.

Preparation of Solid Samples

Specimen-size quantities of anorthite and glauconite were ground in a jar mill and sieved to recover the 38 to 106-μm-size fraction. After sieving, the powders were washed in deionized water with ultrasonic agitation to remove both excess salt and extremely fine and possibly amorphous material that may have been produced by grinding. The powders then were vacuum dried at 40°C for 7 hours. A portion of each material was saved for chemical and mineralogical analysis. Prior to beginning the experiments, the solid phases were characterized by x-ray diffraction (XRD) and scanning electron microscopy (SEM) with

energy dispersive spectroscopy (EDS). In addition, bulk compositions were determined by wet chemical methods. The composition of anorthite was $Ca_{0.91}Na_{0.07}Al_{1.96}Fe_{0.06}Si_{2.02}O_8$, plus trace amounts of Ti and Cr; iron was assumed to be all Fe^{II}. The composition of glauconite is approximate because of uncertainty in the oxidation state of iron. The result was $Na_{0.01}K_{0.33}Ca_{0.10}Fe_{0.56}Al_{0.41}Mg_{0.53}Si_{4.44}O_{10}(OH)_2$, plus trace amounts of Cr, Ni, and P; Fe^{II} and Fe^{III} were assumed to be present in equal amounts; H_2O was not determined.

Experimental Parameters

After attaching tubing and instrumentation lines, vessels were pressurized with high-purity nitrogen gas to detect leaks. The vessels were heated and topped off with nitrogen gas or CO_2 gas to achieve a final total pressure of between 2,000 and 2,500 psi. Sensors to monitor pressure and temperature were connected and the vessels were placed on a shaker table or rocker to agitate the mixtures throughout the course of the experiments. In some runs, small amounts of gas and liquid were collected at interim times to verify the approach toward equilibrium. Table 1 lists the contents and conditions of four experiment runs that are described in this paper.

Table 1. Conditions in Pure Mineral Experiments

Experiment No.	Mineral Contents	T, P_{TOT}, P_{CO2}	Run Duration (days)
2B	Glauconite	50°C, 2,000 psi, 600 psi	30
2C	Anorthite	50°C, 2,000 psi, 600 psi	34
3G	Anorthite	150°C, 2,000 psi, 2,000 psi	30
3H	Glauconite	150°C, 2,000 psi, 2,000 psi	30

Sampling and Analysis Procedures

At the end of each experimental run, a sample of gas was extracted from the pressure vessel and the solid and solution phases were separated by siphoning liquid through a 2 μm-frit mounted inside a tube that extended to the bottom of each vessel (see Figure 1). The solutions were analyzed for total carbon, alkalinity, pH, ORP, and major and minor ions. The solids were rinsed with deionized water, dried, and then analyzed in the same manner as the unreacted samples for comparison. Routine analysis of solid phases consisted of XRD and SEM/EDS. Additional characterization was performed using x-ray photoelectron spectroscopy (XPS), which probes the top 50 to 100 Å of surface. XPS measures elemental concentrations at the surface of mineral grains and can be useful for looking for compositional changes at mineral surfaces.

RESULTS

The following sections present preliminary results and discussion for two sets of experiments using pure mineral phases. These results should be considered preliminary at this time. A more detailed evaluation of all experimental results and comparison with geochemical simulations will be made at the conclusion of the study.

Batch Experiments

Results of the solution analyses are shown in Table 2. The initial brine compositions also are shown for comparison with the reacted mixtures. In general, the solutions analyzed at the end of the experiments were more concentrated in dissolved species, overall. The net increase in total dissolved solids could be

due to any of three factors: (1) dissolution of soluble salts that were not removed by rinsing the ground material before the tests were begun; (2) dissolution of mineral matter (primarily silicates, but may include carbonates and sulfate minerals) during the experiment; and (3) concentration of the brine as a result of evaporation from the reactor.

Table 2. Concentrations of Dissolved Species (mg/L) in Brine after Reaction with Mineral Samples

Sample ID	Brine Solution	Glauconite	Anorthite	Brine Solution	Anorthite	Glauconite
Experiment No.	2	2B	2C	3	3G	3H
Alkalinity	23	327	630	18	610	ND
Chloride	61,200	60,100	69,100	NA	NA	NA
Sulfate	1,080	1,825	1,300	900	600	1,650
Aluminum	ND	1.46	1.31	0.00	ND	0.00
Arsenic	0.26	0.58	0.63	0.37	0.55	0.37
Barium	0.28	0.45	0.34	0.29	0.67	0.30
Calcium	7,840	10,369	10,004	9,400	6,319	9,650
Chromium	0.04	0.06	0.20	0.03	0.06	0.04
Cobalt	0.02	0.92	1.24	0.01	0.23	0.01
Copper	0.29	0.28	0.74	0.33	1.34	0.32
Iron	0.17	4.59	19.38	0.21	117.88	0.23
Lead	0.02	0.00	0.07	0.01	0.35	0.01
Magnesium	1,286	1,873	1,568	1,310	5,560	1,390
Manganese	0.02	22.81	1.17	0.01	3.87	0.01
Nickel	0.09	6.41	8.39	0.06	5.82	0.06
Phosphorus	0.04	0.27	0.03	0.00	ND	0.00
Potassium	793.87	2,493	1,003	987	1,630	987
Scandium	0.01	0.01	0.01	0.00	0.07	0.01
Silicon	1.14	32.0	30.8	0.85	162	0.93
Sodium	22,666	28,794	30,811	24,300	31,755	24,200
Strontium	5.06	6.92	6.42	4.75	120.69	4.65
Tin	0.00	0.00	0.01	0.01	ND	0.02
Titanium	17.27	16.96	19.06	16.90	15.95	17.00
Vanadium	0.43	0.42	0.39	0.31	0.57	0.29
Yttrium	0.00	0.01	0.00	0.01	0.00	0.01
Zinc	0.16	0.90	0.36	0.07	5.97	0.07
Zirconium	0.00	0.00	0.00	0.00	0.01	0.01
pH	ND	6.28	6.11	7.31	6.28	5.35
ORP (mV)	ND	–70.9	42.1	220.1	–73.6	69

ND = Not detected; NA = Not analyzed; ORP = oxidation-reduction potential.

It is important to note that measurements of alkalinity and pH listed in Table 2 are not representative of conditions while the experiment was in progress. This is because the pressure drop upon decanting the solution causes dissolved CO_2 to volatilize and changes the distribution of carbon species in solution.

Results of vapor phase analysis by gas chromatography are shown in Table 3. In Experiment 2, the vapor consisted of approximately 20% CO_2 and 80% N_2. In Experiment 3, the vapor consisted of approximately 95% CO_2 and 5% N_2. The O_2 content was low in both sets of experiments, due to precautions taken to exclude oxygen from the system. The gas composition data were used to model the solution and thereby infer the amount of CO_2 dissolved in the liquid phase.

Table 3. Composition of Gas Phase at End of Experiments (% by Volume)

Experiment No.	Mineral Type	% CO_2	% N_2	% O_2
2B	Glauconite	20.31	78.32	1.37
2C	Anorthite	21.02	77.86	1.12
3G	Anorthite	91.37	8.29	0.34
3H	Glauconite	94.95	3.11	1.94

XPS Analysis

Starting materials and reaction products were analyzed by XPS to determine whether surface composition changed as a result of the experiments. In XPS, binding energies of core shell electrons ejected by x-rays are used to identify compositional elements. Peaks in the XPS spectrum correspond to the abundance of atoms that emit photoelectrons, and are proportional to the concentration of elements in the surface region of the sample. Typically, these emissions account for the top 50 to 100 Å of the surface. For example, the silicon 2p emission occurs at approximately 100 eV in silicates. This energy can vary slightly (i.e. shift) due to the particular structure of the compound containing silicon; and this *chemical shift* effect enables XPS to differentiate elements based on local chemical environment.

Anorthite. Figure 2 compares an XPS spectrum for unreacted anorthite with a spectrum obtained after reacting a sample with CO_2 and brine for 30 days at 150 ºC (Experiment 3G). In this figure, elements were identified according to the binding energy for each type of emission, which are labeled above the peaks. (A spectrum for Experiment 2C was also performed, but is not show in Figure 2). Peaks labeled 1s and 2p are photoelectron emissions and peaks labeled KLL are Auger electron emissions. Peak intensities (height or area) were used to calculate concentrations as percentages of the total intensity.

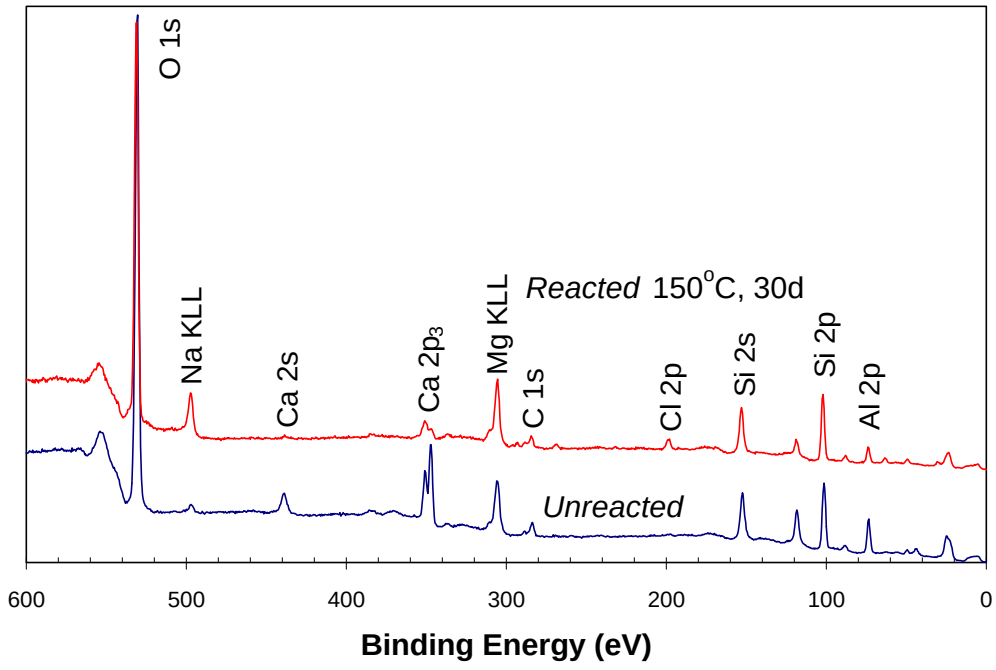

Figure 2. Portion of the XPS Spectrum for Unreacted and Reacted Anorthite (Experiment 3G)

Table 4 summarizes data for anorthite prior to reaction and after reacting at 150 ºC for 30 days. Table 4 also lists elemental percentages for ideal anorthite of composition that is 90% pure end member of the plagioclase feldspar series and 10% albite (sodium end member), or An_{90}. Terms in the brackets next to the element symbols indicate the photoelectron emission used in the analysis.

It can be seen that all of the anorthite specimens contain 4 to 5% carbon. However, none of this carbon is in the carbonate form. Based on the binding energy of the carbon signal, this carbon is likely a hydrocarbon which could have sorbed onto particle surfaces from exposure to vacuum equipment.

Table 4. Results of XPS Analysis of Anorthite in Percent Peak Area

Sample	C[1s]	O[1s]	Na[1s]	K[2p]	Mg[1s]	Ca[2p]	Al[2p]	Si[2p]	Cl[2p]	Fe[2p3]
Ideal An_{90} [(a)]	0.00	61.54	0.77	0.00	0.00	6.92	14.62	16.15	0.00	0.00
Unreacted	4.98	63.46	0.65	0.00	3.42 [(b)]	5.02	8.77	12.94	0.11	0.66
30 day, 150ºC	5.35	60.38	4.90	0.09	5.89 [(b)]	1.45	4.88	15.13	1.16	0.77

(a) Calculated signal area; (b) sample impurity not related to anorthite.

The sodium content of the solid increased as a result of reaction. Also, the calcium content decreased in approximately the same proportion as sodium increased. Because an increase in sodium content could result from incomplete rinsing of brine from the reacted samples, chloride also was analyzed to determine if it behaved similar to sodium. Table 4 shows that chloride was slightly higher in the two reacted samples, indicating that the specimens may have had some residual brine, but the chloride content is several factors less than the increase in sodium. This result indicates that the increase in sodium cannot be attributed entirely to residual salt. Rather, the sodium appears to be incorporated into the structure of the feldspar.

The data in Table 4 were recalculated to remove chloride, magnesium, and carbon impurities. Results are given in Table 5. Now it can be seen that wet chemical and XPS analysis of sodium and calcium in the unreacted sample are in close agreement. In comparison, the aluminum and silicon contents differ somewhat with the bulk analysis. Compared to the bulk analysis (and to the ideal structure for An_{90}), XPS results show that the unreacted sample contain excess silicon and is deficient in aluminum.

Table 5. XPS Analysis of Anorthite - Corrected for Impurities

Sample	Sodium	Calcium	Silicon	Aluminum	Iron
Unreacted [(a)]	0.07	0.91	2.03	1.96	0.06
Unreacted	0.10	0.90	2.33	1.58	0.12
30 day, 150 C	0.72	0.28	2.93	0.95	0.15

(a) Based on bulk chemical analysis of sample.

The inverse relationship between sodium and calcium was examined further by plotting the composition of the specimens against theoretical values for the anorthite-albite series. The left plot on Figure 3 shows that the sodium and calcium content for the unreacted sample falls on the theoretical curve for plagioclase at 90% anorthite and 10% albite, or An_{90}. In these plots, atomic percentages were recalculated without impurities such as carbon and chloride (as in Table 5). When sodium and calcium concentrations in the reacted specimens are plotted on the theoretical curve, the predicted composition is An_{28} for the sample equilibrated for 30 days at 150 ºC.

The relationships of the feldspar reactions depicted in Figure 3 suggests that calcium was partially replaced by sodium during the experiments, and that the extent of replacement is enhanced by higher tem-

perature. Calcium, liberated due to the reaction, is available for precipitating carbon species from solution in the form of calcium carbonate. However, no calcium carbonate was detected at the conclusion of these experiments. The absence of calcium carbonate can be explained by the pH of the solution remaining too low to stabilize a carbonate mineral. In subsequent experiments, carbonate buffer was added to control pH, and kaolinite or smectite were included with the solid components to "seed" the reaction. It is hoped that these measures will encourage precipitation of calcium carbonate.

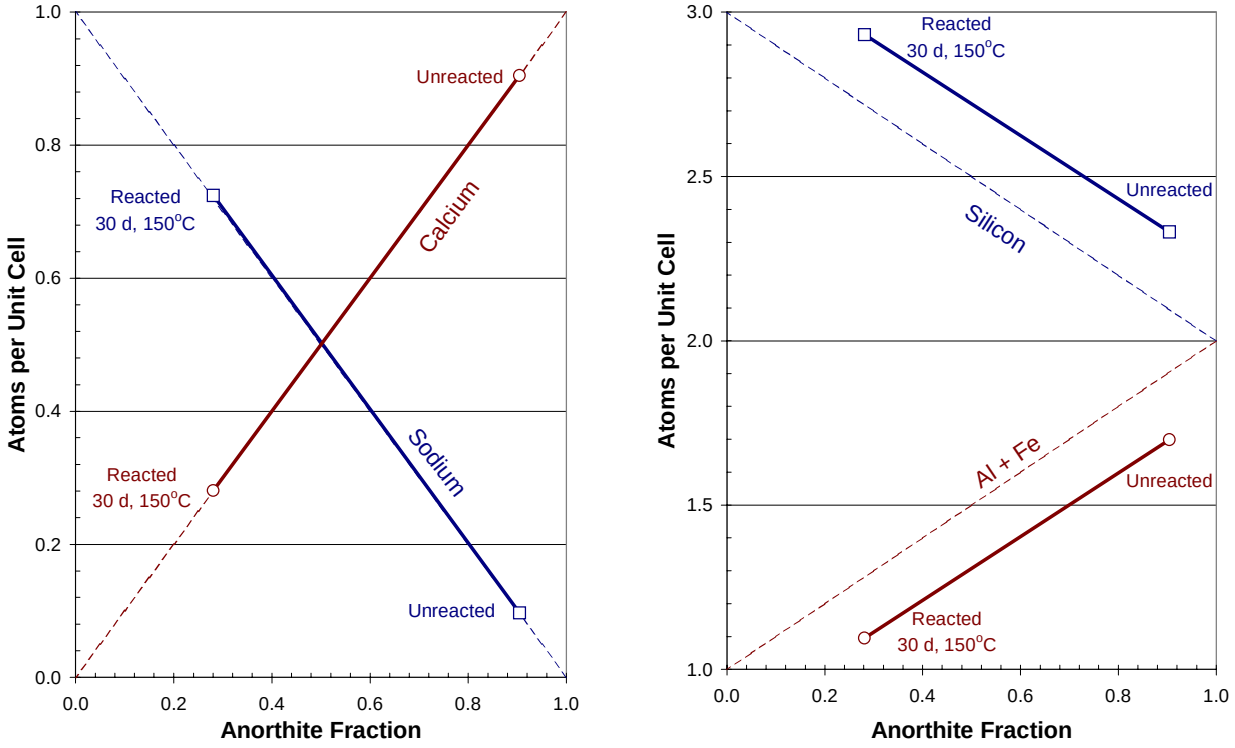

Figure 3. Change in Anorthite Composition as a Result of Mineral Equilibration Reactions (based on data in Table 5); Ideal Formulae Show by Dashed Lines.

Glauconite. Products of experimental runs consisting of glauconite clay, brine and CO_2 also were analyzed by XPS to detect compositional changes after the reaction. As the results in Table 6 show, small but significant differences in composition were observed in the glauconite sample after the equilibration experiment. In particular, the sodium content increased substantially (after correcting for chloride), while the aluminum, magnesium and calcium content was unchanged, and potassium, iron, and silicon decreased. Glauconite was chosen as a starting material for tests in this study because of the potential for iron to precipitate iron carbonate. Although no iron carbonate compound (siderite) was observed in the reaction products, tests will be continued to determine if siderite can be precipitated under suitable (reducing) conditions.

Table 6. Results of XPS Analysis of Glauconite in Percent Peak Area

Sample	C[1s]	O[1s]	Na[1s]	Mg[1s]	Al[2p]	Si[2p]	Cl[2p]	K[2p]	Fe[2p3]	Ca[2p]	F[1s]
Unreacted	1.11	67.49	0.2	2.79	3.46	17.03	0.05	2.86	3.92	0.98	0.11
30 day, 150ºC	2.21	65.32	1.28	2.83	3.45	16.73	0.32	2.49	3.69	1.09	0.58

APPLICATION

Experiments to verify mineral trapping show progress toward that end, but generally are too slow to be completed during short time periods (< 1 year). Surface spectroscopic techniques (e.g. XPS) indicate that elemental compositions at mineral surfaces were modified as a result of the experiments. Moreover, these changes occurred in such a way that agrees with equilibrium modeling calculations. For example, when anorthite (calcium aluminosilicate) was reacted in brine, the calcium and aluminum content at the mineral surface decreased, which is consistent with equilibrium modeling that indicates precipitation of calcium carbonate (calcite) and kaolinite (clay). This, and similar types of behavior, indicate that reaction progress was made, but that time limitations prevented reaching equilibrium.

Geochemical modeling has been used to confirm mineral dissolution behavior and to predict carbonate precipitation under equilibrium conditions. An expanded thermochemical database from Lawrence Berkley Laboratory is now being used to evaluate potential reactions involving CO_2 under geochemical conditions that could occur during carbon sequestration in deep formations. This modeling work, when completed, will provide greater insight into potential reactions that may be occurring over many years or centuries.

FUTURE ACTIVITIES

Results from the full suite of experiments being conducted will be compared with geochemical simulation data. Also, recent changes in experimental parameters are expected to speed reaction progress. For example, some experiments are being "seeded" with kaolinite or montmorillonite clay to help initiate the reactions. In addition, some of experiments now being conducted include a pH buffer, which is expected to stabilize pH and allow carbonate phases to precipitate more readily than in previous experiments. Addition of buffer enhances the conversion of carbonic acid to bicarbonate ion, which helps produce solid carbonates in the presence of divalent ions, such as calcium and iron. In other new experiments, rock samples with natural pyrite present are being used to test whether iron carbonate (siderite) can be formed. This series of tests is designed to show where mineral trapping by carbonates can be demonstrated in the laboratory.

REFERENCES

Sass, B., N. Gupta, L. Smith, and E. Drescher. 1999a. *Experimental Evaluation of Chemical Sequestration of Carbon Dioxide in Deep Saline Formations*. Phase I Topical Report. Prepared by Battelle for the U.S. Department of Energy, Federal Energy Technology Center, under DOE Contract No. DE-AC26-98FT40418.

Sass, B., N. Gupta, J. Sminchak, and P. Bergman. 1999b. "Geochemical Modeling to Assess the Capacity of a Midwestern United States Geologic Formation for CO_2 Sequestration." *Proceedings of Fourth International Conference on Greenhouse Gas Control Technologies, Interlaken, Switzerland, August 30 – September 2, 1998.*

Sass, B., N. Gupta, J. Ickes, P. Bergman, and C. Byrer. 2001. "Experimental Evaluation of Chemical Sequestration of Carbon Dioxide in Deep Saline Formations." *Proceedings of Fifth International Conference on Greenhouse Gas Control Technologies, Cairns, Australia, August 14-16, 2000*.

Gupta, N., P. Wang, B. Sass, P. Bergman, and C. Byrer. 2001. "Regional And Site-Specific Hydrogeologic Constraints on CO_2 Sequestration in the Midwestern United States Saline Formations." *Proceedings of Fifth International Conference on Greenhouse Gas Control Technologies, Cairns, Australia, August 14-16, 2000*.

Gupta, N., B. Sass, J. Sminchak, T. Naymik, and P. Bergman. 1999. "Hydrodynamics of CO_2 Disposal in Deep Saline Formation in the Midwestern United States." Proceedings of Fourth International Conference on Greenhouse Gas Control Technologies, Interlaken, Switzerland, August 30 – September 2, 1998.

L.A. Smith, N. Gupta, B.M. Sass, T.A. Bubenik, C. Byrer and P. Bergman. 2001. "Engineering and Economic Assessment of Carbon Dioxide Sequestration in Saline Formations," *First National Conference on Carbon Sequestration.* Washington DC. May 15-17.

ISSUES RELATED TO SEISMIC ACTIVITY INDUCED BY THE INJECTION OF CO_2 IN DEEP SALINE AQUIFERS

Joel Sminchak (sminchak@battelle.org; 614-424-7392)
Neeraj Gupta (gupta@battelle.org; 614-424-3820)
Battelle Memorial Institute
505 King Avenue
Columbus, Ohio 43201

Charles Byrer [(a)] and Perry Bergman [(b)]
National Energy Technology Laboratory
(a) P.O. Box 880, Morgantown, WV, 26507-0880
(b) P.O. Box 10940, Pittsburgh, PA, 15236-0940

Abstract

Case studies, theory, regulation, and special considerations regarding the disposal of carbon dioxide (CO_2) into deep saline aquifers were investigated to assess the potential for induced seismic activity. Formations capable of accepting large volumes of CO_2 make deep well injection of CO_2 an attractive option. While seismic implications must be considered for injection facilities, induced seismic activity may be prevented through proper siting, installation, operation, and monitoring. Instances of induced seismic activity have been documented at hazardous waste disposal wells, oil fields, and other sites. Induced seismic activity usually occurs along previously faulted rocks and may be investigated by analyzing the stress conditions at depth. Seismic events are unlikely to occur due to injection in porous rocks unless very high injection pressures cause hydraulic fracturing. Injection wells in the United States are regulated through the Underground Injection Control (UIC) program. UIC guidance requires an injection facility to perform extensive characterization, testing, and monitoring. Special considerations related to the properties of CO_2 may have seismic ramifications to a deep well injection facility. Supercritical CO_2 liquid is less dense than water and may cause density-driven stress conditions at depth or interact with formation water and rocks, causing a reduction in permeability and pressure buildup leading to seismic activity. Structural compatibility, historical seismic activity, cases of seismic activity triggered by deep well injection, and formation capacity were considered in evaluating the regional seismic suitability in the United States. Regions in the central, midwestern, and southeastern United States appear best suited for deep well injection. In Ohio, substantial deep well injection at a waste disposal facility has not caused seismic events in a seismically active area. Current technology provides effective tools for investigating and preventing induced seismic activity. More research is recommended on developing site selection criteria and operational constraints for CO_2 storage sites near zones of seismic concerns.

Introduction

Concerns about global warming have prompted investigation into the disposal of carbon dioxide (CO_2) into deep saline rock formations. This option is attractive, since there are regionally extensive aquifers capable of accepting large volumes of CO_2 from power plants without the need for long pipelines. There is also a substantial amount of research available on the subject from projects on enhanced oil recovery and deep well injection of liquid wastes. However, application of the technology to populated areas may involve seismic hazards if the injection facilities are not properly sited and operated. The objective of this paper is to review induced seismic activity as it

relates to the injection of CO_2 into deep saline aquifers in the United States. Basic theory, regulation, monitoring and testing methods, and special considerations on induced seismic activity are addressed. A case study on seismic practices in Ohio is also presented to outline typical procedures followed to monitor seismic activity during deep well injection. Related DOE funded work on geologic storage of CO_2 in saline formations conducted at Battelle includes compositional reservoir simulations (Gupta et al., 2001), evaluation of geochemical aspects through modeling and experiments (Sass et al., 2001a and Sass et al., 2001b), and assessment of economic and engineering aspects (Smith et al., 2001).

Seismic activity was first linked to deep well injection activities near Denver, Colorado, in 1962. Since then, seismic activity triggered by injection wells has been noted at locations worldwide. Due to the uncertainty associated with deep subsurface investigations, an understanding of the lithology, structural geology, and hydrology of the site is critical to determining if injection will induce seismic events. To this end, regulation on injection wells exists to ensure that a site is properly investigated and monitored for seismic vulnerability. In addition, several distinctive processes related to CO_2 injection must be considered for the option of CO_2 disposal. Ramifications of induced seismic events go well beyond the traditional image of earthquake activity. While most seismic events triggered by deep well injection are too small to be noticed, moderate earthquakes have occurred due to injection activity. Most notably, two earthquakes with Richter magnitude of 5.1 and 5.2 were triggered in Denver, Colorado, in 1966. Seismic activity may also affect the injection system itself. In the worst-case scenario, a fault or fracture causes the rupture of the injection well casing and containment is lost. Fractures may also occur in overlying rock units providing a pathway for upward migration of the injection liquid. Continual seismic activity may result in the gradual weakening of the well casing. In addition, formation alteration may affect the performance of the injection system by reducing or increasing the pore space in the injection system. However, through proper siting and operation procedures, seismic events may be prevented. In fact, current technology has provided very effective tools for investigating potential seismic activity induced by deep well injection.

Overview of Induced Seismic Activity

In general, deep well injection weakens the strength of a fault, triggering movement and the resulting seismic event. Wesson and Nicholson (1987) note that deep well injection usually triggers activity in a seismically unstable area rather than causing an earthquake in a seismically stable area. Conceptually, the fluid in a fault is pressurized and assumes the stress of the overlying rock and water. Since the fluid has little shear strength, the frictional resistance along the fault declines and the fault blocks slip, causing a seismic event. These processes are best represented by a stress/strain relationship at very high pressures. Other processes involved in the triggering of seismic activity may include transfer of stress to a weaker fault, hydraulic fracture, contraction of rocks due to the extraction of fluids, subsidence due to the saturation of a rock formation, mineral precipitation along a fault, and density-driven stress loading. Figure 1 shows a conceptual model of processes involved in triggering seismic activity by underground injection wells. Most of these processes are site specific and can be evaluated through site investigations or formation testing.

In terms of stress equations, deep well injection reduces both the principal and confining pressure in the injection formation while keeping the differential pressure constant, moving the system toward failure (Figure 2). Represented on a Mohr's circle, it is easy to see how the injection pressures may move the rock to the point of failure (Figure 3). With respect to deep well injection systems, the confining pressure and the principal pressure may be measured or estimated based on lithology and depth. Consequently, injection pressures may be analyzed to determine if

the changes in pressure may trigger fracture. Key parameters that affect injection pressures are formation permeability and porosity. Rock formations with high permeability and porosity are more receptive to injected fluids. Low permeability and low porosity rock formations will require higher injection pressures and be more susceptible to induced seismicity. Another factor which may influence the stress-strain system is formation pressure. Water trapped in a formation during deposition may reach very high pressures as sediments are deposited on top of the formation throughout time.

At very high injection pressures, rock formations may fracture in a process termed hydraulic fracturing. This process is often used by oil/gas companies to increase the transmissivity of a formation around the well. Hydraulic fracturing occurs when the injection pressure exceeds the intergranular strength of the rock, creating or expanding fractures. 1996 Joule II proceedings suggest that controlled hydraulic fracturing does not induce seismic activity above a magnitude of one. However, unmonitored hydraulic fracturing may produce rather extensive fractures several meters wide and hundreds of meters long which could possibly trigger more substantial seismic activity.

Seismic events can be correlated to injection activities in several ways. A seismic monitoring network is essential to collecting information on earthquakes. Most seismic events triggered by deep well injection are too small to be felt, but they are often precursors to larger events. The most obvious way to link earthquakes to injection wells is an increase in seismic events once injection begins. The frequency of seismic activity compared to previous seismic trends may be examined to reveal changes introduced by the injection practices.

The magnitude of the seismic events is another line of evidence to link earthquakes to injection wells. The seismic activity caused by the injection well may be either smaller or larger in magnitude than the previous trend in seismic activity. For example, numerous small seismic events may happen after injection starts. Trends in the magnitude of seismic activity may be recognized by comparing frequency-magnitude charts. The geographic location of the earthquake foci should be in the general area of the injection radius of influence. It should be noted that the radius of influence of the injection system may be kilometers to tens of kilometers from the injection wells. Similarly, the depth of the earthquakes may be in the affected injection interval; although, earthquakes have been triggered several kilometers below the injection well. More advanced analysis methods can determine the orientation of faults from the seismic response and compare the orientations to the location of the injection well to see if the two are somehow related.

Operations data on injection pressure at the wellhead and/or injection volumes can be valuable to studying seismic events. The frequency of the seismic activity over time is often related to the injection pressure or injection volume history over time. There may be a lag of days to years between the two events since an earthquake may be triggered by a propagating pressure wave. In addition, sudden pressure changes at the wellhead itself may result from an earthquake event.

Another method of linking earthquakes to deep well injection is the analysis of critical fluid pressures capable of causing failure along a fault. Based on formation pressures at depth and induced pressure, the Mohr-Coloumb failure criteria may be used to determine if conditions capable of triggering a fault would be created in the injection zone. However, these calculations involve several assumptions concerning fault strength and pressures. The method provides less certainty than direct evidence from monitoring instruments. For example, Davis and Pennington (1989) found that injection pressures at thousands of sites in the state of Texas were high enough to trigger seismic activity but do not exhibit seismicity. The value of stress analysis is that the

work may be performed in site selection and system design before any fluid is actually injected. Information for evaluation of critical fluid pressure may be obtained from compression tests, hydraulic testing, and analysis of the orientation of the stress tensors.

Reservoir modeling may be used to analyze the migration of injection pressure. Reservoir modeling uses the hydraulic properties of the injection formation with analytical or numerical equations to simulate the progression of pressure or liquid. These models are useful in determining whether deep well injection may have caused seismic activity a long distance from the injection well(s). Similar models are available to determine what pressures will trigger hydraulic fracture and the extent of the fracturing.

Seismic activity induced by deep well injection has been observed at locations throughout the world. However, only a few case studies have been well studied due to the large amount of monitoring and testing required to demonstrate a conclusive relationship between earthquakes and deep well injection. Table 1 summarizes documented case studies of induced seismic activity. Earthquakes were first linked to deep well injection in 1962 at the Rocky Mountain Arsenal near Denver, Colorado (Healy et al., 1968). This remains one of the best-studied occurrences of seismic activity triggered by deep well injection. Researchers suggest that these earthquakes were likely triggered by pressure waves that continued to propagate after injection was stopped. Hsieh and Bredehoft (1981) reassessed the Denver earthquakes with reservoir modeling. The authors found that they could use modeling to simulate the arrival of critical pressure levels in a faulted zone where earthquakes occurred. The modeling results were comparable to the earthquake control studies by Raleigh et al. (1976) that demonstrated that earthquakes could be controlled by monitoring injection pressure and seismic activity. Increased seismic activity has also been observed at numerous oil/gas drilling sites, due to either fluid extraction or injection. Motivated by the Denver earthquakes, the USGS conducted an experiment in 1976 to control earthquakes at a nearby oil well site in Rangely, Colorado (Raleigh et al., 1976). Injection pressures were increased to critical levels, then decreased. The frequency of earthquakes decreased after the initial pressures declined. Similar research was performed in Matsushiro, Japan.

Issues Related to Induced Seismic Activity

Regulation

Injection wells in the United States are regulated by the federal Underground Injection Control (UIC) program, which provides minimum rules for the siting, testing, installation, operation, monitoring, reporting, and abandonment of underground injection wells (Title 40 Code of Federal Regulation Parts 146 and 148). UIC rules are enforced by regional and/or state Environmental Protection Agency (EPA) offices, which dispense permits for UIC wells. Injection wells are classified according to the type of fluid injected and the injection interval in relation to underground sources of drinking water (USDW). CO_2 disposal wells have yet to be classified by the EPA. However, they will likely be held to the same type of seismic regulation as Class I wells because of depth considerations. The UIC program requires testing on formation materials to ensure that injection pressures will not fracture rock formations in the injection interval. The program also requires regular monitoring to retain injection permits.

Overall, UIC regulation does not extensively address induced seismic activity. However, two sections are fairly explicit in providing rules related to earthquake activity:

40CFR146.13 Except during stimulation, injection pressure at the wellhead shall not exceed a maximum which shall be calculated so as to assure that the pressure in the injection zone during injection does not initiate new fractures or propagate existing fractures in the injection zone. In no case shall injection pressure initiate new fractures or propagate existing fractures in the injection zone. In no case shall injection pressure initiate fractures in the confining zone or cause the movement of injection or formation fluids into an underground source of drinking water.

This rule is aimed at preventing formation of transmissive faults and fractures which may allow injected fluids to migrate vertically and reach sources of drinking water. The CFR addresses the issue of seismic activity induced by deep well injection in 40CFR146.68. The UIC guidance provides the enforcing agency more than enough leeway to require extensive testing and monitoring:

40CFR146.68 The Director may require seismicity monitoring when he has reason to believe that the injection activity may have the capacity to cause seismic disturbances.

Testing and Monitoring

Many types of tests are available to detect faulting or fractures that could lead to induced seismic activity including down-hole geophysical tests as well as more traditional testing methods that may be performed within the borehole. Another type of testing is pressure fall-off/shut-in testing that involves monitoring pressure buildup in the well. Testing methods are summarized below:

2-D or 3-D seismic surveys
Core sample collection from major units during drilling
Down-hole caliper logging to detect fractures
Down-hole resistivity logging to detect fractures and lithologic changes
Down-hole spontaneous potential logs
Down-hole gamma ray logging to detect formation changes
Down-hole density testing
Fracture-finder logs to detect fractures
Compression tests on formation samples to determine rock strength
Geotechnical tests on formation samples (porosity, density, permeability)
Compatibility test of injection fluids with formation unit and confining unit
Pressure fall-off/shut-in tests
Radioactive tracer survey.

Monitoring is another important part of assessing induced seismic activity from an injection well. Table 2 summarizes typical monitoring requirements at an underground injection facility to aid in evaluating seismic activity. Monitoring at the well may include recording of injection volume, rate, and pressure, continuous monitoring of annulus pressure. Abrupt changes in these parameters may signal a seismic event. Well workovers to assure mechanical integrity and detect weakening of well casing may also suggest faulting at depth. Other monitoring methods may include reservoir pressure/ambient monitoring and groundwater monitoring to detect upward migration of injection fluids through fractures.

Seismic monitoring should be performed before injection activities start to obtain baseline conditions. Depending on the frequency of seismic activity at the injection site, months to years of monitoring may be required to achieve an adequate depiction of baseline seismic conditions prior to injection. This may involve the installation of several subsurface seismic sensors around the proposed injection site. Seismic monitoring considerations may also be integrated into well installation so that down-hole sensors can be installed while drilling. The Joule II report suggests that at minimum a network of subsurface sensors should be installed at the injection site. Another monitoring method to consider is measuring changes in elevation due to expansion, subsidence, or movement along fault blocks. Tiltmeters may also be considered to monitor changes in fracture orientation at depth. Monitoring should be continued once injection activities begin. Aside from the frequency of seismic events, the location, depth, and magnitude of the seismic events should be analyzed to determine if the events are related. Geophysical methods may also be used to determine the extent of injected fluid as proposed for the Sleipner Aquifer CO_2 Storage operation in the North Sea of Norway (International Energy Agency, 1998). Since seismic velocities vary according to the density of the material, the density contrast between the formation waters and injected CO_2 may provide evidence of the extent of the injected fluid.

Modeling can be a valuable tool in evaluating the potential for deep well injection to trigger earthquakes. Overall, modeling refers to making a simplified representation of actual conditions or processes. Reservoir modeling involves using numerical equations to simulate the migration of pressure and/or fluid from the injection well. With respect to seismic activity, modeling may be used to predict if and when critical pressures are reached in a seismically sensitive area. Modeling may also be used to address uncertainty regarding rock strength, formation pressure, and other factors to see if more testing is required to characterize the injection system. Simple one- or two-dimensional models as used by Hsieh and Bedehoeft (1981) to complex three-dimensional models like UTCOMP (Chang, 1990) may be used for CO_2 injection simulation. Davis and Pennigton (1989) modeled pressure buildup in the Cogdell oil reservoir and showed a correlation between earthquake epicenters and zones of high pressure.

Special Considerations

Supercritical Liquid Properties

For deep well disposal, CO_2 is generally injected in a supercritical phase at pressures above 6.9 MPa (1,000 psig) to minimize the injected volume. Consequently, injection formations must be deeper than approximately 1,000 m to ensure that CO_2 will remain in a supercritical state. Supercritical CO_2 has a density of about 0.60 to 0.75 g/cc while the density of saline formation fluid ranges from 1.0 to 1.2 g/cc. Supercritical CO_2 is also less viscous than saline waters, resulting in more uniform flow migration. Czernichowski-Lauriol, et al. (1996) note that about 50 g of CO_2 will dissolve in 1 kg of typical formation water. Consequently, the injected CO_2 must be addressed as a multiphase system. Special considerations for underground disposal of CO_2 are mostly related to the unique properties of supercritical CO_2.

Formation Dissolution/Weakening

Supercritical CO_2 has the potential to dissolve, weaken, or transform the minerals in the injection formation. In the supercritical state, CO_2 becomes a “supersolvent.” Thus, there is potential for the fluid to dissolve and weaken the rocks in the injection formation. If the rock formation is weakened, the potential for hydraulic fracturing increases. Dissolution of minerals precipitated

along a fault will reduce the strength of the fault, possibly moving the fault to frictional sliding conditions where failure is more likely to occur.

Another aspect of deep well CO_2 disposal is the compatibility of the injected fluid with the formation waters and the formation rocks. There is potential for the injected fluid to precipitate out minerals. Mineral precipitation has the potential to significantly decrease formation porosity and permeability (Melcer and Gerrish, 1996). These changes may result in unexpected pressure buildup and formation faulting or fracture. Minerals may also bond along a previously aseismic fault. Thus, stress is increased and builds. The ensuing failure event is much larger than would have occurred without precipitation.

With respect to induced seismic activity, mineral dissolution and precipitation may have the greatest potential to affect a fault. Mineral precipitation in the pore space may cause a decrease in permeability, resulting in the buildup of pressure and hydraulic fracturing or pressure-induced faulting. Many shallow injection wells experience clogging due to similar processes as fine sediments accumulate in pore space around the well. Mineral precipitation or dissolution along fault planes may affect the stress regime of a fault system. Precipitation along a fault could "lock up" a previously aseismic fault. As stress accumulates, the potential for a more significant fault becomes greater. Conversely, mineral dissolution along a previously bonded fault may reduce the strength of the fault.

Radius of Influence

Deep well injection activities commonly affect a formation far beyond the location of the injection well(s). The earthquakes may occur after injection activities are stopped, as shown by the Denver earthquakes which occurred over one year after injection activities were stopped. Finally, earthquakes may be induced in formations well below the injection formation. For these reasons, the effective radius of influence must be examined for the injection well(s). Injecting 200 million tons of CO_2 into a formation 20 m thick with a porosity of 15% and a storage efficiency of 6% will require a radius of influence of approximately 22 km. Thus, it must be demonstrated that there are no faults of fractures within the radius of influence that might be susceptible to earthquakes. Simple calculations or modeling methods may be used with site characterization data to estimate the radius of influence. The radius of influence for the pressure front created by the injection practices may be even larger than the injection capacity indicates. Therefore, modeling may be necessary to evaluate this aspect of the injection process.

Density Driven Flow

Most other waste disposal wells attempt to match the density of the injection liquid with the formation fluids. However, the density of supercritical CO_2 is 0.60 to 0.75 g/mL while the density of most deep saline formation waters ranges from approximately 1.0 to 1.2 g/mL. Consequently, this density contrast may produce density-driven flow as the lighter, injected fluids migrate upward. Given the large volumes of fluid involved in CO_2 disposal operations, the impact of the density contrasts could be capable of influencing stress conditions at depth. Conceptually, the less dense fluid will migrate upward until it reaches a confining layer/cap rock. Once at the caprock, the upward force exerted by the lighter fluid could weaken the caprock or transfer stress to overlying faults. Stress transfer due to deep well injection was identified as a potential cause of seismic activity in Cogdell, Texas (Davis and Pennington, 1989). Similarly, injected CO_2 may produce seismic activity related to density-driven flow of free-phase CO_2 at depth. It should be noted that when the CO_2 is injected, much of the fluid will mix and dissolve into the formation

waters. Whether density-driven flow will pose a significant seismic threat is best addressed with multiphase modeling and chemical experiments.

Case Study: Seismic Aspects of Deep Well Injection in Ohio

Deep well injection practices and seismic activity in Ohio were examined to determine the potential for induced seismicity in the state. All five active deep well injection systems in Ohio have been investigated for seismic hazards to some extent. Of the operational facilities, BP Chemical injects the most, with a cumulative injection volume of over 20 million metric tons. Most deep well injection in Ohio is into the Mt. Simon formation, a fine-grained sandstone with a relatively high porosity and permeability. The formation overlies Precambrian basement rock, with a top depth of approximately 800 m in northwestern Ohio to over 3,000 m below ground surface in eastern Ohio. The unit is generally less than 100 m thick throughout the state and thins toward the northeast. Rock formations overlying the Mt. Simon are generally less permeable shale, limestone, dolomite and sandstone. However, permeable layers exist at various depths in certain areas. In eastern Ohio, many oil and gas wells penetrate the Clinton sandstone 1,000 to 1,100 m below the surface. In general, there are several intervals of rocks which may be suitable for deep well injection in Ohio. The depth intervals and hydraulic properties of the receptive formations appear to vary throughout the state, but are fairly constant within the anticipated radius of influence of an injection facility.

Most faults in Ohio are associated with Precambrian basement rocks at depths over 1 km below land surface. Several faults have been identified in northwestern Ohio, while relatively few faults have been identified in the rest of the state. The Anna Seismogenic Region is one of the most active seismic zones in Ohio (Figure 4). The zone is located in west-central Ohio. While many faults have been proposed in the area, only a few are well accepted. The faults are mostly northeast-southwest or northwest-southeast oriented. Analysis of seismic effects in that area suggests that the faults are steeply dipping with strike-slip movement. Seismic activity in the Anna area is generally deeper than 10 kilometers. Other major faults southeast of Ohio are related to the Kentucky River Fault Zone. Faults have also been proposed in various other areas throughout the state, most notably the Ashtabula fault in northeastern Ohio.

The seismic history of Ohio dates back to 1811 when a series of earthquakes with epicenters near New Madrid, Missouri, were felt in Cincinnati. Since then, many seismic events have occurred in Ohio. The largest earthquakes have had a Richter magnitude in the range of 5.0-5.5, or a Mercalli Modified Index of VII-VIII. In general, most seismic activity indicates strike-slip movement along steeply dipping faults. Based on the USGS Seismic Hazard mapping project, there is a low probability for damage from earthquakes for Ohio, except in the Anna Seismic Area, which has a moderate hazard.

The Anna Seismic Seismogenic Region in west-central Ohio has been identified as one of the most active seismic areas in the Midwest. The area has a substantial history of seismic activity dating back to the mid-1800s. The largest earthquake observed in the area had a Modified Mercalli intensity of VIII in 1937. In general, seismic activity indicates northeast-southwest strike-slip movement oriented perpendicular to the predominant stresses in the area. Analysis of the seismic activity indicates foci in Precambrian bedrock at depths of over 10 km below ground surface. A number of faults have been proposed in the area, but most activity appears to occur near the trend of the proposed Anna-Champaign Fault. Overall, the Anna Seismic Area is considered a seismically active area. However, since most activity is well below potential injection formations, the potential for induced seismic activity is not likely. In fact, no substantial induced seismic activity has been observed at the BP Chemicals injection facility, which is

located 50 km northeast of the Anna Seismic Area. Based on the study of Ohio, a properly sited and operated injection facility may be located in a region with moderate seismic activity.

Conclusions and Future Work

The possibility for seismic activity induced by deep well injection must be considered when evaluating the disposal of CO_2 in deep saline aquifers. The potential for seismic events is greatest in seismically vulnerable locations with a history of faulting and earthquakes. Seismic activity may be prevented, through proper siting, installation, and monitoring. To this end, federal guidance exists to regulate underground injection facilities. Special considerations related to the properties of supercritical CO_2 may have seismic effects.

Future work on induced seismic activity associated with disposal of CO_2 into deep saline aquifers should involve improving methods for detecting seismic activity induced by injection activities, integrating seismic monitoring with the evaluation of the migration of the injected CO_2, characterization of regional seismic suitability for injection activities, and the assessment of fractured rock formation injection capacities and limitations.

Acknowledgement: The work presented here was conducted with funding from the U.S. Department of Energy's National Energy Technology Laboratory as part of project number DE-AF26-99FT0486.

References

BP Chemicals. 1991. UIC No Migration Demonstrations. Pursuant to 40 CFR Part 148.

Chang, Y. 1990. "Development of a Three-Dimensional, Equation-of-State Compositional Reservoir Simulator for Miscible Gas Flooding." Ph.D. Dissertation, The University of Texas at Austin.

Czernichowski-Lauriol, B.S., C. Rochelle, K. Bateman, J. Pearce, and P. Blackwell. 1996. "Area 5. Inorganic Geochemistry." In S. Holloway (Ed.), *The Underground Disposal of Carbon Dioxide.* Contract No. JOU2 CT92 0031, Final Report. British Geological Survey. February.

Davis, SD., and W.D. Pennington. 1989. Induced Seismic Deformation in the Cogdell Oil Field of West Texas. Bulletin of the Seismological Society of America, vol. 79, no. 5, p. 1477-1494.

Gupta, N., B.M. Sass, J.R. Sminchak, and J.E. Hicks. 1998. *Carbon Dioxide Sequestration in Deep Saline Aquifers in the Midwest: Data Compilation and Modeling Aspects, Interim Report*. Battelle Report prepared for U.S. Department of Energy, Pittsburgh Energy Technology Center.

Gupta, N., P. Wang, B. Sass, P. Bergman, and C. Byrer. 2001. "Regional And Site-Specific Hydrogeologic Constraints on CO_2 Sequestration in the Midwestern United States Saline Formations." *Proceedings of Fifth International Conference on Greenhouse Gas Control Technologies, Cairns, Australia, August 14-16, 2000.*

Healy, J.H., W.W. Rubey, D.T. Griggs, and C.B. Raliegh. 1968. The Denver Earthquakes. *Science*, vol.161, no. 3848, p. 1301-1310.

Hsieh, P.A., and J.D. Bredehoeft. 1981. A Reservoir Analysis of the Denver Earthquakes: A Case Study of Induced Seismicity. *Journal of Geophysical Research*, v. 86, p. 903-920.

Holloway, S. (ed.). 1996. The Underground Disposal of Carbon Dioxide. Contract No. JOU2 CT92 0031, Final Report of the JOULEII Project, British Geological Survey.

International Energy Agency. 1998. Proceedings of the Sleipner Carbon Dioxide Storage Workshop, 25th-26th November 1997, Trondhiem, Norway. Report PH3/1.

Melcer, A., and H.W. Gerrish. 1996. Effects of Formation Damage on Injection Operations and on Pressure Transient Tests. *Deep Injection Disposal of Hazardous and Industrial Waste*, J.A. Apps and Chin-Fu Tsang, eds. p. 277-286.

Ohtake, M. 1974. Seismic Activity Induced by Water Injection at Matsushiro, Japan. J. *Phys. Earth*, 22, p. 163-174.

Raleigh, C.B., J.H. Healy, and J.D. Bredehoeft. 1976. An Experiment in Earthquake Control at Rangely, Colorado. *Science*, v. 191, p. 1230-1237.

Sass, B., N. Gupta, J. Ickes, P. Bergman, and C. Byrer. 2001a. "Experimental Evaluation of Chemical Sequestration of Carbon Dioxide in Deep Saline Formations." *Proceedings of Fifth International Conference on Greenhouse Gas Control Technologies, Cairns, Australia, August 14-16, 2000*.

Sass, B., N. Gupta, J. Ickes, M. Engelhard, D. Baer, P. Bergman, and C. Byrer. 2001b. "Interaction of Rock Minerals with Carbon Dioxide and Brine: A Hydrothermal Investigation." *First National Conference on Carbon Sequestration, Washington, D.C., May 15-17.*

Smith, Lawrence A., N. Gupta, B. Sass, T. A. Bubenik, C. Byrer, and P. Bergman. 2001. Engineering and Economic Assessment of Carbon Dioxide Sequestration in Saline Formations. *First National Conference on Carbon Sequestration, Washington, D.C., May 15-17.*

Wesson, R.L. and C. Nicholson. 1987. "Earthquake Hazard Associated with Deep Well Injection." Prepared by the U.S. Geological Survey. Open-File Report 87-331.

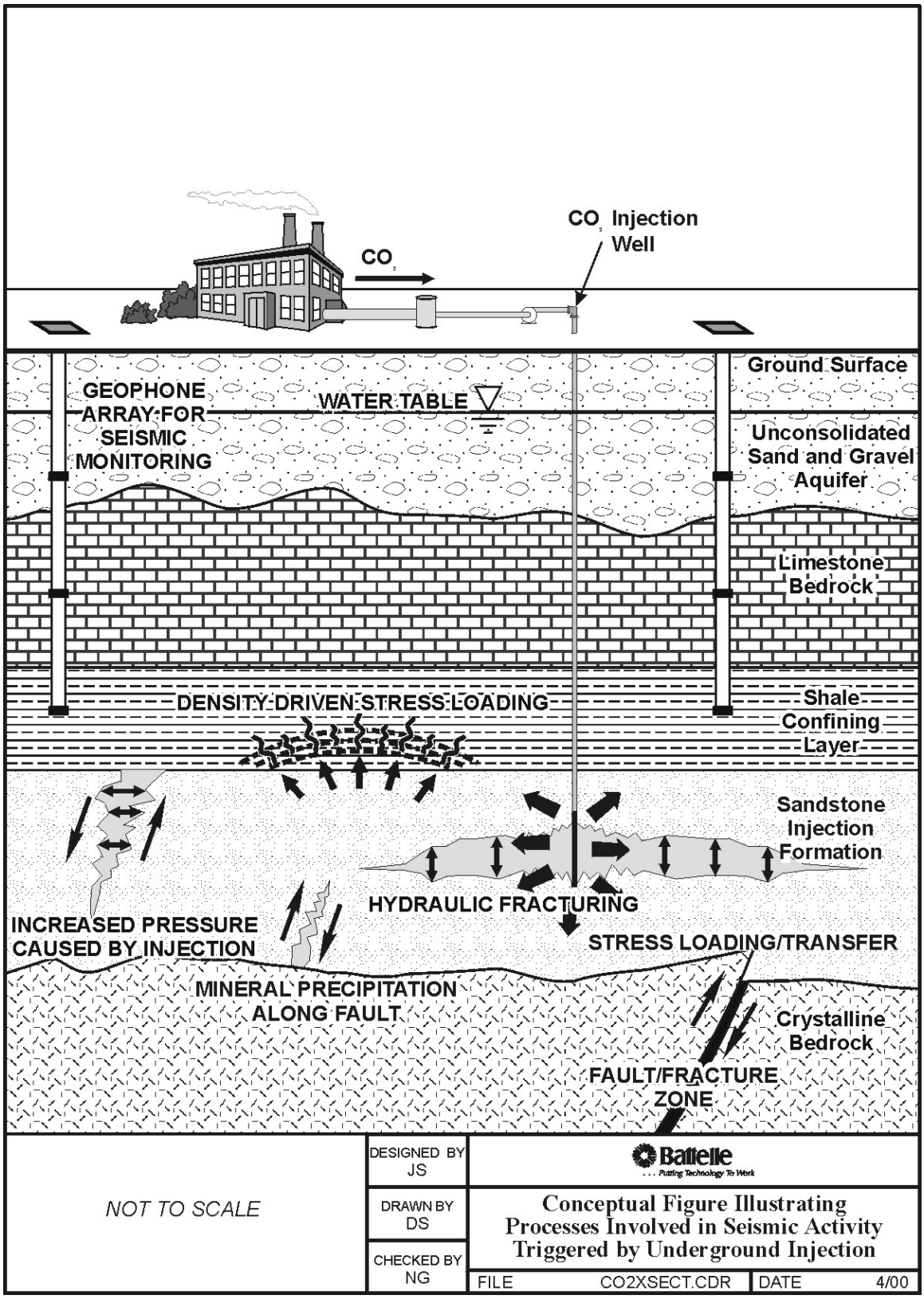

Figure 1. Conceptual figure illustrating processes involved in seismic activity induced by underground injection wells.

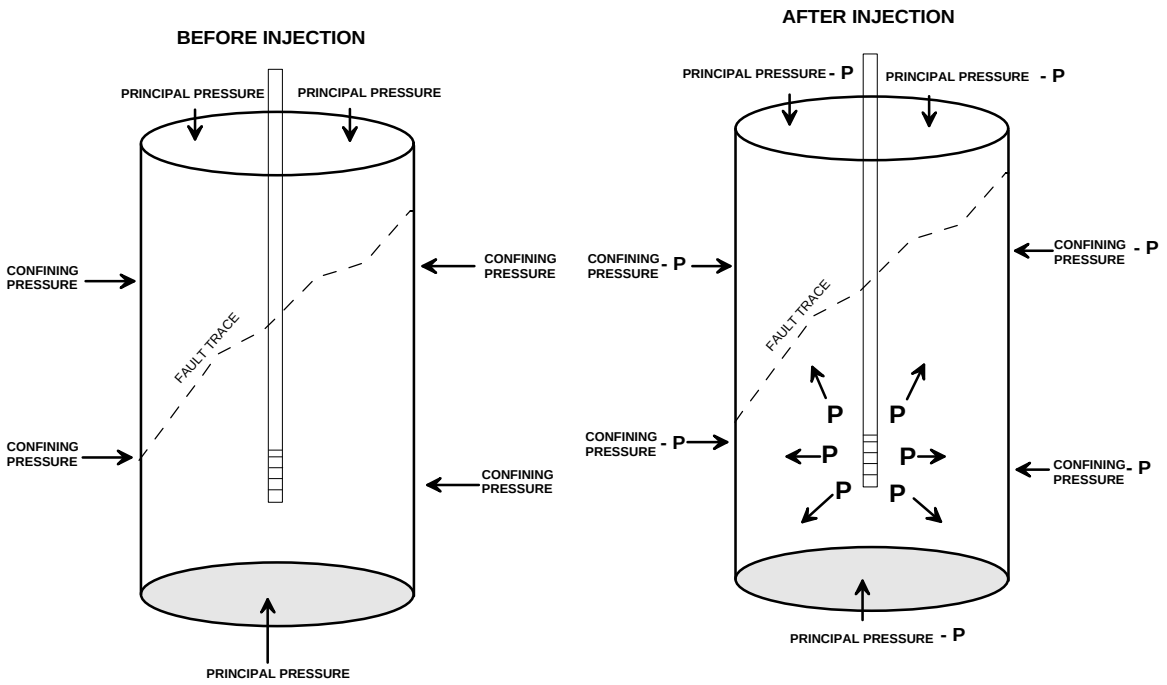

Figure 2. Diagram illustrating how injection pressures (P) reduce the effective confining and axial strength of a rock formation. Injection pressure counteracts confining and axial pressures, reducing the strength of the rock and causing fracture or faulting.

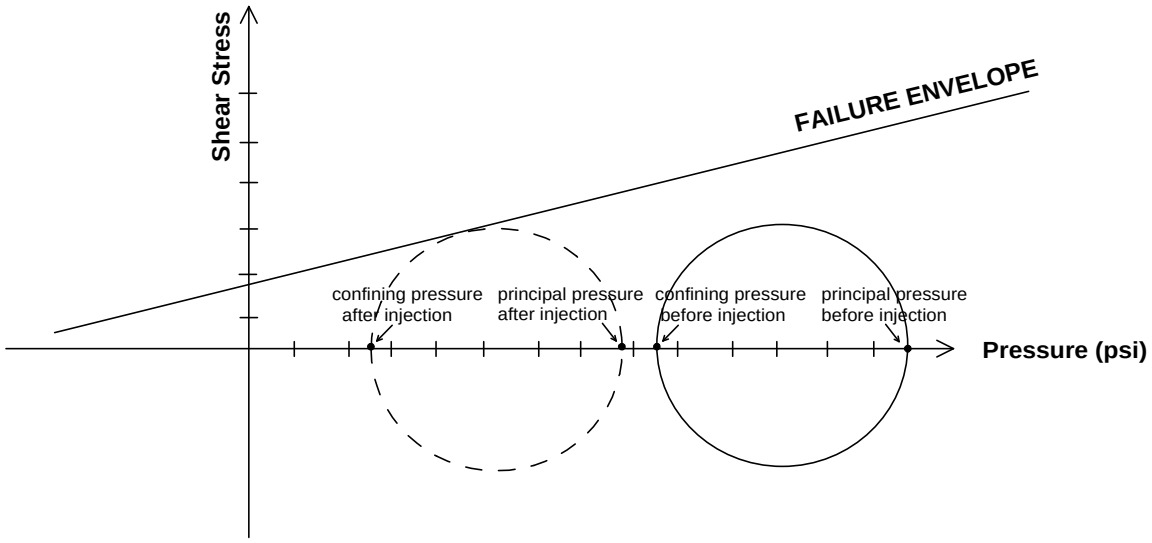

Figure 3. Mohr diagram showing how injection pressures bring a faulted rock to the point of failure.

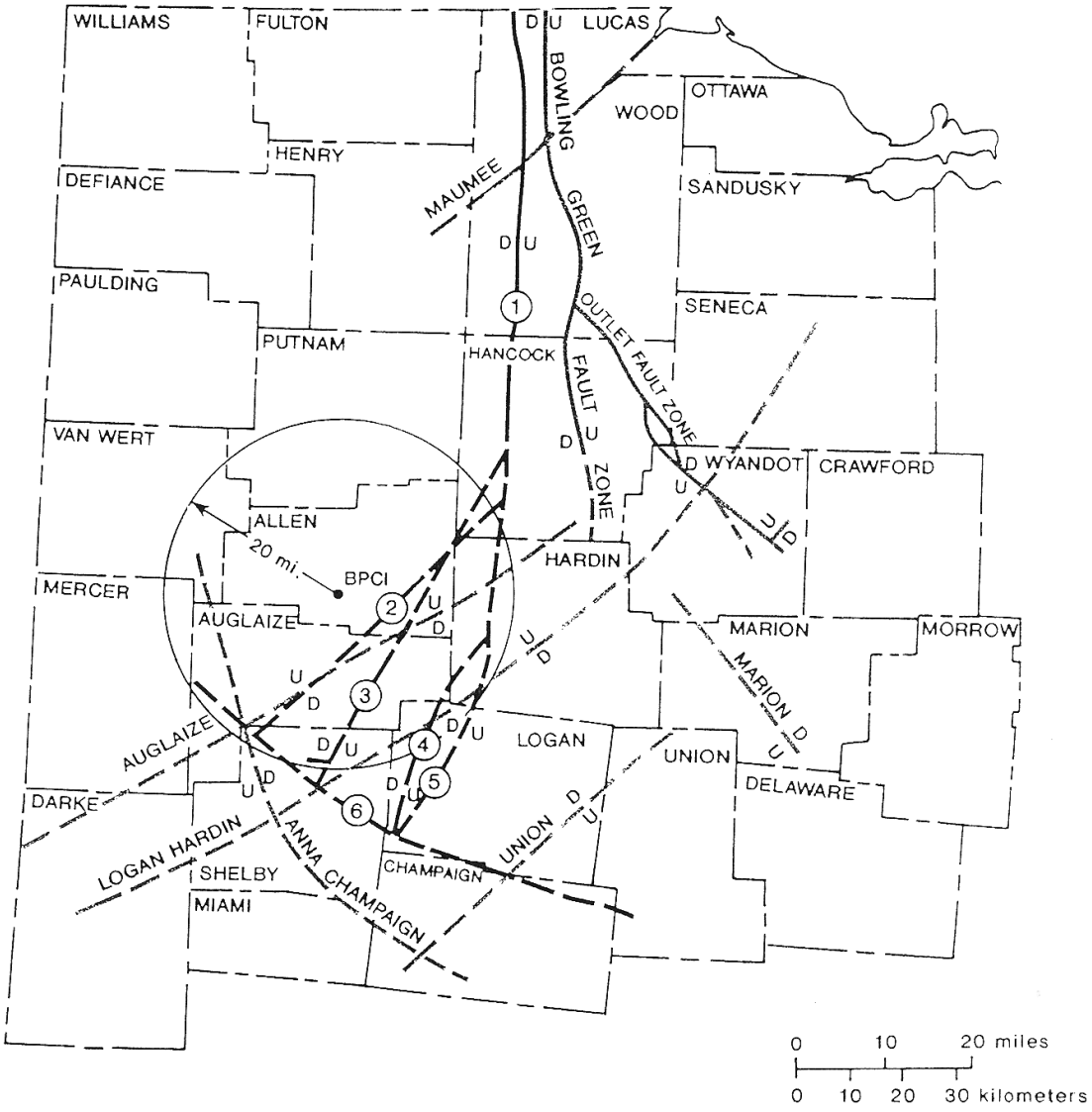

BPCI = BP LIMA INJECTION FACILITY
1. BOWLING GREEN FAULT
2. TEAYS TRIBUTARY FAULT
3. AUGLAIZE FUALT
4. BOWLING GREEN EXTENSION FAULT
5. LOGAN-HARDIN FAULT
6. ANNA-CHAMPAIGN FAULT
(DASHED LINES INDICATE PROPOSED FAULTS)

Figure 4. Faults in Northwestern Ohio (Source: BP Chemicals, 1991)

Table 1. Documented cases of induced seismic activity.

Location	Type	Depth (m)	Injection Pressure (MPa)	Maximum Earthquake Magnitude
Denver, CO	Waste disposal	3,671	7.6	5.5
Fenton Hill, NM	Geothermal	2,700	20.0	<1.0
The Geysers, CA	Geothermal	3,000	(extraction)	4.0
Matsushiro, Japan	Research	1,800	5.0	2.8
Dale, NY	Solution mining	426	5.5	1.0
Central Michigan	Gas storage	320	1.5-4.3	NA
Germigny Reservoir, France	Gas storage	750	<3	<1?
Cogdell, TX	Secondary recovery	2,071	19.9	4.0
Rangely, CO	Secondary recovery	1,900	8.3	3.1
Gobles Field, Ontario	Secondary recovery	884	NA	2.8
Sleepy Hollow, NE	Secondary recovery	1,150	5.6	2.9
Snipe Lake, Alberta	Secondary recovery	NA	NA	5.1
Dollarhide, TX	Secondary recovery	2,590	13.8	~3.5
Dora Roberts, TX	Secondary recovery	3,661	43.1	~3.0
Kermit Field, TX	Secondary recovery	884	10.6	~4.0
Keystone Field I, TX	Secondary recovery	975	10.3	~3.5
Keystone Field II, TX	Secondary recovery	2,987	17.6	~3.5
Monahans, TX	Secondary recovery	2,530	20.7	~3.0
Ward-Estes Field, TX	Secondary recovery	914	11.7	~3.5
Ward-South, TX	Secondary recovery	741	13.8	~3.0

(after Wesson and Nicholson, 1986); NA = not available

Table 2. Typical Monitoring Requirements for a Class I Underground Injection Facility

Parameter	Monitoring Requirements	Reporting Requirements
Injection Pressure	Continuous	Monthly
Bottomhole Pressure	Calculated every 4 hours	Monthly
Annulus Pressure	Continuous	Monthly
Interannulus pressure	Continuous	Monthly
Temperature	Continuous	Monthly
Flowrate	Continuous	Monthly
Specific Gravity	Weekly	Monthly
PH	Weekly	Monthly
Composition of Injectate	Every 6 months	Monthly
Cumulative Volume	Daily	Monthly
Annulus Sight Glass Level	Daily	Monthly
Groundwater monitoring	Quarterly	Quarterly
Seismic monitoring (if required)	Continuous	Monthly

A Perspective On The Potential Role Of Geologic Options In A National Carbon Management Strategy

David A. Beecy (David.Beecy@hq.doe.gov; 301-903-2787)
U.S. Department of Energy, Office of Environmental Systems
19901 Germantown Rd., FE-23, Building GTN
Germantown, MD 20874

Vello A. Kuuskraa (vkuuskraa@adv-res.com; 703-528-8420)
Advanced Resources International, Inc.
1110 N. Glebe, Suite 600
Arlington, VA 22201

Charles Schmidt (Charles.Schmidt@netl.doe.gov; 412-386-6090)
U.S. Department of Energy, National Energy Technical Laboratory
626 Cochrans Mill Road
Pittsburgh, PA 15236

Abstract. Carbon sequestration is the critical "third-option" for addressing greenhouse gas emissions, along with increased energy efficiency and expanded use of low-carbon fuels. Together with technology progress, these three options can provide the Nation with the ability to sustain economic growth through affordable energy, while meeting environmental and carbon emission goals (Beecy and Kuuskraa, 2000).

Carbon sequestration in geologic formations, one of the options for carbon management, entails adapting natural processes that have been storing CO_2 and methane (CH_4) (another greenhouse gas) for geologic times. Some nearly pure CO_2 is extracted from geologic formations (or industrial processes) and reinjected back into geologic formations to enhance recovery of oil and coalbed methane. Future research may even unlock the process for converting CO_2 back into methane. As such, there are both near-term opportunities and longer-term possibilities for geologic sequestration to be a major option for carbon management.

Introduction. As concerns increase about the adverse impacts of anthropogenic emissions of greenhouse gases on global climate, it may become necessary to significantly reduce these emissions. From the perspective of fossil fuels, the source of a substantial portion of these anthropogenic greenhouse gas emissions, the industry has three major options: (1) improving the efficiency of energy production and use; (2) reducing the carbon content of fuels through increased use of natural gas and non-carbon fuels (eg. renewables and nuclear); and, (3) sequestering the emission of carbon dioxide. The third option, carbon sequestration, is increasingly seen as a cost-effective strategy for achieving deep reduction in carbon dioxide (and carbon) emissions (Herzog, Drake and Adams, 1997).

Carbon sequestration is a relatively new field of science and technology. However, interest in it has been growing rapidly. In 1998, the Department of Energy's Office of Fossil Energy (DOE/FE) and Office of Science (DOE/OS) set forth their joint "roadmap" for carbon sequestration as an option for addressing climate change concerns.

The roadmap identifies several alternatives for sequestering carbon including enhancing natural carbon sinks, capturing CO_2 and storing it in geologic formations or the deep ocean, and converting CO_2 to benign solid materials or fuels through biological or chemical processes. The DOE's Office of Fossil Energy, in partnership with industry, the International Energy Agency's Greenhouse Gas Research and Development Programme and others, has underway a Carbon Sequestration Research and Development Program that addresses a broad range of sequestration options. In parallel and closely coordinated, the Office of Science has launched their Carbon Management Science Program.

Vision for Geologic Sequestration. The vision for the Sequestration R&D Program is to develop the essential scientific understanding of sequestration and develop cost efficient options that ensure environmentally acceptable sequestration to reduce anthropogenic CO_2 emissions.

> In the near term, the program will emphasize options for "value-added" geologic sequestration with multiple benefits, such as using CO_2 for enhanced oil recovery and coalbed methane production.
>
> Over the long-term, the program will pursue R&D on biogenic conversion of CO_2 to methane, first by better understanding the natural conversion processes that have been underway over geologic time. The program will also examine the feasibility of other value-added sequestration options such as enhanced gas recovery and will seek to better understand the options for CO_2 storage provided by the nation's extensive saline formations. The program seeks to use early successes in niche, value-added applications to attract industry interest and participation in advanced sequestration concepts and R&D.

Putting the Carbon Back in the Ground. With the passage of time, plus temperature and pressure, the carbon in plants and fossils buried underground has been converted to petroleum, coal and other fossil fuels. These are the same fossil fuels that are the source of the carbon dioxide emissions that we now seek to reduce. The vision for geologic sequestration is "putting this carbon back in the ground."

Under the surface of the earth, in the U.S. and many areas of the world, are structures that once were filled with oil and gas but now have space that could be used for storing CO_2. Under the right geologic setting, a portion of this injected CO_2 may be converted to fixed minerals or, in the presence of methanogens, back to methane (Beecy and Ferrell, 2000).

Other structural settings, lacking the presence of hydrocarbons, are filled with saline waters left over from pre-historic seas. These structures could also serve as sites for carbon dioxide storage, displacing the water in the structures or becoming dissolved in the saline water itself, much as is the case with natural mineral water – "mit gaz."

Role of Natural Analogs. One of the main issues surrounding geologic sequestration is its reliability for long term CO_2 storage. Opportunities exist for understanding the long term behavior and safety of these underground carbon dioxide storage sites from rigorous study of "natural analogs." In certain geologic and high temperature settings, the hydrocarbons in a reservoir have been converted to carbon dioxide. In other settings, carbon dioxide from deeper sources has migrated and become trapped in these underground structures. In either case, the carbon dioxide in these "natural analogs" has existed and been stored for millions of years. Understanding the interactions of carbon dioxide with formation water, rock and minerals and assessing the seals and leakage (if any) of natural CO_2 storage sites can provide valuable insights and data obtainable in no other manner.

Value-Added Geologic Sequestration. As introduced above, some of the geologic settings offer the potential for value-added byproducts, helping defray some of the costs of carbon sequestration. Notable examples are the injection of carbon dioxide for enhanced oil recovery and enhanced coalbed methane production. Numerous barriers still exist in using these options for carbon dioxide storage, such as reconciling the conflicts between achieving lowest cost oil/methane recovery and maximizing CO_2 sequestration. In all cases, adding appropriate long term monitoring and verification to the CO_2 injection and storage process will be essential.

The adaptation of these existing technologies can provide viable near term options for geologic sequestration. In the longer term, considerable research and technology demonstration will be required to fully define and lower the costs of advanced options, such as saline formation storage, biomineralization, or even CO_2 conversion through methanogens or biomimetic approaches.

Capacities of Geologic Sinks. Numerous natural sinks exist for storing carbon in the form of carbon dioxide -- depleted oil and gas reservoirs, deep coal seams, saline formations, rock caverns and mined salt domes. These geologic sinks hold considerable capacity, both in the U.S. and worldwide, sufficient to store all expected increases in carbon dioxide emissions for the next many hundreds of years.

The technology for injecting carbon dioxide back into the ground is established. Oil producers in the Permian Basin of West Texas and in the Rocky Mountains have been injecting carbon dioxide for enhanced oil recovery (EOR) for more than 25 years. In addition, the operation of the underground natural gas storage system, with its annual cycles of natural gas injection and withdrawal, offers a considerable base of geologic and engineering experience relevant to carbon dioxide injection and sequestration.

Depleted Oil and Gas Fields. Depleted oil and gas fields provide some of the largest, geographically diverse value-added geologic sinks. The "value-added" is from the additional production of oil (and possibly natural gas) which would help defray some of the costs associated with carbon dioxide transportation and injection.

A recent study by Advanced Resources Int. for the International Energy Agency's Greenhouse Gas R&D Programme and the Department of Energy assessed the potential for sequestering CO_2 in depleted oil and gas fields (Stevens, Kuuskraa and Taber, 1999). This study established that 98 billion metric tons (Bt) of CO_2 (27 Btc) storage capacity exists in the U.S. with 923 Bt of CO_2 (252 Btc) storage capacity worldwide, Table 1.

Currently, an estimated 30 million metric tons (MMt) of CO_2 (8 MMtc) is injected annually into oil fields as part of enhanced oil recovery, including 6 MMt of CO_2 (2MMtc) of high purity anthropogenic waste CO_2 from gas processing, fertilizer and coal gasification plants. One of the most visible new international field projects is in the Weyburn oil field, Saskatchewan, Canada where vented CO_2 from the Dakota Gasification Plant in North Dakota is transported by a 300 kilometer pipeline to the field site. A total of 20 MMt of CO_2 (6 MMtc) will ultimately be sequestered at Weyburn.

Deep Coal Seams. Deep, unminable coal seams offer a second set of geologic sinks for sequestering carbon dioxide. As in oil fields, the injection of carbon dioxide can lead to enhanced recovery of methane from these coal seams, providing a second value-added storage site. An update to an earlier study by Advanced Resources Int. (Stevens and Kuuskraa, 1998) shows that deep coals have 52 Bt of CO_2 (15 Btc) storage capacity in the U.S. with 220 Bt of CO_2 (60 Btc) of storage capacity worldwide, Table 2.

Currently, a field scale demonstration pilot involving injection of carbon dioxide into coals for enhanced coalbed methane recovery is underway in the deep Fruitland Formation of the San Juan Basin. Burlington Resources, the operator of the demonstration pilot, is injecting approximately 70 thousand metric tons of CO_2 annually into the deep coal formation with promising results. A second, smaller enhanced coalbed methane R&D project involving CO_2 injection is being conducted by the Alberta Research Council in Canada, and a new, field based ECBM effort is being launched in the San Juan Basin involving Advanced Resources, BP and Burlington Resources.

Gas Shales. Organically rich gas bearing shales, such as the Devonian shales in the Appalachian Basin, also provide an opportunity to store carbon dioxide while enhancing the recovery of gas from shales (EGSR). While substantial basic information and R&D are required to better understand the value-added opportunity, the carbon storage capacity of gas shales may approach that of deep coal seams.

Saline Formations. The largest but least defined of the geologic sinks occur in deep saline formations. Such formations are broadly distributed across the US and much of the world. While these sinks offer no value-added products, they have the advantage of being in close geographic proximity to CO_2 emission sources. The estimated carbon dioxide storage capacities for saline formations are large, though still to be defined, in the U.S. and several thousand billion tonnes worldwide.

An innovative test of CO_2 storage in saline formations is underway at Sleipner Field in the middle of the North Sea. Approximately 1 million metric tons of CO_2 is being injected annually into the saline Utsira Formation at Sleipner, with 2.5 million metric tons having been injected to date.

Summary. The currently defined storage capacity in geologic sinks is large, sufficient for many hundreds of years of carbon sequestration. Moreover, as these sinks are further assessed for maximizing carbon dioxide storage, these capacities will undoubtedly increase. The next major challenges for geological storage are to: (1) understanding the requirements and costs of adapting these sites for long term storage of carbon dioxide; (2) ensuring that the carbon dioxide will be stored in a safe and environmentally sound manner; and, (3) establishing the appropriate monitoring and verification systems for the broad geologic spectrum of storage options.

Current Status and Future Directions. Currently, the highest priority research activities for geologic sequestration are those which can help resolve technical, economic and environmental uncertainties that would enable CO_2 sequestration using enhanced oil and coal bed methane recovery to move forward to large-scale deployment. Major emphasis will be placed on developing acceptable monitoring and verification processes. As additional funding becomes available, research will begin to address value-added CO_2 storage options, such as gas-bearing shales and other gas reservoirs, and sequestration in deep saline formations.

For the longer term, we will seek to explore more challenging scientific frontiers. One area is to determine whether the emerging knowledge base about biogenic methane, produced by the reduction of CO_2, can lead to commercially viable processes for the conversion of man-made CO_2 to methane at sites specifically designed for that purpose. If economically viable concepts can be developed in this area, this could provide a pathway to a sustainable "methane economy".

The U.S. Congress has appropriated $19 million of R&D funds for fiscal year 2001, which started on October 1, 2000. R&D funding required to maintain the schedule of the 15-year plan, outlined in Table 2, is $40 million in 2002. The program is also exploring funding opportunities to expand technology deployment of carbon sequestration in cooperation with industry and developing nations.

In the coming years, the program will be seeking to expand its partnerships. In May 2001, the program is sponsoring the First National Carbon Sequestration Conference, in Washington, D.C. The conference theme is "Progress Through Partnerships" and will cover all aspects of sequestration. As the recently funded partnership projects get underway, the program will be exploring opportunities to expand collaborative R&D in cooperation with industrial partners, using these projects as "host-sites" for expanded international cooperation in a manner similar to what is occurring with the Sleipner Saline Formation CO_2 Storage (SACS) Joint Industry Program (JIP) in the North Sea.
We also look forward to expanding our existing cooperative efforts with the European Commission, Canada and Australia, including the GEODISC Consortia, and to building new "Partnerships For Progress".

If you are interested in working with the Carbon Sequestration Program, please visit the DOE or NETL website or establish contact with the persons listed below.

DOE Carbon Sequestration Page @
http://www.fe.doe.gov/coal_power/sequestration/index.html
NETL Carbon Sequestration Page @ http://www.netl.doe.gov/technologies

Chuck Schmidt
National Energy Technology Laboratory
Office of Fossil Energy
(412) 386-6090 or
Schmidt@netl.doe.gov

David Beecy
Office of Environmental Systems
Office of Fossil Energy
(301) 903-2786 or
david.beecy@hq.doe.gov

References

Beecy, D., Kuuskraa, V., et al, "The Economic Benefits of Carbon Capture And Sequestration R&D Under Uncertainty" presented at the Fifth International Conference on Greenhouse Gas Control Technologies, August 2000.

Beecy, D., Ferrell, F., et al, "The Potential Role of Geologic Storage and Carbon Dioxide In A Sustainable Fossil Fuels Future", presented at the National Meeting of the American Chemical Society, August 2000

Carbon Sequestration: Overview and Summary of Program Plans, U.S. DOE FE and NETL, April 2000

Herzog, H., Drake, E., Adams, E., CO2 Capture, Reuse, and Storage Technologies for Mitigating Global Climate Change – A White Paper, January, 1997

Stevens, S., Kuuskraa, V., "Enhanced Coalbed Methane Recovery: Worldwide Application and CO_2 Sequestration Potential", Report prepared for IEA Greenhouse Gas R&D Programme, 1998

Stevens, S., Kuuskraa, V., Taber, J., "CO_2 Sequestration in Depleted Oil and Natural Gas Fields", IEA Greenhouse Gas R&D Programme, 1999

Table 1. Capacities of Geologic Sinks				
	U.S.		Worldwide	
	CO_2 (Bt)	Carbon (Bt)	CO_2 (Bt)	Carbon (Bt)
Depleted Oil and Gas Fields	98	27	923	252
Deep Coals	52	15	220	60
Gas Shales	equal to coal?		TBD	TBD
Saline Formations	large	large	very large	very large

Table 2. 15-year Resource Requirements for the Carbon Sequestration Program (millions of 1999 U.S. dollars)															
2000	2001	2002	2003	2004	2005	2006	2007	2008	2009	2010	2011	2012	2013	2014	2015
9.2	19.5	40	57	63	73	75	80	85	80	75	70	60	50	45	40

Sequestration of Carbon Dioxide in Coal Seams

K. Schroeder (schroede@netl.doe.gov; 412.386.5910)
U.S. Department of Energy
National Energy Technology Laboratory
P.O. Box 10940
Pittsburgh, PA 15236

E. Ozdemir (ekost4+@pitt.edu; 412.624.9656)
B.I. Morsi (morsi@engrng.pitt.edu; 412.624.9650)
University of Pittsburgh
Chemical & Petroleum Engineering Department
1244 Benedum Hall
Pittsburgh, PA 15261

Introduction

The sequestration of CO_2 in coal seams is seen as a possible way to mitigate the rising atmospheric concentrations of CO_2 (Reichle et al. 1999). Technologies that have been developed for enhanced oil recovery and enhanced coal bed methane recovery could be applied to the long-term disposal of CO_2. In order to determine which, if any, coal seams would be good disposal sites and under what environmental conditions the sequestered CO_2 would remain stable, a better understanding is needed of the chemistry of the coal-CO_2 (or combustion gas) system(s). Among the R&D priorities for coal seam sequestration listed in the Reichle report are: adsorption/desorption of CO_2, interaction with SO_x and NO_x and coal swelling behavior caused by CO_2 adsorption (Reichle et al. 1999). Studies in these and related areas will help define the CO_2 trapping mechanisms.

One of the earliest studies of the adsorption of CO_2 on coal used the BET equation to calculate the CO_2 surface areas of anthracites (Walker and Geller 1956). That the diffusion of CO_2 through coals of various ranks is an activated process was established not long afterward (Nandi and Walker 1965). Despite of the fact that these, and many studies since then, have been performed at low pressure and often at low temperature in order to investigate the surface area of the coal (Mahajan 1991, and references therein), they have provided information which is relevant to today's sequestration projects. The large CO_2 adsorption capacities of coals and the CO_2-induced swelling of coals are two properties that were documented early (Mahajan 1991). The adsorption of CO_2 and other gases, especially methane, has also been studied in efforts to increase the safety of coal mining. In this regard, it has long been recognized that, although the gas in coal seams can exist as free gas in cracks and fractures, most of the gas in coal is adsorbed on the internal surface of the micropores (Kim and Kissell 1986). More recently, CO_2 adsorption on coal has been studied as a means of enhancing the gas production in coal bed methane recovery projects. Amoco has studied the adsorption of nitrogen, methane, carbon dioxide, and their mixtures to provide data for the modeling of gas recovery from coal bed methane reservoirs (Chaback et al. 1996, DeGance et al. 1993). Burlington Resources, the largest producer of coal-bed methane, has been injecting CO_2 to enhance methane production since 1996 (Stevens et al. 1998). Thus, there is at

present a large body of scientific studies and practical information to lend credence to the coal-seam sequestration scenario.

The Problem

The extent to which coal can adsorb CO_2 is affected by a number of factors. The nature of the coal will determine the maximum adsorption capacity under a given set of conditions, but the sequestration environment will determine the extent to which that ultimate capacity will be realized. The effect of both physical and chemical changes need to be understood. Parameters such as temperature, pressure, and pH might be expected to have a moderate to large influence; salinity might be expected to be less important.

Coal contains a wide variety of organic and mineral phases in a complex, porous, 3-dimensional network which varies from one coal deposit to another and from one location to another within the same seam. The organic portion of the coal is thought to capture CO_2 via surface adsorption, pore filling, and solid solution (Larsen et al. 1995). Less recognized is the possibility that the mineral phases present in the coal may assist via mineral carbonate formation. Thus, the nature of the coal seam itself is an important variable to be considered.

In the absence of external influences, underground temperatures tend to be constant over time but increase with depth. The adsorption of CO_2 is exothermic (Starzewski and Grillet 1989) and will provide a heat source, at least during the active pumping phase of sequestration. Also, some sequestration scenarios would provide additional heating mechanisms such as by the dissolution of co-sequestered acidic gases (SO_x, NO_x) or by reaction with residual oxygen in the combustion gas. Thus, it is important to know how temperature will affect the CO_2 adsorption onto the coal and whether the magnitude of this effect is universal for all coals or is rank or maceral dependent.

Even if initially dry, the seam will certainly become wet as a result of drilling operations, fracturing of the coal bed and over-lying strata, and the deposition of a combustion gas which may contain residual water of combustion. Thus, an aqueous phase will be present and will vary in composition according to its source and the nature of the coal bed and the surrounding minerals with which it is in contact. In natural systems, pH is often an important parameter (Stumm and Morgan 1996) and it will change during sequestration. Because of the formation of carbonic acid, the pH within the sequestration media will drop to around 3 at high CO_2 pressures, favoring the dissolution of calcite. This may be beneficial if mineral dissolution provides better access to the organic matrix, but would be detrimental if dissolution of cap-rock resulted. The effect of the sequestration on pH would be more dramatic for those scenarios in which the SO_x and NO_x were not removed by prior separation and are sequestered along with the CO_2. Little is known about the potential effect of such a pH change on the ability of the organic matrix to adsorb CO_2. It is well recognized that adsorption of on solid surfaces is affected by the pH of the surrounding media (Stumm and Morgan 1996). Solids in contact with solutions with a pH above their isoelectric point acquire a net negative surface charge; those in contact with solutions with a pH below their isoelectric point acquire a net positive surface charge. The extent to which pH changes will affect the CO_2 adsorption capacity of coals has not been investigated.

Depending on the capture technology, the CO_2 stream may be nearly pure CO_2, raw combustion gas, or something in between. In addition, gases such as hydrogen, methane, ethane, and higher hydrocarbons may be present in the coal seam (Kim and Kissell 1986) and act to inhibit or enhance the CO_2 sequestration. In the case of a gassy coal seam, it may be advantageous to displace and capture the

methane as a profit-making part of the operation. This displacement may be enhanced by secondary combustion gases in the CO_2 such as SO_x and NO_x.

The composition of the post sequestration gas and liquid phases may change with time. Even slow reactions can become important over geologic-sequestration time scales. Also, microbes have an uncanny ability to adapt to many environments and are known to populate even deep geologic strata, at least to 9000 feet below the surface (Amy and Haldeman 1997). Under oxic conditions, gases such as SO_x, NO_x, and CO may be produced either chemically or biologically. Under anoxic conditions, methane and H_2S may be produced by anaerobic microbes. These gases may displace CO_2 and thus limit the durability of the sequestration.

Knowledge of the extent to which coals can adsorb CO_2 under a variety of conditions is necessary to evaluate the long-term storage capacity of candidate seams. The nature of the coal will determine its maximum adsorption capacity, but the dynamic nature of the sequestration environment will determine the extent to which that capacity can be realized. In order to evaluate the long-term storage capacity of a coal seam, possible changes in the sequestration environment need to be anticipated and their effect understood.

Approach

In this paper, the interaction of one of the Argonne Premium Coal Samples with CO_2 is studied under a variety of conditions. Argonne samples, which include a representative sample of every rank, are among the most widely studied coals in the world. Because of this, there exists a vast database of measurements and studies which can aid in the interpretation of results (Vorres 1993). Our approach is to investigate the effect of various parameters such as pressure, temperature, pH, and salinity on the adsorption isotherms of these coals. Herein, the effects of temperature, pressure, and pH on the CO_2 adsorption capacity of one of these samples, the Upper Freeport coal, are described.

Project Description

Gas-phase carbon dioxide adsorption isotherms were obtained using a manometric technique (Nodzenski 1998). In the set of experiments described here, the temperature and pressure were maintained at values below the critical temperature and pressure of carbon dioxide, and the temperature was held above the condensation temperature, thereby maintaining gas-phase conditions.

The manometric apparatus consists of a reference cell of known volume from which all gas transfers were made, and a sample cell, also of known volume. The reference cell, contained within a temperature-controlled bath ($\pm$ 0.1 ºC), was pressurized to the desired level as indicated on a pressure transducer. The maximum pressure for any given isotherm was limited by the operating temperature and the condensation pressure of carbon dioxide at that temperature. A sample cell of known void volume, which was also placed within the same bath, was pressurized from the reference cell. Using the change in pressure in the reference cell and accounting for the gas compressibility, the number of moles of gas transferred from the reference cell was calculated. Similarly, the number of gas-phase moles in the sample cell after the gas transfer was calculated from the post-transfer sample-cell pressure. The missing moles of gas were accounted to the adsorption of CO_2 onto (into) the coal. The reference cell was then pressurized to a higher pressure and the process was repeated. The individual incremental gas adsorption values (dn) were summed to generate the adsorption isotherm in a step-wise fashion. The adsorption isotherm for a given

temperature was plotted as the total number of millimoles of carbon dioxide adsorbed per gram of coal (y-axis) versus the equilibrium sample-cell pressure (x-axis). This method of isotherm construction is shown graphically in Figure 1. The incremental number of moles adsorbed for each pressure change (dn) are shown as the triangles. These increments slowly decrease as higher pressures are attained. The total moles adsorbed (n) are obtained by summing the individual increments and are shown as the circles in Figure 1.

In the experiments investigating the effect of temperature, after completing the experiment at one temperature, the sample was depressurized and evacuated overnight at 22°C. The temperature of the bath was then raised and the process was repeated. From the temperature dependence of the adsorption isotherms, the isosteric heat of adsorption, $Q_{isosteric}$, was calculated from the modified Clausius-Clapeyron equation (Daniels et al. 1962).

$$\ln (P_2/P_1) = Q_{isosteric} (T_2-T_1) / RT_1T_2$$

Because coals rapidly and irreversibly adsorb atmospheric oxygen (Schmidt 1945), efforts were devoted to maintaining an oxygen-free environment. The precautions taken during the collection, processing and packaging of the Argonne samples (Vorres 1993) and our efforts to maintain an oxygen-free environment ensured that the measured coal properties reflect the activity of the virgin coal as closely as possible under laboratory conditions. Vials of the Argonne Premium coal were opened in accordance with the provided mixing instructions. Vials were opened and all operations were performed in an inert-gas flushed glove bag under a positive pressure of nitrogen gas. Aqueous solutions, when used, were prepared from de-ionized water which had been sparged with and stored under inert gas to remove dissolved oxygen. Coal samples were removed from the glove bag only after they had been placed in the sample cell and capped.

The effect of pH was investigated by pre-treating the coal in aqueous slurries to pH values of 2.4, 6.2, and 12. All procedures were performed in a nitrogen-flushed glove bag. The pH value of 2.4 was achieved by the slow addition of 3.1mM H_2SO_4 to the coal-water slurry. The pH of 12 was achieved in a similar fashion using 10 mM NaOH. The value of 6.2 represents the solution pH resulting from the simple mixing of only the coal and water. The coals were filtered and dried overnight in a vacuum oven at 60°C prior to being loaded into the sample cells.

Results

Effect of Temperature

The temperature dependence of the carbon dioxide adsorption isotherms for the Argonne Premium Upper Freeport Coal is shown in Figure 2. The isotherms obtained for the three lower temperatures were self-consistent and the entire range of data is plotted. At the highest temperature (55°C), the extent of adsorption at pressures above 300 psia continued to increase linearly and, at 700 psia, had surpassed the extent of adsorption observed at the lower temperatures. While this may indicate a physical change in the coal at the highest temperature, the reproducibility of this result needs to be confirmed and so this portion

of the isotherm is not depicted in Figure 2. Within the pressure-temperature range shown in Figure 2, the carbon dioxide adsorption isotherms appear to be non-Langmuir. They fail to approach a limiting value at high pressures as would be predicted by the Langmuir equation. Instead, the amount of carbon dioxide adsorbed becomes nearly linear in the higher pressure region. It should be mentioned that the critical temperature and pressure of carbon dioxide are about 31 C and 1070 psia, respectively (Weast 1979). At temperatures below the critical temperature, increasing pressure will ultimately result in condensation of the carbon dioxide and the apparent amount of "adsorbed" CO^2 would rapidly increase. At temperatures and pressures above the critical point, CO^2 exists as a supercritical fluid. The conditions of the experiments depicted in Figure 2, lie in the gas phase region of the CO^2 phase diagram.

The incremental amount of carbon dioxide that can be adsorbed by the coal drops off dramatically at higher pressures. For example, the amount of carbon dioxide adsorbed during the application of the first 100 psi of CO^2 pressure (0-100 psia) amounts to 0.6 to 0.9 mmole per gram of coal, depending on the temperature. However, the additional amount of CO^2 adsorbed during the addition of the last 100 psi of CO^2 pressure (600-700 psi) amounts to less than an additional 0.1 mmole per gram. From a practical stand-point, this means that disproportionately higher pumping costs per pound of CO^2 will be incurred at higher sequestration pressures.

In the pressure-temperature region studied, the CO^2 capacity of the coal did not exceed 1.4 mmole CO^2 /g coal. This adsorption value corresponds to a CO^2 storage density of about 85 kg CO^2 /m coal. For comparison, the density of liquid phase CO^2 is 600 kg/m (at 30 C).

The effect of increasing temperature is to decrease the equilibrium adsorption capacity of the coal. This is expected because higher temperatures increasingly favor the gas-phase due to the $T\Delta S$ entropy term in the free energy expression. This means that otherwise equivalent, but deeper, warmer seams will adsorb less CO^2 at a given pressure than shallower, cooler ones.

The average isosteric heat of adsorption was calculated to be 4.85 ± 0.26 kcal per mole of CO^2 adsorbed (20.3 ± 1.1 kJ/mole). This is higher than the heat of vaporization of CO^2 in this temperature range which is only about 1.3 kcal/mol, even at the lowest temperature. However, this value is lower than the 12 kcal/mol (50 kJ/mol) value measured via calorimetry, albeit at very low coverage (Starzewski and Grillet, 1989). Nodzenski (1998) found a range from 6 to 14 kcal/mol (26-59 kJ/mol) for a selection of hard coals. Coal contains a wide variety of adsorption sites. Thermodynamics would suggest that the most active sites would be occupied first and provide the greatest heat of adsorption. Thus, it is to be expected that the heat evolved per mole of CO^2 at low coverage would be higher than the heat evolved at high coverage. We find that the strength of the average, high-coverage, interaction is about the same as for a hydrogen bond, about 5 kcal/mol. This is in qualitative agreement with results that have related the CO^2 adsorption capacity to oxygen functionality (Nishino 2001). Thus, it appears that the binding energy found here falls between simple condensation and the higher energy adsorption onto the more active sites.

The change in the heat of adsorption with increasing extent of adsorption is shown in Figure 3. The slight drift to higher heat values at coverages below 1 mmole/gram amounts to less than ½ kcal/mole. This may reflect small changes resulting from fresh adsorption sites being made available during coal swelling. Coals swell upon exposure to CO^2 and the extent of expansion increases with increasing CO pressure (Reucroft and Patel 1986, Reucroft and Sethuraman 1987). However, the application of an external load limits the extent of coal swelling (Walker et al. 1988) so its practical influence on coal-seam sequestration may be limited by the over-burden pressure. The sharp decrease in the heat of adsorption at coverages above 1.2 mmole/gram may be due to the saturation of more reactive adsorption sites on the coal.

Effect of pH

The effect of pH on the chemistry of aqueous CO_2 is well known (Stumm and Morgan 1996). At a pH of 9, dissolved CO_2 exists as the carbonate ion and mineral carbonates are stable. At a pH of 2, mineral carbonates dissolve, the CO_2 that can remain dissolved exists as H_2CO_3 and $CO_{2(aq)}$, and $CO_{2(gas)}$ is produced. The pH of an aqueous solution also affects the surface of a material it is in contact with. In the case of coal, at the higher pH value, the carbonaceous surface, being in an environment above its isoelectric point, assumes a net negative charge. At the lower pH value, the carbonaceous surface assumes a net positive charge. While a pH of 9 will favor, and a pH of 2 disfavor, the aqueous capture of CO_2, the effect of being above, or below, the carbonaceous isoelectric point is not so obvious. An example of the importance of aqueous parameters to coal-gas interactions can be seen in the case of the coal floatation process where not only pH but also salinity is important for bubble attachment (Li and Somasundaran 1993). Because of the potential importance of pH, we have studied its effect on the ability of the organic matrix to adsorb CO_2 in the absence of the aqueous phase as a confounding factor.

The effect of the coal surface pH was investigated by pre-soaking the coal using aqueous slurries at pH values of 2.4, 6.2, and 12. The coals were filtered and dried overnight in a vacuum oven at 60°C prior to being loaded into the sample cells. These three samples were then compared to each other and to an untreated aliquot of the same coal which had not been oven dried. The effect of these treatments on the CO_2 adsorption capacity of the coal is shown in Figure 4. Note that the coal weights have been adjusted to a dry, ash-free (daf) basis to account for the different levels of mineral matter and moisture in the original sample and these laboratory-generated samples.

The major difference observed is the lower extent of adsorption for those samples that were treated, regardless of treatment. Because these samples were all oven dried whereas the virgin sample was not, the assumption that such mild drying would not affect the results may not be valid. Moisture removal is know to affect the porosity and transport properties of coals, especially lignite and subbituminous coals, but the effects are usually mild for higher rank coals when the drying temperature is below 100°C (Suuberg et al. 1993). Yet, this trend is opposite to that found for the methane adsorption capacity which increased when the moisture was removed from the coal pores by drying (Joubert et al. 1974). Because of the uncertain effect of the drying, it is reasonable to limit the discussion of pH effects to the three treated samples.

As seen in Figure 4, both acid treatment to a pH of 2.4 and a base treatment to a pH of 12 result in an increase in adsorption capacity compared to the coal treated with only de-ionized water. The Upper Freeport coal has a low-temperature ash content of 15%, which includes acid soluble minerals such as calcite (Vorres 1993). The proximate analysis of the acid-washed coal showed an ash reduction from 13.0% to 11.8%. If removal of acid-soluble minerals resulted in increased accessible pore volume, then increased CO_2 capacity would be expected. The ash content of the base treated coal was reduced by only 0.2%. In this case it seems more likely that any increase in capacity would be due to surface-adsorbed NaOH. If water is also present, alkali metal hydroxides react with CO_2 to form carbonates. Whatever the mechanism, the acid treatment appears to have a greater effect than the base or neutral treatments in these initial experiments.

Application

Adsorption isotherms and related information are needed for effective CO_2 sequestration modeling. For example, parameters such as the heat and rate of CO_2 adsorption, the heat capacities of the coal seam components, and the thermal conductivity of the surrounding media must be known or estimated in order to calculate coal-bed temperature rises for various pumping scenarios. As shown in this work (Figure 2), the temperature dependence of the adsorption isotherms can seriously affect the sequestration capacity. Incompletely filled coal seams, or time wasted while waiting for a seam to cool, eventually affects the cost of the sequestration. Similarly, the estimated cost of alternative sequestration scenarios, such as co-sequestration of acid gases, need to take into account changes in the sequestration chemistry, such as increased pore capacity due to mineral dissolution or other surface changes.

Future Activities

In addition to completing the experiments discussed above, a task devoted to the study of these interactions using techniques adopted from inverse chromatography (IC) will be pursued. One of the major advantages of IC is the ability to generate the entire adsorption and desorption isotherm from a single experiment. The application of IC to physicochemical research is well established (Paryjczak 1975) and has been implemented in both gas chromatography (GC) and high pressure liquid chromatography (HPLC). Here, we will be employing conditions appropriate to supercritical fluid chromatography (SFC) as well. In the IC experiment, properties of the solid, stationary phase are investigated using known solutes (probes), as opposed to the typical chromatography experiment in which a known stationary phase is used to study an unknown gas mixture. Techniques including frontal analysis, displacement chromatography, elution-on-a-plateau, thermo-desorption, and pulse injection can be used to obtain physicochemical measurements such as the extent of irreversible adsorption, adsorption isotherms, and energies of interactions. Some techniques, such as those that require linear chromatography conditions, may not be possible under the conditions we wish to explore for geologic sequestration, whereas others, such as elution-on-a-plateau, seem directly applicable.

References

Amy P. and Haldeman D.L. (1997) *The Microbiology of the Terrestrial Deep Subsurface*. CRC Press, New York.

Chaback J.J., Morgan W.D., Yee D. (1996) Sorption of nitrogen, methane, carbon dioxide and their mixtures on bituminous coals at in-situ conditions. *Fluid Phase Equilibria* ***117*** , 289-296.

DeGance A.E., Morgan W.D., Yee D. (1993) High pressure adsorption of methane, nitrogen and carbon dioxide on coal substrates. *Fluid Phase Equilibria* ***82*** , 215-224.

Daniels F., Williams J.W., Bender P., Alberty R.A., Cornwell C.D. (1962) *Experimental Physical Chemistry*. McGraw-Hill Book Co., Inc., New York.

Joubert J.I., Grein C.T., Beinstock D. (1974) Effect of moisture on the methane capacity of American coals. *Fuel*, ***9***, 186-191.

Kim A.G. and Kissell F.N. (1986) Methane formation and migration in coalbeds. In, *Methane control research: summary of results, 1964-80. U.S. Dept. of the Interior, Bureau of Mines Bulletin/1988, Bulletin 687,* Deul M. and Kim A.G (eds.) Chapter 3, pp. 18-25.

Larsen J.W., Hall P., Wernett P.C. (1995) Pore structure of the Argonne premium coals. *Energy & Fuels **9**,* 324-330.

Li C. and Somasundaran P. (1993) Role of electrical double layer forces and hydrophobicity in coal floatation in NaCl solutions. *Energy & Fuels **7**,* 244-248.

Mahajan O.P. (1991) CO_2 surface area of coals: the 25-year paradox. *Carbon **29**,* 735-742.

Nandi S.P. and Walker, Jr. P.L. (1965) The diffusion of nitrogen and carbon dioxide from coals of various rank. *Fuel **44**,* 385-393.

Nishino J. (2001) Adsorption of water vapor and carbon dioxide at carboxylic functional groups on the surface of coal. *Fuel **80**,* 757-764.

Nodzenski A. (1998) Sorption and desorption of gases (CH_4 ,CO_2) on hard coal and active carbon at elevated pressures. *Fuel **77,*** 1243-1246.

Paryjczak T. (1975) *Gas Chromatography in Adsorption and Catalysis*. John Wiley & Sons, New York.

Reichle D. Houghton J., Kane B., Ekmann J., Benson S., Clarke J., Dahlman R., Hendry G., Herzog H., Hunter-Cevera J., Jacobs G., Judkins R., Ogden J., Palmisano A., Socolow R.,Stringer J., Surles T., Wolsky A., Woodward N., York M. (1999) Carbon Sequestration Research and Development, *U.S. Department of Energy Report DOE/SC/FE-1*. Available at www.ornl.gov/carbon_sequestration/

Reucroft P.J. and Patel H. (1986) Gas-induced swelling in coal. *Fuel **65**,* 816-820.

Reucroft P.J. and Sethuraman A.R. (1987) Effect of pressure on carbon dioxide induced coal swelling. *Energy & Fuels **1**,* 72-75.

Schmidt L.D. (1945) Changes in coal during storage. In: *Chemistry of Coal Utilization*, H.H. Lowry (Ed.), Chapter 18, pp. 627-676.

Starzewski P. and Grillet Y. (1989) Thermochemical studies of adsorption of He and CO_2 on coals at ambient temperature. *Fuel* **68,** 375-379.

Stevens S.H., Kuuskraa V.A., Spector D., Riemer P. (1998) CO_2 Sequestration in Deep Coal Seams: Pilot Results and Worldwide Potential. Paper presented at GHGT-4 in Interlaken, Switzerland, 30 Aug. - 2 Sep. 1998. Available at: http://www.ieagreen.org.uk/pwrghgt4.htm

Stumm W. and Morgan J.J.(1996) *Aquatic Chemistry: Chemical Equilibria and Their Rates in Natural Waters.* John Wiley & Sons, New York.

Suuberg E.M., Otake Y., Yun Y., Deevi, S.C. (1993) Role of moisture in coal structure and the effects of drying upon the accessibility of coal structure. *Energy & Fuels **7**,* 384-392.

Vorres K.S. (1993) Users Handbook for the Argonne Premium Coal Sample Program. *ANL/PCSP-93/1*, Argonne National Laboratory.

Walker, Jun. P.L. and Geller I. (1956) Change in surface area of anthracite on heat treatment. *Nature **178**,* 1001.

Walker, Jr. P.L., Verma S.K., Rivera-Utrilla J. (1988) A direct measurement of expansion in coals and macerals induced by carbon dioxide and methanol. *Fuel **67**,* 719-726.

Weast R.C. (1979) *Handbook of Chemistry and Physics*. CRC Press, Inc., Boca Raton, Fl.

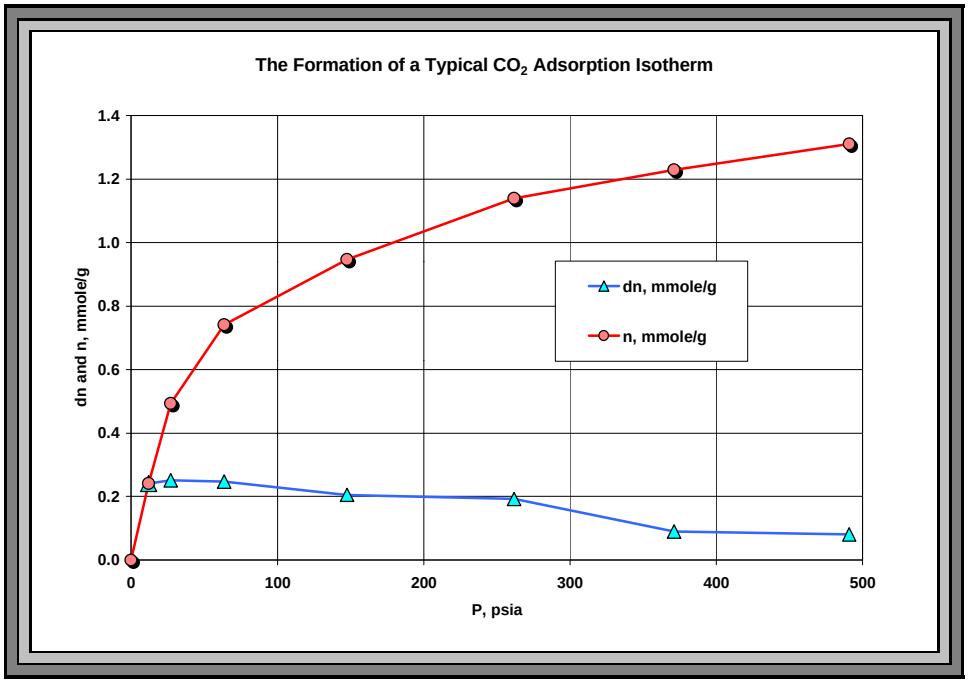

Figure 1. Formation of the Adsorption Isotherm by Summing the Incremental Moles Adsorbed

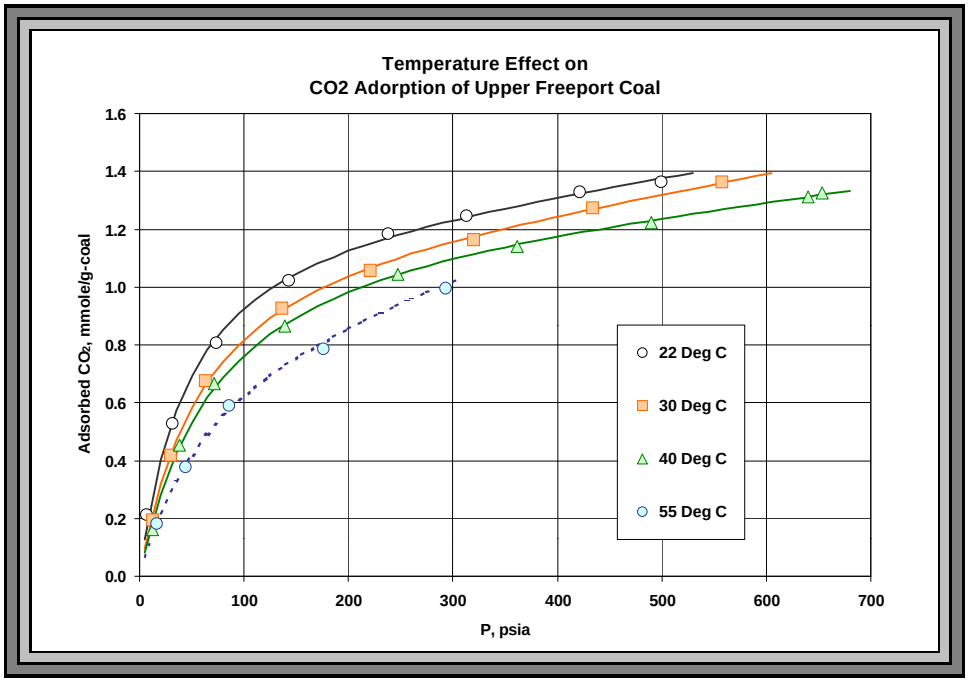

Figure 2. Effect of Increasing Temperature on the Upper Freeport Adsorption Isotherm.

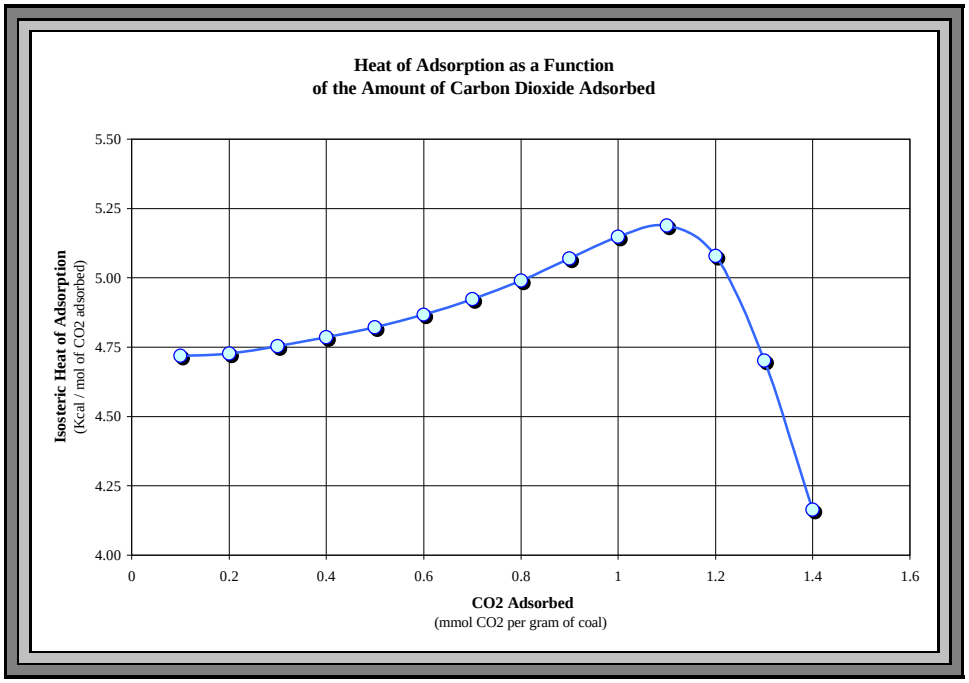

Figure 3. Change in the Isosteric Heat of Adsorption of CO_2 as a Function of Coverage.

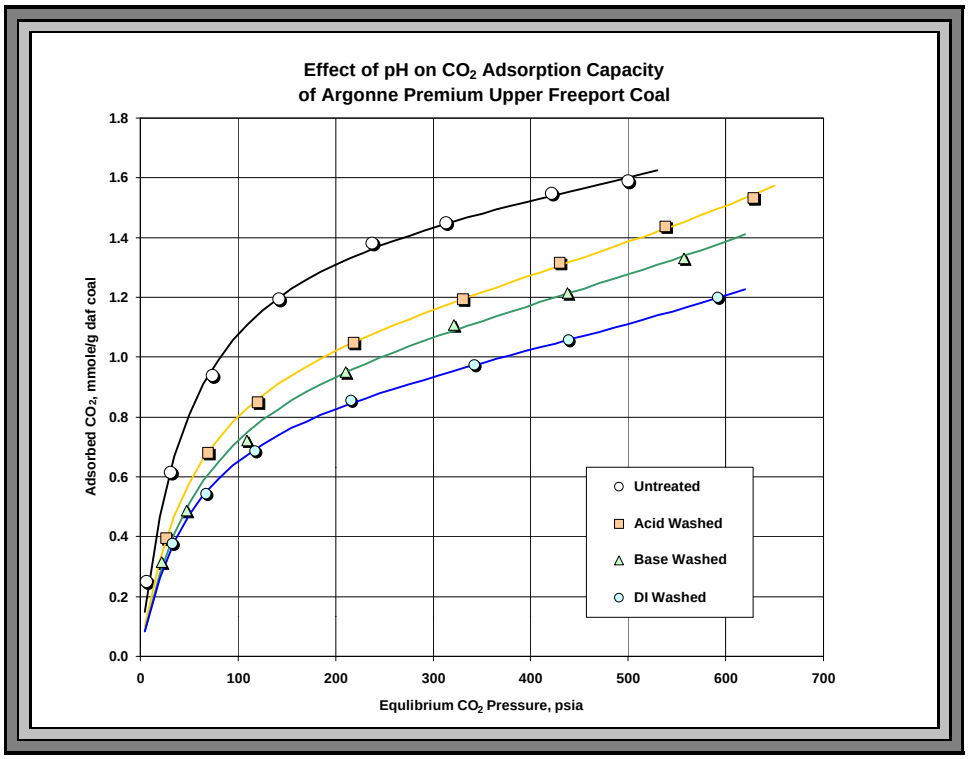

Figure 4. Effect of Prior Treatment on the Adsorption Isotherm of Upper Freeport Coal.

Sequestration of CO_2 in a Depleted Oil Reservoir: An Overview

H. Westrich (hrwestr@sandia.gov; 505-844-9092)
J. Lorenz (jcloren@sandia.gov; 505-3695)
S. Cooper (spcoope@sandia.gov; 505-844-3977)
C. Jove Colon (cfjovec@sandia.gov; 505-284-5494)
N. Warpinski (nwarpi@sandia.gov; 505-844-3640)
Geoscience and Environment Center
Sandia National Laboratories
Albuquerque, NM 87185-0750

D. Zhang (dongzhang@lanl.gov; 505-667-3541)
C. Bradley (cbradley@lanl.gov; 505-665-6713)
P. Lichtner (lichtner@lanl.gov; 505-667-3420)
R. Pawar (rajesh@lanl.gov; 505-665-6929)
Earth & Environmental Sciences Division
Los Alamos National Laboratory
Los Alamos, NM 87545

Bruce Stubbs (pecos@lookingglass.net; 505-624-2800)
Pecos Petroleum Engineering, Inc.
Roswell, NM 88202

R. Grigg (reid@baervan.nmt.edu; 505-835-5403)
R. Svec (bsvec@prrc.nmt.edu; 505-835-6142)
Petroleum Recovery Research Center
New Mexico Tech University
Socorro, NM 87801

C. Byrer (cbyrer@netl.doe.gov; 304-285-4547)
Fuel Resources Division
National Energy Technology Lab
Morgantown, WV 26507-0880

Abstract

Geologic sequestration of CO_2 in depleted oil reservoirs, while a complex issue, is thought to be a safe and effective carbon management strategy. This paper provides an overview of a NETL-sponsored R&D project to predict and monitor the migration and ultimate fate of CO_2 after being injected into a depleted oil reservoir as part of a micropilot scale field experiment. The Queen Formation sandstone, located in the West Pearl Queen field in SE NM, was identified as the CO_2 injection site for this project. Core samples of this formation were obtained for lithologic analysis and laboratory experimentation. Preliminary flow simulations were run using this data and suggest that at least 2000 tons of CO_2 can be injected into the reservoir over a period of one month. Our planned suite of computer simulations, laboratory tests, field measurements and monitoring efforts will be used to calibrate, modify and validate the modeling and simulation tools. Ultimately, the models and data will be used to predict storage capacity and physical and chemical changes in oil reservoir properties. Science or technology gaps related to engineering aspects of geologic sequestration of CO_2 also will be identified in this study.

Introduction

Carbon dioxide sequestration in geologic formations is the most direct carbon management strategy for long-term removal of CO_2 from the atmosphere, and is likely to be needed for continuation of the US fossil fuel-based economy and high standard of living. Subsurface injection of CO_2 into depleted oil reservoirs is a carbon sequestration strategy that might prove to be both cost effective and environmentally safe. Part of this confidence is due to an extensive knowledge base about site-specific reservoir properties and subsurface gas-fluid-rock processes from the mining and petroleum industries, including those from recent EOR CO_2 flooding activities (Morris, 1996). However, CO_2 sequestration in oil reservoirs is a complex issue spanning a wide range of scientific, technological, economic, safety, and regulatory concerns, requiring more focused R&D efforts to better understand its cost and consequences (DOE Offices of Science and Fossil Energy report, 1999).

Objective

Our project, "Sequestration of CO_2 in a Depleted Oil Reservoir: A Comprehensive Modeling & Site Monitoring Project," is funded by the DOE/NETL Carbon Sequestration program. One of the program's stated goals is to provide the science and technology basis to properly evaluate the safety and efficacy of long-term CO_2 sequestration in geologic formations. The specific objective of our project is to better understand CO_2 sequestration processes in a depleted oil reservoir. Because of the nature of an oil reservoir and the presence of multiple phases, CO_2 sequestration mechanisms can include hydrodynamic trapping, aqueous solubility or mineralization. Viscous fingering, gravity separation, miscible fluids, reaction kinetics, and possible leakage through fractures are but a few of the processes that also can affect geologic sequestration effectiveness. Broad project goals include computer simulations and laboratory measurements of fluid flow and reaction, as well as a field experiment in order to better understand the complex nature of geosequestration processes. The micropilot field experiment calls for injection of several thousand tons of CO_2 into a depleted oil reservoir. An ideal site for this project would be located in a geologically simple setting in porous and permeable sandstone, having a recent development and production history, and where no secondary water or enhanced CO_2 treatments have been used. These site parameters allow for simplified modeling and easier interpretations of field results. Specific R&D objectives for this project include:

- Characterization of oil reservoir and its capacity to sequester CO_2
- Prediction of multiphase fluid migration & interactions
- Development of improved remote (geophysical) monitoring techniques
- Measurement of CO_2-reservoir reactions

Approach

The West Pearl Queen field, which is owned and operated by Strata Production Company of Roswell, NM, was chosen as our field demonstration site to study geologic sequestration of CO_2. This field is located near Hobbs, New Mexico and was first developed in 1984, producing about 250,000 barrels of oil. Production has slowed in recent years as the reservoir pressure in some wells fell below levels required for profitable oil recovery. This field has not been subjected to secondary or enhanced oil recovery operations with water or CO_2. The main producing zone for this field is the Queen Formation, which is a small structural dome of arkosic sandstone about 25 feet in thickness (Figure 1). The Pearl Queen field seems to be an ideal site to study CO_2 migration and interactions after injection into a depleted oil reservoir. Injection is planned for Stivason-Federal #4 well, while other wells (Stivason-Federal #1, 3 & 5) will be used for remote monitoring.

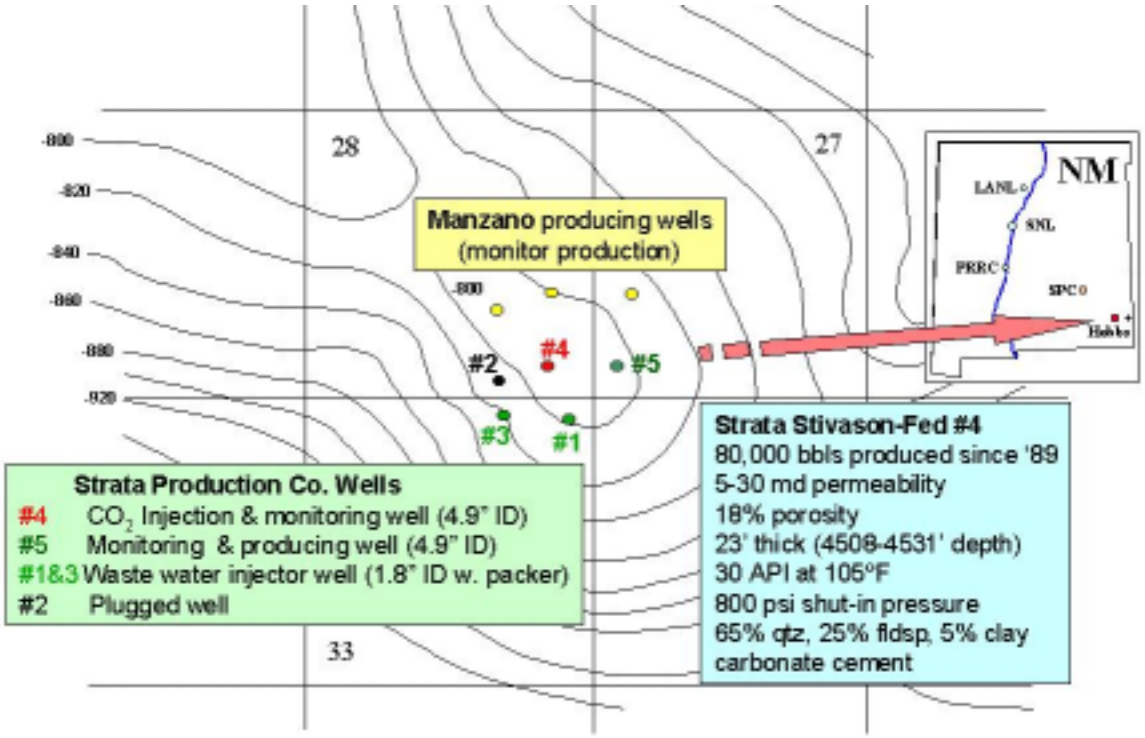

Figure 1. Location of the West Pearl Queen Field, and Structure map for top of Queen F. (20' contour interval; datum S. L.)

This project utilizes a suite of computer simulations, laboratory tests, field measurements and monitoring efforts to understand those physical and chemical processes governing geologic sequestration of CO_2 in oil reservoirs. The micropilot demonstration calls for injection of several thousand tons of CO_2 into the Queen Formation, followed by a comprehensive suite of geophysical field surveys to monitor the advance of the CO_2 plume and lab experiments to measure geochemical changes in reservoir mineralogy and permeability. Specific field and lab observations will be used to calibrate, modify and validate the modeling and simulation tools. The field demonstration, however, will be the ultimate test of our computer simulations.

Project Description

This field demonstration project has three phases: I) baseline characterization, II) CO_2 injection and soaking, and III) post-injection characterization. Phase I includes compilation of a geologic model for the depleted reservoir, evaluation of available flow and reaction simulators, well preparation, acquisition of legal permits, collection of reservoir fluids, and baseline geophysical surveys of the reservoir. Phase II of this project involves the design of the micropilot field test, preparation of surface injection facilities, refinement of computer simulation models, injection of 2000-4000 tons of CO_2 over a one month period, measurement of fluid pressure changes or plume breakthroughs and geophysical surveys of the plume. Phase III of the project includes wellhead venting of the injected CO_2, and downhole pumping of residual fluids and final geophysical surveys. Our project combines geologic, flow and reaction path modeling and simulations, injection of CO_2 into the oil-producing formation, geophysical monitoring of the advancing CO_2 plume and laboratory experiments to measure reservoir changes with CO_2 flooding. The field data will provide a unique opportunity to test, refine and calibrate the computer model(s) that will simulate those subsurface interactions. Iteration of modeling, laboratory and field data is crucial to the improvement of simulation tool methodologies.

<u>Modeling and Simulation</u>

Our ability to accurately predict the migration and fate of CO_2 in oil reservoirs is limited by inadequate reservoir characterization as well as the lack of a comprehensive simulator to model coupled chemical, hydrological, mechanical and thermal (CHMT) processes. However, existing commercial and research codes, such as ECLIPSE and FLOTRAN, are available and will be

used to simulate some of the important geoprocesses involved during CO_2 sequestration (e.g., three-phase flow and geochemical reactions). The goal of this task is to choose one or more codes that have the ability to simulate the coupled processes that occur during injection and migration of CO_2 in the depleted oil reservoir. These codes will be evaluated based on availability, cost, ease of use, robustness and flexibility to modification. With the selected code(s) and input data from a geologic model, a computer model will be built for a depleted oil reservoir, which will incorporate site-specific information and previous characterization results. This model will be used to aid in designing a micropilot field study of high-flow CO_2 injected in the depleted oil reservoir. The geologic model will integrate available data on stratigraphy and reservoir rock properties, including wireline logs, structure-contour and isopach maps, core samples from the Stivason-Federal well #1, and appropriate regional geologic data.

Geophysical Monitoring

State of the art geophysical techniques are one of the few ways to remotely characterize oil reservoir properties and changes due to injection of CO_2. Remote geophysical sensing techniques will be used prior to, during and after CO_2 injection, consisting of borehole geophysics, surface to borehole surveys, and surface reflection seismic surveys. These surveys will identify and characterize formation changes due to saturation and injection effects (Knight et. al., 1998; Withers and Batzle, 1997). The borehole geophysics will include dipole sonic logs, limited microseismic surveys during injection and multi-level, 3C crosswell seismic surveys. The surface to borehole seismic surveys will include a Vertical Seismic Profile (VSP) in which receivers are placed in the injection wellbore to detect arrivals from surface shots (e.g., Lizarralde and Swift, 1999). The 4D, 9C seismic surveys will be run before and after injection, as well as a third survey conducted after flow-back of the injected CO_2.

Field Demonstration

Our micropilot demonstration calls for injection of several thousand tons of CO_2 into the Queen Formation at a depth of about 4500 feet using the Stivason-Federal well #4 as the injection well. This reservoir is geologically simple and consists of a small structural dome of thinly bedded sandstones. Although the reservoir is pressure depleted (<3.0 MPa), it has not been subjected to secondary oil recovery treatment with water or CO_2, and is therefore an ideal site to study the effects of CO_2 injection in a depleted oil reservoir. Strata Production Company will coordinate all field preparations, surveys and injection operations.

Laboratory Tests

Mineralization is the geochemical interaction of CO_2 with sedimentary minerals to form stable and environmentally benign carbonate phases, and is a desired sequestration end stage. However, the nature and kinetics of CO_2-dominated fluid/mineral interactions is not well understood. This knowledge is essential for the prediction of carbonation reactions and the formation of carbonate minerals that will be responsible for the long-term confinement of CO_2 into the reservoir. Our project will examine static and non-static flow experiments of pure CO_2 and CO_2-H_2O mixtures interacting with plugs of Queen Formation sandstone for time periods up to 15 months at reservoir conditions (P=4.5 MPa, T=40°C). Static tests will explore the effects of fluid chemistry and flow on mineral dissolution and precipitation reactions. Non-static flow (percolation) tests will elucidate the effects of fluid-mineral interaction on rock porosity and permeability. Solid and liquid samples from these tests will be analyzed for chemical, structural and morphological changes using standard geochemical techniques. These results should provide critical information on the mechanisms and rates of CO_2-mineral interactions in a depleted oil reservoir.

Results

Geology

Approximately 30 ft of discontinuous, four-inch diameter core of the Queen Formation (Shattuck Sandstone Member) from the Stivason Federal #1 well was available for study and to develop a geologic model. This well is approximately 1200' from our injection well and its core should be representative of the reservoir. No natural fractures are present in this core, although it is not precluded for the rest of the reservoir. In general, the Shattuck Sandstone consists of irregularly bedded sandstones, siltstones, and sandy siltstones, containing irregular anhydrite beds and nodules. The sandstones are a heterogeneous mix of oxidized detrital sands and siltstones, with detrital and authigenic cements of dolomite, gypsum, anhydrite, and halite. The main reservoir lithology (lithology C in Figure 2) is a poorly cemented, oil stained sandstone exhibiting between 15-20% porosity and irregular permeabilities up to 200 millidarcies (Figure 2). The percentage of the reservoir represented by this lithology is unknown due to missing core, although about a third of the core available consists of this facies. The upper parts of the core represent the confining strata rather than the reservoir rock. The likely reservoir sandstone represents about

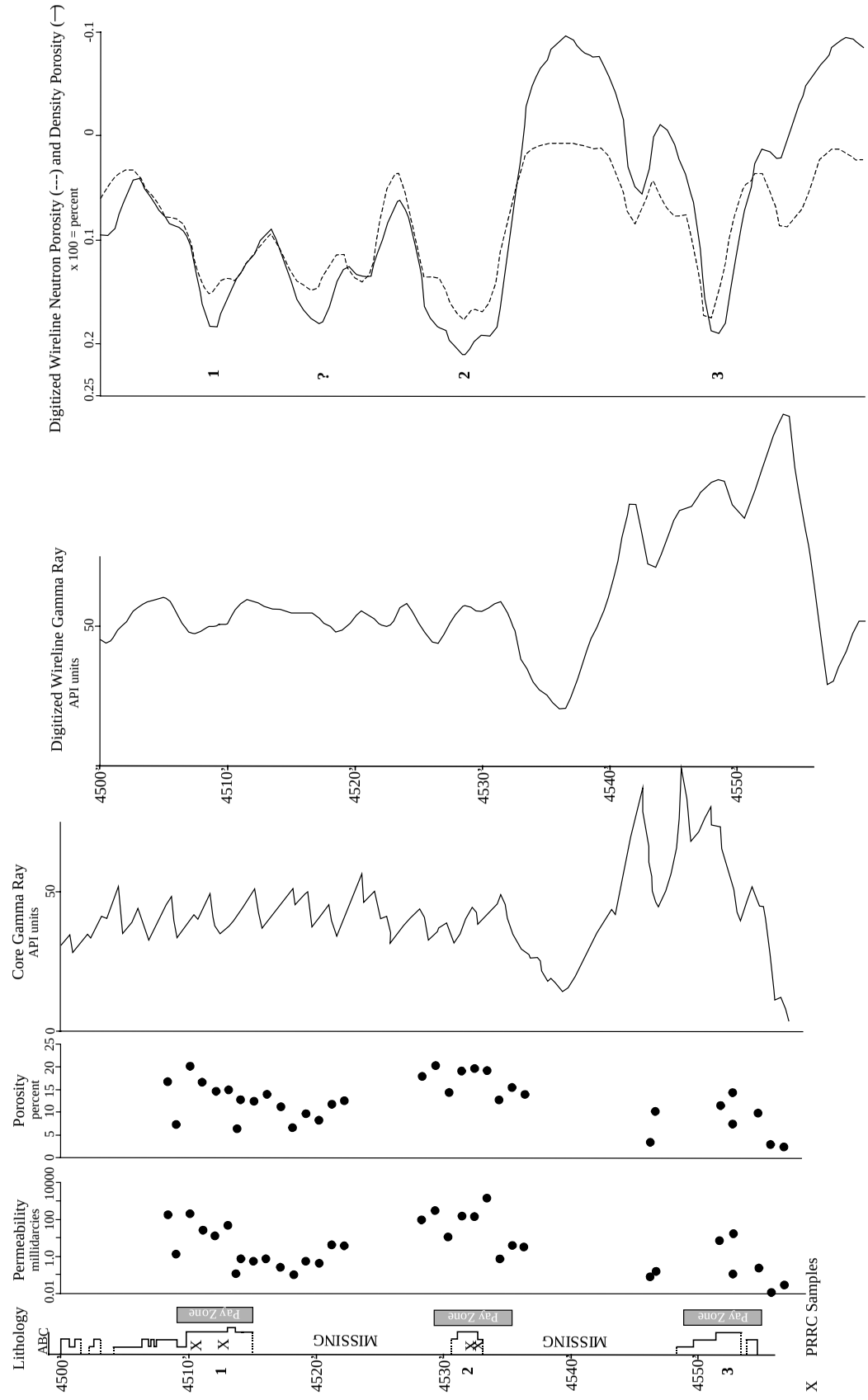

Figure 2. Chart showing the lithologic and geophysical properties of the Stivason Federal well #1 core with depth, and correlated to permeability, porosity and gamma ray logs; shaded intervals are oil stained and are likely sequestration zones.

80% of the core available from the designated main reservoir intervals. Oil staining suggests high porosities and that they will be the primary hosts for injected CO_2 as long as local hydrofracture pressure is not exceeded during injection. The variability in oil staining and measured permeability shown by this lithology suggests that some of the residual oil may be difficult to displace during CO_2 injection.

Non-reservoir strata contain more pore-lining illite and chlorite, as well as illite/smectite and anhydrite cements (Mazzullo, et al., 1991). Mineralogic changes caused by CO_2 injection into these heterogeneous strata would probably occur in the cementing mineral phases, most likely in the carbonates and sulfates. The heterogeneity of the cements suggests that a thorough base-line characterization prior to injection would be necessary in order to fully understand and document any changes caused by injection.

Flow Modeling

Porous media flow simulations were used to match the historic production data. Values of a number of unknown reservoir rock and fluid properties had to be determined by trial and error due to lack of appropriate data. The reservoir model was subsequently used to determine feasibility of injecting CO_2 over a period of one month. A number of injection scenarios were tested to determine the response of the reservoir over a wide range of operating conditions and regulatory operational constraints. The preliminary injection studies indicate that the injected CO_2 plume can be dispersed in the Shattuck Formation sandstones to such an extent that it can be characterized through a variety of proposed monitoring techniques. More details of the geologic and flow modeling can be found in Pawar, et al. (2001).

Pearl Queen Brine Chemistry

Brine samples taken from wells Stivason Federal #4 and Stivason Federal #5 (see Figure 1) were analyzed for cations and anions using Direct Current Plasma (DCP) spectroscopy and ion chromatography (IC); pH was measured using a pH electrode. The chemical analyses (Table 1) show that these oil-field brines are mainly composed of Na and Cl with an ionic strength of ~2.4 Molar. There is a charge imbalance of about 0.3 Molar (due to an excess of negative charges), and the Al concentrations in the brines are suspiciously high, perhaps due to the presence of colloids. Additional chemical analyses should resolve these concerns, and will allow for subsequent calculation of equilibrium mineral phases. We suspect that the Pearl Queen brine is

close to equilibrium with gibbsite, kaolinite, dolomite, calcite and quartz. Total carbon analyses are scheduled soon. Preliminary reaction path modeling of CO_2 mixing with the brine shows an initial sharp decrease in pH as expected. Preliminary modeling of low pH fluid interactions with the estimated major modal mineralogy of the Shattuck Member sandstone (75% quartz, 10%-15% K-feldspar, and 5%-10% dolomite cement), and for several modal fractions of initial dolomite, shows the resulting fluid pH ranges from 4-5 after reaction with these minerals. This preliminary result is an indication of the potential buffering capacity of the reservoir when the low pH CO_2-brine reacts with the Queen Formation during injection. Further modeling trials are needed when considering different CO_2 fugacities and initial mineral fractions.

Table 1. Chemical analyses of brines from Stivason Federal wells # 4 and #5[1]

Well #	pH	Al[2]	Si	Na	K	Mg	Ca	Cl	Br	SO_4
#5	6.786	0.000414	0.00014533	2.085	0.00268	0.123	0.056	2.99	0.0041	0.0208
#5	6.852	0.000410	0.00013823	2.044	0.00307	0.122	0.056	3.12	0.0040	0.0220
#4	7.181	-	-	1.797	0.00264	0.110	0.049	-	-	-

[1] Analyses performed at the NMBMMR, Socorro, NM on same samples yielded similar results.

[2] Elemental compositions reported as molarity (moles/L)

Geophysical Monitoring

Negotiations are underway to schedule pre-injection geophysical surveys, including dipole sonic logs, a deviation survey and a 3 component crosswell survey. We are planning to have the 3C Vertical Seismic Profile survey and the 3D, 9C surface seismic surveys completed by the end of FY01, immediately prior to CO_2 injection.

Application

Ultimately, the models and data resulting from this CO_2 sequestration project will be used to predict geologic storage capacity and physical and chemical changes in reservoir properties, such

as fluid composition, porosity, permeability and phase relations. Development of accurate monitoring tools will also permit validation of the computer simulations that will be needed for future performance and risk assessments. Science or technology gaps related to engineering aspects of CO_2 sequestration will be identified in the course of this study. In addition, a better understanding of CO_2-reservoir interactions resulting from this project should improve industrial EOR flooding practices.

Future Activities

Current geologic and preliminary flow simulation results indicate the feasibility of CO_2 injection in a depleted oil reservoir. These results also provide guidelines for upcoming geophysical monitoring (e.g., spacing of seismic sources and receivers). Geochemical lab experiments with Shattuck Member sandstones have been initiated to evaluate mineralization reaction kinetics. Preparation for CO_2 injection and acquisition of geophysical surveys has begun and should be completed by the end of FY01. CO_2 injection is scheduled for the beginning of FY02. Final characterization and modeling efforts will be completed in FY03. Upon completion of this project, the West Pearl Queen reservoir will be one of the most completely characterized oil reservoirs, setting the stage for follow-on DOE/NETL CO_2 sequestration experiments. This field site could be used for field demonstration experiments of greater scope and duration, including injection of larger volumes of CO_2, soaking of CO_2 for a duration significantly longer than a month, drilling of additional observation wells or sampling of the reservoir for actual core analysis.

Acknowledgements

The authors wish to acknowledge the financial support from the Department of Energy's National Energy Technology Laboratory, as well as the overall support of Mark Murphy from Strata Production Company.

References

Department of Energy, Carbon Sequestration: Research and Development, Officesof Science and Office of Fossil Energy report, December 1999.

Knight, R., Dvorkin, J. and Nur, A., Acoustic Signatures of Partial Saturation, Geophysics, 63(1), 132-138, 1998.

Lizarralde, D. and Swift, S., Smooth Inversion of VSP Traveltime Data, Geophysics, 64(3), 659-661, 1999.

Mazzullo, J., Malicse, A., and Siegel, J., 1991, Facies and depositional environments of the Shattuck Sandstone on the Northwest Shelf of the Permian Basin: Journal of Sedimentary Petrology, vol. 61, p. 940-958.

Morris, G., More CO_2 floods start up in West Texas. Oil & Gas Journal, 87-88, 1996.

Pawar, R., Zhang, D., Stubbs, B., and Westrich, H., Preliminary Geologic Modeling and Flow Simulation Study of CO_2 Sequestration in a Depleted Oil Reservoir,, NETL Carbon Sequestration Conference Proceedings, May 15-17, 2001.

Withers, R.J. and Batzle, Modeling Velocity Changes Associated with a Miscible Flood in the Prudhoe Bay Field, Geophysics, 62(5), 1442-1455, 1997.

Translating Lessons Learned From Unconventional Natural Gas R&D To Geologic Sequestration Technology

Vello A. Kuuskraa (vkuuskraa@adv-res.com; 703-528-8420)
Advanced Resources International, Inc.
1110 N. Glebe Road, Suite 600
Arlington, VA 22042

Hugh D. Guthrie (hugh.guthrie@netl.doe.gov; 304-285-4632)
United States Department of Energy
P.O. Box 880
Morgantown, WV 26507

Abstract. The gloomy, almost crisis-like outlook for the future of domestic natural gas in the late 1970's set in motion a set of national-level energy initiatives for adding new gas supplies. Two of the most valuable of these were: (1) the joint government/industry R&D programs in tight gas, gas shales and coalbed methane by the Department of Energy's Office of Fossil Energy (DOE/FE) that established the essential exploration and production technology for these resources; and, (2) the unconventional gas economic incentives (Section 29 tax credits) that buffered the economic risks faced by the early set of unconventional gas developers and helped attract scarce investment capital to this emerging resource.

Now, twenty years later, unconventional gas offers one of the impressive technology success stories. A poorly understood, high cost energy resource is now providing major volumes of annual gas supplies and helping meet the growing domestic demand for natural gas.

> Unconventional natural gas provided 4,500 Bcf of supply in 1999, up threefold from about 1,600 Bcf twenty years ago.
>
> Proved reserves of unconventional gas are 53 Tcf, up from less than 20 Tcf when the R&D and incentive programs started.
>
> Assessed recoverable resources of unconventional gas are now estimated at 400 to 500 Tcf, providing confidence that with technology progress the contribution of unconventional gas will continue to grow.

Behind these spectacular numbers are a host of dedicated activities, occasional failures and many successes, all underlain by substantial investments in R&D and technology. Tight gas, the flagship of unconventional gas, is now pursued routinely by independents and majors alike in over a dozen major domestic basins. Gas shales development has expanded from the Appalachian Basin to new basins in Michigan (Antrim) and North Texas (Barnett). Coalbed methane, a resource once labeled "moonbeam gas", has been converted from a mining hazard to an economic source of new gas reserves. Ironically, geopressured methane, the resource stated as

holding "a 1,000 years of gas", came up short once the bright, hot light of serious scientific inquiring was turned on.

The look at the history of unconventional gas also provides a rich set of "lessons learned". These "lessons" demonstrate that combining a well managed joint government/industry R&D technology program with performance-based incentives for early application of new technology can be highly successful, providing significant economic benefits to the U.S. economy.

Introduction. After decades of plentiful supplies, low costs and public indifference, in the 1970s natural gas finally moved to the center of national attention. The winter of 1975-76 saw worrisome curtailments in natural gas supplies leading to closing of schools and public facilities. In the following winter the problems of supply curtailments grew worse, leading to Congressional hearings and a scramble for explanations.

While numerous reasons were posed for the cause of the problem, the one set of answers that gained broad public and political acceptance was that "the nation was rapidly running out of natural gas supplies." Prominent in the winning debate were two dominating figures, M. King Hubbert and the Federal Power Commission, both painting a pessimistic, depleting future:

> King Hubbert, who had gained considerable credibility among energy policy and Congressional staff by correctly forecasting the peak and subsequent decline in domestic oil production, applied his same forecasting methods to natural gas. In widely followed Congressional testimony, he set forth a future of limited natural gas resources and a pending crisis in gas supplies. Hubbert viewed a low domestic natural gas resource base of 1,050 Tcf of which nearly one-half had already been produced. He predicted that the peak in natural gas productions would occur shortly (in 1977) followed by a dramatic decline, Figure 1.
>
> The Federal Power Commission, responsible for regulating the price and profitability of natural gas production, confirmed its stance for continued price controls defending it by stating -- why deregulate natural gas when there is so little left to find?

Search for New Resources. The bleak, uncertain outlook for natural gas set the stage for ground breaking legislation -- phased removal of wellhead price controls, incentives for new natural gas development, and restrictions on gas use for electric generation (NGPA, Public Law 95-621). The concern over future gas supplies also set in motion a search for new sources of natural gas, in settings that had been previously overlooked.

> A Federal Power Commission task force identified that 600 Tcf of gas in place existed in three large Western basins. These gas resources were held in geologically complex, extremely low permeability ("tight") reservoirs where existing technologies were insufficient for ensuring economic production.
>
> The Bureau of Mines identified that considerable volumes of methane (pure natural gas) were being vented for safety reasons from coal mines, wasting a valuable resource.

> Gas bearing Devonian-age shales were judged to hold several thousand Tcf of gas in the Appalachian Basin, "one of the least defined domestic gas producing regions."
>
> And, public interest was stirred by major articles in Fortune and The Wall Street Journal that a new natural gas resource -- geopressured aquifers -- could provide gas for a 1,000 years.

Numerous special purpose studies and narrowly focused R&D efforts were initiated to further understand and pursue these large, little-understood natural gas resources, Figure 2.

Foundation for a Coordinated R&D Program. Faced with a growing body of new, sometimes promotional information on unconventional natural gas, the Energy Research and Development Administration (ERDA) commissioned a comprehensive study of these resources. Advanced Resources International, then called Lewin and Associates, with Mr. Vello Kuuskraa as Study Director, was contracted to perform this broadly scoped, landmark study. The introductory page of this study, "Enhanced Recovery of Unconventional Gas (Volumes I, II, and III)," February 1978, pointedly set forth the challenge:

"As conventional domestic natural gas supplies dwindle, the nation must seek ways to slow these trends and obtain new supplies. The choices faced are controversial, costly and risky. They entail difficult balancing among higher prices, accelerated development, reliance on imports and new technology. This study has been conducted to assist public decision-makers select among these many choices by addressing two questions:

> How severe is the need for additional future supplies of natural gas?
>
> What is the economic potential of providing a portion of future supply through enhanced recovery from unconventional natural gas resources?"

As important, the study set forth the framework for an aggressive, coordinated program of research and development on unconventional natural gas "… the study serves to assist the Department of Energy (the successor to ERDA) design a cost-effective research and development program to stimulate industry to recover this unconventional gas and to produce it sooner."

Objectives, Design And Implementation Of The Program. The Department of Energy's unconventional gas R&D/incentives program has had many political twists and policy turns during its twenty years of existence. The outline and objectives of the original Enhanced Gas Recovery Program, that responded to the supply crisis atmosphere of the late 1970's, was set forth in the FY 1978 Congressional Budget Request. Subsequent administrations, reflecting their own National priorities and energy strategies, shaped and modified this program continuously.

Original DOE R&D Program Objectives. The strategic policy goal was to develop and stimulate the deployment of advanced exploration, development and production technologies for recovering new gas supplies from the massive but complex unconventional gas resources -- tight gas, coalbed methane, gas shales and geopressured methane. The technical objectives were to increase per well gas recovery efficiencies and lower unit development costs while providing incentives (through tax credits) for prompt, orderly development of the nation's gas resources.

In addition, two quantitative, national-level natural gas supply goals were set forth for the Enhanced Gas Recovery Program:

> *Increase gas production by an incremental 3 billion cubic feet per day by 1986, and Add 10 Tcf of producible reserves by 1985.*

Changing Horses in Mid-Stream. Even before the results were in, the political winds and market conditions shifted. The Reagan administration, in 1980, first scaled back the R&D program and then pushed to eliminate government involvement in short-term gas supply R&D, citing that "the private sector has the financial and technical resources to develop the technology needed for new unconventional gas resources." Congressional intervention maintained the program, although only at a life-support level.

In 1991/92, with the publication of the administration's National Energy Strategy and the growing R&D role of the Gas Research Institute in unconventional gas, much of the remaining DOE R&D program was eliminated, with only the low permeability ("tight sands") area surviving. When, in 1994, the Gas Research Institute also shifted its priorities, terminating its focus on unconventional gas in favor of a more generic technology-based R&D program, for all practical purposes public R&D on unconventional gas came to an end. With subsequent loss of public support, the Gas Research Institute's R&D program on gas supply is now also being phased out.

Program Definition, Design and Implementation. The original DOE R&D program had its roots in Volume III of the study -- "Enhanced Recovery of Unconventional Gas (1978) -- and was shaped considerably by industry and outside technical input. Unfortunately, in subsequent years the political process rather than science and analysis shaped much of program design. In contrast, the GRI R&D program on unconventional gas was able to stay, at least during its formative years, outside the political process. The two R&D programs complemented each other, with the DOE program often conducting the exploratory, fundamental science and the GRI program providing the applied science and technology transfer.

Each organization relied greatly on outside technical experts, research organizations and industry to perform and commercialize its R&D. This helped to bring valuable cost-efficiency and cost-sharing to the program, particularly during the field documentations stages, and to accelerate technology commercialization.

Supporting Policy Mechanisms. Two economic incentives were set forth in Congressional legislation to encourage the development of unconventional gas - - incentive pricing and tax credits.

Incentive Pricing Under NGPA. The first set of economic incentives for encouraging exploration and development of unconventional gas were set forth in the Natural Gas Policy Act of November, 1978. Section 107 of this act deregulated the well-head sales price of natural gas from Devonian-age gas shales, coal seams and geopressured brines. Section 102 of this Act enabled tight gas to become eligible for the highest ceiling price within the NGPA regulated categories, providing this resource with modest economic incentives.

Section 29 Tax Credit. A separate set of economic incentives for unconventional gas were placed into the Crude Oil Windfall Profits Tax Act of 1980. Section 29 of this act provided tax credits to qualified unconventional gas wells and formations. While producers initially needed to select which set of incentives to use, the deregulation of natural gas in 1981 made this choice moot. With amendments, the Section 29 tax credit qualifying period for new unconventional gas wells lasted until the end of 1992, with tax credits provided for gas produced through 2002.

The incentive provisions of the Section 29 tax credit were designed to reward efficient unconventional gas development and performance. During a time when national average wellhead natural gas prices were between $1.50 and $2.50 per Mcf, the tax credit for tight gas was about $0.50 per Mcf and for gas shales and was on the order of $1.00 per Mcf for coalbed methane, adding considerable economic value to the efficient production of these resources. The tax credits also helped justify the high investment needed for initial infrastructure.

Response to Incentives. Not surprisingly, industry's development and production of unconventional natural gas responded strongly to these incentives:

> The production of Section 29 "legally eligible" tight gas, a resource with many undeveloped basins and readily available technology, grew from 240 Bcf in 1980 to 1,180 Bcf in 1986, plateauing thereafter. Overall production from this resource, including "legally" and "geologically" defined tight gas, was considerably higher as numerous low permeability areas and pre-existing tight gas production remained unapproved by FERC or a FERC-designated State agency.
>
> Lacking a sufficient base of technology, coalbed methane had little opportunity to use the tax credits until the end of the 1980's. Even with this late start, over 5,000 CBM wells were drilled and completed before the qualifying period for tax credits expired.
>
> Drilling for gas shales increased substantially in the Appalachian Basin and with R&D opening up the Michigan Basin drilling boomed, averaging over 1,200 wells per year in the last six years of tax credits.

Post Tax Incentive Activity. A most significant outcome of the tax incentive program was that unconventional gas well drilling and completions stayed strong after the expiration of the tax credits:

> After a brief lull, tight gas well completions rebounded to 3,000 wells per year.
>
> Coalbed methane well completions slumped somewhat in the mid-1990's but now have reached new highs with the strong activity in the Powder River Basin.
>
> Gas shale well drilling has averaged 900 wells per year for the six years since the expiration of the tax credits, only somewhat less than the 1,200 wells per year prior.

The reason for the strong post tax incentive activity was that unconventional gas exploration and development technology had progressed sufficiently and the infrastructure was in place such that the industry remained economic and could attract capital without the need for further incentives or subsidies.

Monitoring And Evaluation. The initial DOE and GRI unconventional gas R&D programs placed considerable emphasis on establishing reliable, efficient monitoring and evaluation systems. Explicit supply enhancement goals, detailed R&D program plans, and benefit to cost analyses were used in annual budget justifications. However, as the gas supply conditions moved from shortage to surplus and the political support for public R&D waned, the rules of the game and the measures of success changed.

The DOE R&D Program. The initial DOE R&D program's monitoring and evaluation process, involving independent outside technical experts, served the program well. As new information was collected and compared with expectations, a series of significant shifts in the program occurred. For example, the geopressured methane resource was found to be geologically flawed, the program was terminated. At the same time, other priorities and budget shifts occurred with increases for tight gas and coalbed methane and decreases for gas shales, bringing the individual technology area budgets into closer line with their resource potential.

However after a few years, as the gas shortage turned into a gas surplus, much of the national level evaluations and mid-course adjustments became politically driven rather than analytically founded. The coalbed methane R&D program was essentially shut down. The gas shale R&D program stayed on life support only due to Appalachian Basin political support. Subsequently the program was terminated in 1992. Tight gas R&D survived, but at a dramatically reduced level.

In recent years, DOE's R&D monitoring and evaluation process has again become much more analytical and rigorous. While no sense of urgency has yet emerged for using R&D or incentives to stimulate additional natural gas production (even though natural gas prices are at an all time high and concerns exist again about gas curtailments), several important management steps have been taken. A Strategic Center for Natural Gas has been established at the National Energy Technology Laboratory and a National Research Council/National Academy of Sciences evaluation of the accomplishments and benefits of each of the unconventional gas technology areas is underway.

The GRI R&D Program. From its inception, the Gas Research Institute was mandated by the Federal Energy Regulatory Administration (FERC) to perform extensive cost-benefit analyses, set forth rigorous budget justifications, and hold several levels of advisory board review. This process and a clear focus on unconventional gas served GRI and its R&D program well. In 1994, however, GRI switched from a resource-based program addressing unconventional gas to a generic E&P technology-based program. At that point, GRI began to look like any other industrial R&D shop, lost its national gas supply mandate, and found difficulties justifying its program costs and benefits to industry.

Discussion Of Results. Unconventional gas offers one of the great success stories of national benefits and progress in technology. A poorly-understood, high-cost energy resource, one that the U.S. Geological Survey had not even included in its national appraisals of future gas resources (until their most recent 1995 assessment), is now providing major volumes of annual gas supplies and helping meet growing domestic natural gas demand (Table 1):

Unconventional natural gas provided 4,500 Bcf of supply in 1999, up from 1,600 Bcf twenty years ago.

Proved reserves of unconventional gas are 52 Tcf, up from 20 Tcf twenty years ago; remaining recoverable resources of unconventional gas are estimated at 400 Tcf to 500 Tcf, Table 2.

Looking ahead, based on projections by DOE/EIA's National Energy Modeling System (in AEO 2001), considerable further development of this resource base is expected, assuming a continuing strong pace of technology progress. By 2010, annual unconventional gas production is expected to reach 6,700 Bcf. The recent NPC Natural Gas Study expects a similar contribution from unconventional gas, estimating 6,800 Bcf of supply in 2010 from these resources.

These lofty expectations for unconventional gas depend on continued strong technology progress. Recent cutbacks in industrial R&D, the small size of DOE's gas supply program, and the termination of the Gas Research Institute's public R&D on unconventional gas raise serious concerns on the future pace of technology progress. The NPC Study highlights its concerns by stating, "However, recent (declining) trends in research and development spending raise concerns regarding this (aggressive pace of technology improvement) assumption."

1. Tight Gas Sands. By the mid-1970's, industry knew that large quantities of natural gas resources existed in tight (low permeability) formations. However, the flow and production of gas from most of these tight formations were too low to support economic recovery. A handful of independents explored for areas where nature had sufficiently fractured this tight rock to make it productive, but generally with a poor record of success.

The combined DOE, GRI and industry R&D programs, plus a set of modest tax incentives, unlocked the gas resource held in these tight rocks. The gas play, born in the Appalachian and San Juan basins, expanded rapidly into the major Rocky Mountain gas basins and more recently into Texas and the Mid-continent. By 1999, annual tight gas production was 2,900 Bcf, up from 1,500 Bcf in the mid 1970's. Proved tight gas reserves were 35 Tcf from over 50,000 producing wells (not including the numerous older low producing tight gas wells in the Appalachian Basin), with 50 Tcf of tight gas having been produced since the initiation of the R&D program.

2. Gas Shales. At the start of the DOE R&D Program, the Appalachian Basin gas shales were a small, declining resource providing 70 Bcf per year. Annual new well drilling averaged only 200 wells and proved reserves were below 1 Tcf. Wells were being completed open hole, with little definition of productive pay zones, and were being stimulated with nitroglycerine (a remnant of early 1900's technology). Much of the activity was centered in the Big Sandy area of eastern Kentucky. Little understanding existed on key gas storage and production mechanisms nor about geologically similar gas shale plays in other parts of the country.

By 1999, annual gas shale production had reached 370 Bcf. Proved reserves were 5 Tcf, with another 4 Tcf having been produced in the twenty years from 1978 to 1998. Stimulated by Section 29 tax credits and the expansion into new gas shale basins in Michigan and North Texas, well drilling climbed sharply. Over 17,000 productive gas shales wells were drilled from 1978 to 1999 with a peak of 1,700 gas shale wells completed in 1992, the last year wells could qualify for tax credits.

3. Coalbed Methane. The combination of building a scientific base of knowledge, fostering appropriate technology and providing economic incentives launched the birth of a new natural gas industry -- coalbed methane -- now with nearly $10 billion of capital investment. Much of the early development was by independent production companies such as Devon Energy, Meridian Oil and Taurus Energy, who saw their gas production, reserve holdings and market capitalization rise sharply.

Coalbed methane production climbed from essentially zero at the start of the R&D program to 1,250 Bcf in 1999, from three significant basins. Proved reserves were 13 Tcf from over 7,000 producing wells, with another 8 Tcf having already been produced. The introduction and continuing adaptation of technology enabled the industry to remain profitable and vigorous, even after the 1992 expiration of Section 29 tax credits. Today, several new coalbed methane basins and plays are being actively developed, including the Powder River (Wyoming), Raton (Colorado), and Uinta (Utah), providing a base for continued growth.

4. Geopressured Methane. While considerable geologic and reservoir knowledge was gained, no commercial natural gas production was established for this resource. Still, the R&D program in geopressured methane helped bring a strong dose of reality and understanding on the viability, or lack of, for this gas resource and helped dispel the speculation that "a 1,000 years of natural gas" was at hand.

Lessons Learned.

Twenty years have passed since the DOE R&D and incentive programs were launched in unconventional natural gas. What lessons and insights might one be able to draw from this rich base of experience that would be relevant to other emerging DOE R&D programs such as Carbon Sequestration? Among the many "lessons learned," ten stand out:

1. When rigorously planned and managed, government supported R&D can be highly successful, providing significant benefits to the domestic economy. The DOE and GRI R&D programs introduced knowledge and hardware that turned low productivity, high cost resources into a reliable source of new natural gas reserves and supply. Using a net profits value of $0.50 per Mcf of additional natural gas production and reserves due to advances in technology and economic incentives, the national economic benefits of unconventional gas are over $50 billion, not including future development.

2. Establishing a scientifically-based knowledge base "the intellectual foundation," is an essential first step. The negative outlook for coalbed methane, that stemmed from an ill-advised and unsuccessful "drill and hope" field demonstration project, was overcome when a strong scientific foundation was established.

3. Joint industry/government partnerships and implementation help leverage R&D resources, bring practicality to the program, and accelerate commercial implementation. The GRI unconventional gas program regularly benefited from industry cost sharing and advice. DOE began to realize similar values when it increasingly turned to industry/government partnerships for implementing tight gas and gas shales R&D.

4. A critical mass of funding and sufficient time are essential for achieving success, particularly for ambitious, breakthrough efforts. The timely and efficient development of the coalbed methane resource had a major setback when the DOE R&D was prematurely terminated. Fortunately, GRI continued the R&D on this resource and made it one of its high priorities, enabling the technology to mature, to be rigorously field tested and to achieve success.

5. Economic and tax incentives can greatly accelerate industry's adoption of technology by helping justify capital, by lowering economic risk and by challenging the financial community's imagination. The tremendous boost in new investment and well drilling, seen by all three of the unconventional gas resources, is a testament to the power of properly structured economic and tax incentives.
6. Special purpose "performance based" rather than broadly structured or "input based" economic incentives are a key to success. The highly focused Section 29 tax had considerably larger impacts credits to the unconventional gas industry than the general purpose R&D tax credit available to all industry.

7. For maximum effectiveness, the incentives need to be sufficiently attractive and long lasting but also have a "sunset provision." Section 29 tax credits significantly improved project economics during the initial risky phase of unconventional gas development. As the technology and resource understanding matured, these risk premiums became less, enabling the unconventional gas industry to compete for project approval and capital without the need for continued incentives.

8. Independent evaluation of fundamental assumptions, data and results, is essential for avoiding wasting scarce R&D resources. The independent review of the geology and science of geopressured methane helped close down a large R&D program targeting this geologically flawed and economically non-viable resource.

9. Cost reductions and efficiency improvements in geologically based technologies rely as much on adapting the technology to the geologic setting as on fundamental breakthroughs. Successful results in the various coalbed methane and gas shale basins required selectively adapting technology rather than blindly applying methods that worked in other geologic settings. Assembling detailed geologic and reservoir data on each of the high potential basins needs to be a priority for R&D.

10. Efficiently disseminating technology to industry requires a comprehensive program of technology transfer ranging from publications for the informed layman to high visibility "flagship" field demonstrations. GRI's publication of the "Quarterly Review of Methane from Coal Seams Technology," the numerous articles prepared by its technical contractors and the major field laboratory at Rock Creek coupled with direct greatly reduced the time for technology penetration and implementation by industry.

References

National Petroleum Council: *Natural Gas, Meeting the Challenges of the Nation's Growing Natural Gas Demand*, Final Report, December 1999.

Energy Information Administration: *Annual Energy Outlook 2001*, DOE/EIA-0383, U.S. Dept. of Energy, December 2000.

Energy Information Administration: *Documentation of the Oil and Gas Supply Module (OSGM)*, DOE/EIA-MO63/1, Volume I, U.S. Dept. of Energy, December 1999.

Model of Unconventional Gas Recovery (MUGS). Internal DOE/FE and DOE/EIA unconventional gas model. (July 2000).

Enhanced Recovery of Unconventional Gas – Volume II. Prepared for the U.S. Dept. of Energy by Lewin and Associates, Inc. HCP/T2705-02, Dist. Category NC-92a, October 1978.

Eastern Devonian Gas Shales Technology Review, Volume I through Volume 5, Gas Research Institute, 1984 – 1988.

Devonian Gas Shales Technology Review, Volume 6 through Volume 8, Gas Research Institute, 1989 – 1993.

"New Basins Invigorate U.S. Gas Shales Play", Reeves, Kuuskraa and Hill, Oil and Gas Journal, January 1996.

"Barnett Shale Rising Star in Fort Worth Basin", Kuuskraa, Koperna and Schmoker, Oil and Gas Journal, May 1998.

"U.S. Crude Oil, Natural Gas and Natural Gas Liquid Reserves, 1999 Annual Report", Energy Information Administration, December 2000.

Figure 1. Past Outlook for U.S. Gas Production

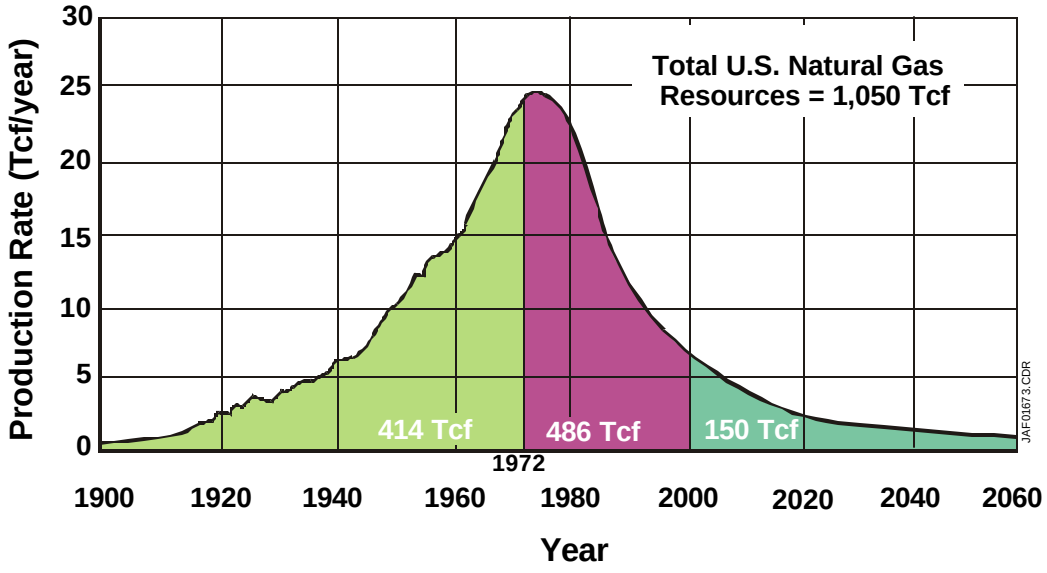

(Modified from Hubbert, 1974)

Figure 2. Natural Gas Resource Pyramid Lower-48 States

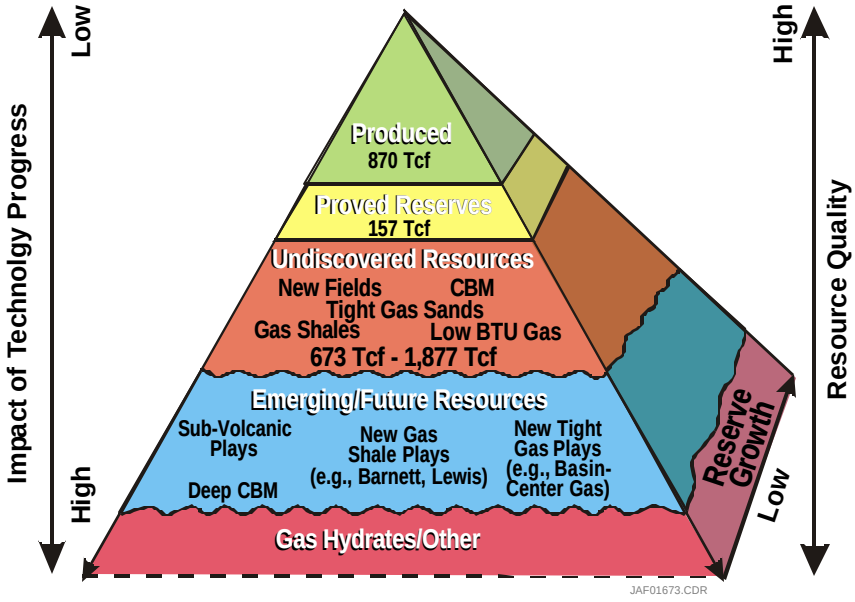

Table 1. Unconventional Gas: Past and Present

	1978	1999
Tight Gas Sands		
• Production (Bcf)	1,560	2,900
• Reserves (Tcf)	19	35
Gas Shales		
• Production (Bcf)	70	370
• Reserves (Tcf)	1	5
Coalbed Methane		
• Production (Bcf)	-	1,250
• Reserves (Tcf)	-	13
TOTAL		
• Production (Bcf)	1,630	4,520
• Reserves (Tcf)	20	53

Table 2. Status Of Natural Gas Resources (Lower-48) (Tcf)

	Proved Reserves	Additional Resources
• Conventional Onshore	72	586
• Unconventional	53	371
• Federal Offshore	33	352
• Deep Gas	7	*
TOTAL (L-48)	158	1,309

Included in conventional onshore

ENGINEERING FEASIBILITY OF CO_2 CAPTURE ON AN EXISTING US COAL-FIRED POWER PLANT

Nsakala ya Nsakala (nsakala.y.nsakala@power.alstom.com; 860-285-2018)
John Marion (john.l.marion@power.alstom.com; 860-285-4539)
Carl Bozzuto (carl.bozzuto@power.alstom.com; 860-285-5007)
Gregory Liljedahl (greg.n.liljedahl@power.alstom.com; 860-285-4833)
Mark Palkes (mark.palkes@power.alstom.com; 860-285-2676)
ALSTOM Power Inc.
US Power Plant Laboratories
2000 Day Hill Rd.
Windsor, CT 06095

David Vogel (david.c.vogel@us.abb.com; 713-821-4312)
J.C. Gupta (jcgupta@us.abb.com; 713-821-5093)
ABB Lummus Global Inc.
3010 Briarpark
Houston, TX 77042

Manoj Guha (mkguha@aep.com; 614-223-1285)
American Electric Power
1 Riverside Plaza
Columbus, OH 43215

Howard Johnson (hjohnson@odod.state.oh.us; 614-644-8368)
Ohio Coal Development Office
77 South High St, 25th Floor
Columbus, OH 43216

Sean Plasynski (plasynsk@fetc.doe.gov; 412-386-4867)
US DOE NETL
626 Cochrans Mill Rd.
Pittsburgh, PA 15236

For Presentation at the
First National Conference on Carbon Sequestration
May 15-17, 2001, Washington DC

ABSTRACT

ALSTOM Power Inc.'s US Power Plant Laboratories (ALSTOM) has teamed with American Electric Power (AEP), ABB Lummus Global Inc. (ABB), the US Department of Energy National Energy Technology Laboratory (DOE), and the Ohio Coal Development Office (OCDO) to conduct a comprehensive study evaluating the technical feasibility and economics of alternate CO_2 capture and sequestration technologies applied to an existing US coal-fired electric generation power plant. Three retrofit technology concepts are being evaluated, namely:

- Concept A: Coal combustion in air, followed by CO_2 separation with Kerr-McGee/ABB Lummus Global's commercial MEA-based absorption/stripping process
- Concept B: Coal combustion with O_2 firing and flue gas recycle
- Concept C: Coal Combustion in air with Oxygen Removal and CO_2 Separation by Tertiary Amines

Each of these technologies is being evaluated against a baseline case and CO_2 tax options from the standpoints of performance and impacts on power generating cost. A typical existing US domestic pulverized coal fired power plant is being used in this evaluation. Specifically, AEP's 450 MW Conesville Unit No. 5, located in Conesville, Ohio is the power plant case study. All technical performance and cost results associated with these options are being evaluated in comparative manner. These technical and economic issues being evaluated include:

- Boiler performance and plant efficiency
- Purity of O_2 produced and flue gas recycled
- Heat transfer into the radiant and convective sections of the boiler
- NO_X, SO_2, CO and unburned carbon emissions
- Heat transfer surface materials
- Steam temperature control
- Boiler and Steam Cycle modifications
- Electrostatic Precipitator system performance
- Flue Gas Desulfurization system performance
- Plant systems integration and control
- Retrofit investment cost and cost of electricity (COE)

ALSTOM is managing and performing the subject study from its US Power Plant Laboratories office in Windsor, CT. ABB, from its offices in Houston, Texas, is participating as a sub-contractor. AEP is participating by offering their Conesville Generating Station as the case study and cost sharing consultation, and relevant technical and cost data. AEP is one of the largest US utilities and as the largest consumer of Ohio coal is bringing considerable value to the project. Similarly, ALSTOM and ABB are well established as global leaders in the design and manufacturing of steam generating equipment, petrochemical and CO_2 separation technology. ALSTOM's world leaders in providing equipment and services for boilers and power plant environmental control, respectively, and are providing their expertise to this project. The DOE National Energy Technology Laboratory and the Ohio Coal Development Office provided consultation and funding. All participants contributed to the cost share of this project.

The motivation for this study was to provide input to potential US electric utility actions to meet Kyoto protocol targets. If the US decides to reduce CO_2 emissions consistent with the Kyoto protocol, action would need to be taken to address existing power plants. Although fuel switching to gas may be a likely scenario, it will not be a sufficient measure and some form of CO_2 capture for use or disposal may also be required. The output of this CO_2 capture study will enhance the public's understanding of control options and influence decisions and actions by government, regulators, and power plant owners to reduce their greenhouse gas CO_2 emissions.

TECHNICAL ANALYSIS

The technical approach followed and results obtained therefrom are presented in this paper. The investment costs and economic analysis are currently under study, and will be presented in subsequent publications.

Study Unit Description.

The unit analyzed in this study was AEP's Conesville Unit #5. The sectional side elevation drawing of the study unit steam generator is shown in Figure 1. This unit can be described as a nominal 450 MWe-gross, tangentially coal fired, subcritical pressure, controlled circulation, radiant reheat unit. Its generator produces 463 MW of electric power at maximum continuous rating (MCR). The furnace is a single cell design utilizing five elevations of tilting tangential coal burners. The unit fires mid-western bituminous coal. The coal is pulverized in five 903-RP bowl mills and fed into the boiler through five elevations of tilting-tangential fuel nozzles. The 903-RP bowl mill has a design base capacity of 119,000 lb/h of coal with a Hardgrove Grindability Index of 55, and is pulverized to 70% through 200 mesh. The unit is

configured in a “Conventional Arch” type design and is representative in many ways of a large number of coal fired units in use today. The unit is designed to generate about 3.1 x 10^6 lbm/hr of steam at 2400 psig and 1005 ^oF with reheat also to 1005 ^oF. These represent the most common steam cycle operating conditions for existing utility scale power generation systems. Outlet steam temperature control is provided with de-superheating spray and burner tilt. The other major components of Unit #5 are identified in Figure 1.

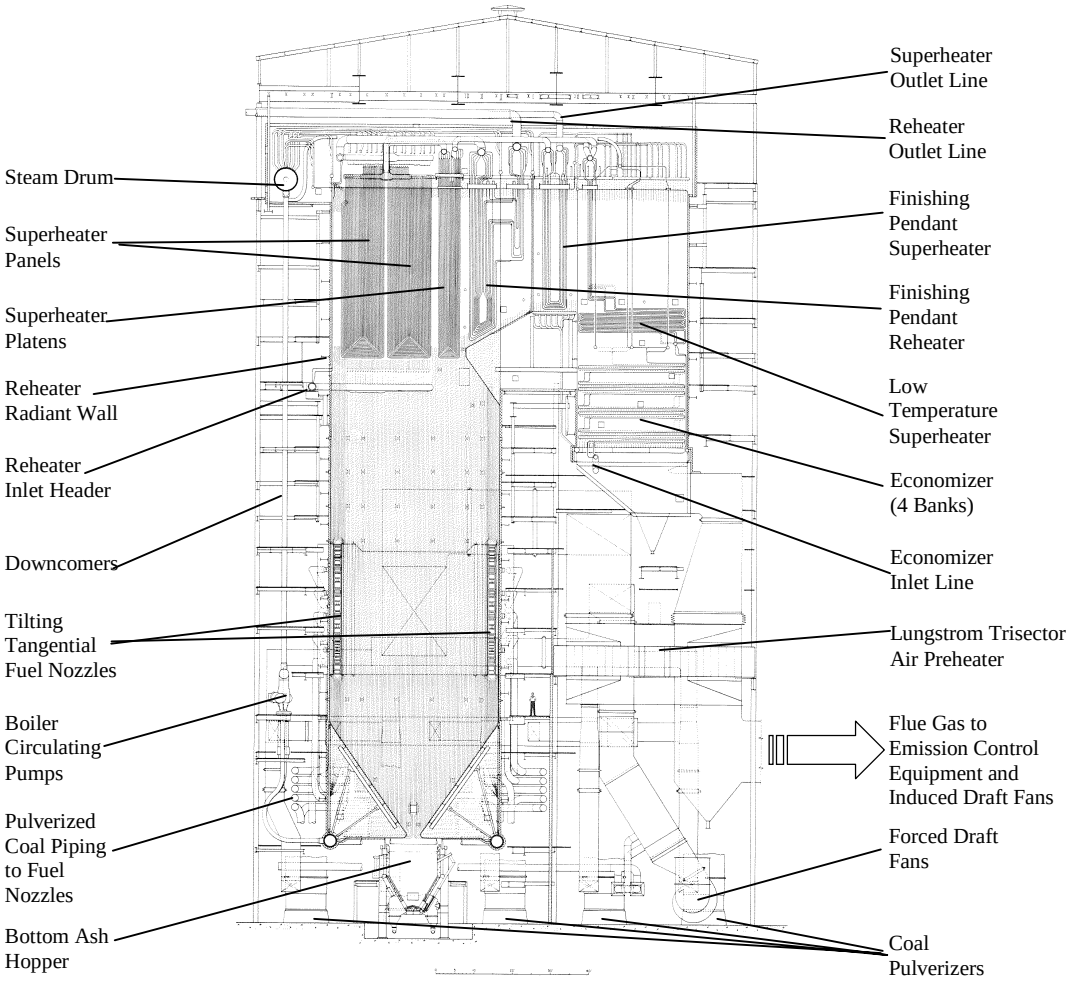

Figure 1: Side Elevation of AEP’s Conesville Unit No. 5

Base Case Analysis.

The Base Case represents the “business as usual” operating scenario and was used as the basis of comparison for the three CO_2 capture concepts investigated in this study. The first step in the development of a Base Case was to set up ALSTOM’s proprietary computer model of the boiler. The computer model was calibrated, using test data supplied by Conesville Plant personnel. The calibrated boiler model was then used for analysis of the Base Case and the three CO_2 capture concepts.

Using the calibrated boiler model and providing it with steam side inputs (mass flows, temperatures, and pressures) from the agreed upon MCR steam turbine material and energy balance, the model was run

and performance was calculated for the Base Case. The simplified gas side process flow diagram for the Base Case is shown in Figure 2.

Steam temperature control was achieved through the use of burner tilt and de-superheating spray. The performance analysis results indicated the reheater circuit required about 3.1% spray to maintain the reheat outlet temperature at the design value. The superheater circuit required about 3.6% spray to maintain the superheat outlet temperature at the design value. The burner tilt was set at –10 degrees, the minimum value the customer uses.

Boiler efficiency was 88.13%, the net plant heat rate was 9,749 Btu/kWh, and overall plant thermal efficiency was about 35%. Auxiliary power and net plant output were 29,700 kW and 433,778 kW, respectively. Carbon dioxide emission was 866,156 lbm/hr or about 1.997 lbm/kWh.

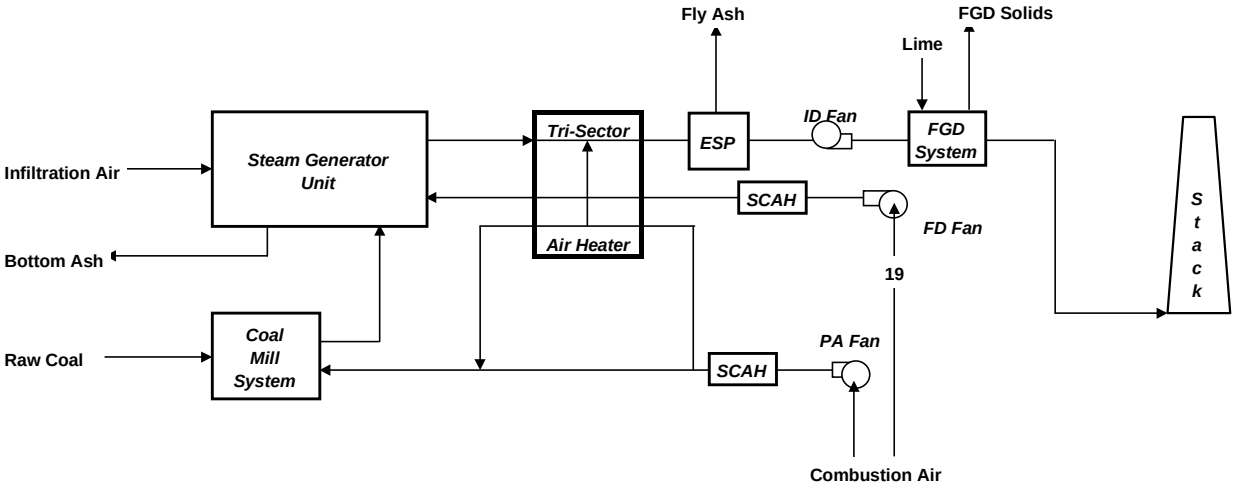

Figure 2: Simplified Existing Power Plant Gas Side Process Flow Diagram

Concept A: CO_2 Separation with Monoethanolamine (MEA) Absorption

Concept A is a process entailing the following: Coal is burned conventionally in air. A commercially proven Kerr-McGee/ABB MEA-based CO_2 recovery process, installed downstream of the flue gas desulfurization unit, is integrated into the power plant to strip CO_2 from the effluent gas stream (containing about 15% CO_2 by volume).

Overall System Description. A simplified process flow diagram for the modified unit is shown in Figure 3. It should be noted that the flue gas desulfurization (FGD) unit was modified with the addition of a secondary absorber to reduce the SO_2 content to about 10 dppmv as required by the amine system downstream. The flue gases leaving the modified FGD system are cooled with a direct contact cooler and ducted to the MEA system where more than 96% of the CO_2 is removed, compressed, and liquefied for usage or sequestration. The remaining flue gases leaving the new MEA system, consisting of primarily oxygen, nitrogen, water vapor and a relatively small amount of sulfur dioxide and carbon dioxide, is discharged to the atmosphere.

Boiler performance for this case was identical to the Base Case. Boiler efficiency was 88.13%. The net plant heat rate, on the other hand, increased significantly to 16,217 Btu/kWh due to steam cycle changes and increased auxiliary power. Hence, the overall plant thermal efficiency was about 21%, or 60% of the Base Case value. Auxiliary power increased to 70,655 kW and the net plant output was reduced to

260,757 kW. Carbon dioxide emission was 31,049 lbm/hr or about 0.119 lbm/kWh (or about 6% of the Base Case).

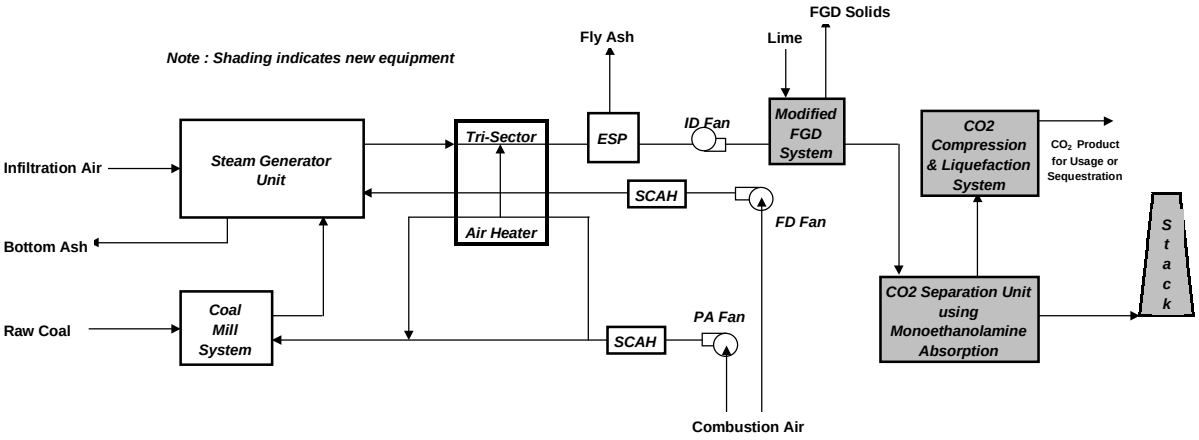

Figure 3: Simplified Gas Side Process Flow Diagram for CO_2 Separation by MEA Absorption (Concept A)

Steam Cycle Modifications and Performance. The steam cycle system for Concept A was modified as described below. About 79% of the IP turbine exhaust is extracted from the IP/LP crossover pipe. This steam is expanded to about 65 psia through a new steam turbine generating 62,081 kW. The exhaust from the new turbine, at about 478 ^{o}F, is de-superheated and then provides the heat requirement for the reboilers of the MEA CO_2 recovery system. The condensate from the reboilers is pumped to the deaerator. The modified existing steam cycle system produces 269,341 kW. The total output from both generators is 331,422 kW. This represents a gross output reduction of 132,056 kW (about 28%) as compared to the Base Case.

Carbon Dioxide Separation and Compression System. The Kerr-McGee/ ABB amine technology is used for the Concept A CO_2 removal system. This system is the most proven of the three processes analyzed in this study. An important feature of this CO_2 recovery technology is its flexibility to operate with boilers or co-generation systems that fire fuels ranging from natural gas to high-sulfur coal and coke. The process tolerates oxygen in the flue gas via the addition of proprietary additives as well as limited amount of sulfur dioxide. Low corrosion rates and minimal loss of the circulating solvent used to absorb CO_2 ensure economical and reliable operation. For cost effectiveness, it was decided to add a secondary absorber to the FGD system and eliminate the causticizer from the front end of the MEA process.

The technology is based on conventional absorption / stripping using 20 wt.% MEA solution (1). The treated gas from the desulfurization system, after cooling and water removal, is sent to an absorber where it is scrubbed with MEA to recover most of the CO_2 (Figure 4). The scrubbed flue gases are vented to the atmosphere after water washing to minimize MEA losses. Rich amine solution from the absorber is preheated

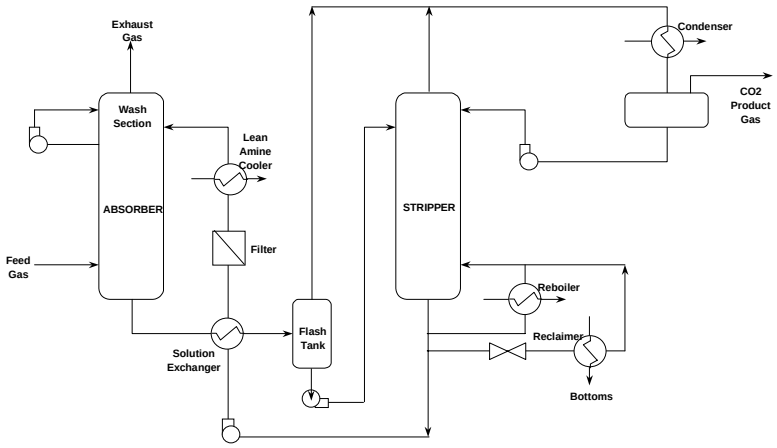

Figure 4: Kerr-McGee/Lummus Crest MEA-Based CO_2 Recovery System

in the solution exchanger against the lean amine solution and then sent to a flash tank. The flashed liquid solution is sent to the stripper and the flashed vapors are combined with the stripper overhead vapors and sent to the condenser where water vapor is condensed. The wet CO_2 product stream leaving the condenser is compressed, cooled, dried, liquefied and pumped to 2000 psig. Water condensed from the stripper overhead is returned to the system. The lean amine solution leaving the solution exchanger is filtered, cooled and returned to the absorber. The system recovers more than 96% of the CO_2.

Auxiliary power requirement for the overall system is 45013 kW. The plot plan required for the equipment is about 5 acres. The ultimate CO_2 liquid product in this study was found to have the following characteristics: CO_2 = 99.95 vol. %; N_2 = 0.05 vol. %; temperature = 82 ^oF; and pressure = 2000 psig. This product would meet the specifications for current pipeline practices (2).

Concept B: CO_2 Separation with Oxygen Firing and Flue Gas Recirculation

The basic concept of the overall system is to replace air with oxygen for combustion in the furnace. A stream of re-circulated flue gas to the furnace is required to maintain thermal balance in the existing boiler between the lower furnace region where evaporation takes place and the convective heat transfer surfaces where steam is superheated and reheated to the required temperature level. This arrangement produces a high carbon dioxide content flue gas which, after leaving the boiler system, is further processed to provide high-pressure carbon dioxide liquid product.

Overall System Description. A simplified system diagram for the modified unit is shown in Figure 5. The system was designed to provide maximum flexibility of operation and facilitates combustion of coal in either air or oxygen and recirculated flue gas mixture environment. Approximately two-thirds of the mass is recirculated to the boiler in order to maintain the thermal balance between heat transferred in the radiant furnace and the convective heat transfer surfaces and to generate required boiler performance. In addition, gas temperatures throughout the unit must be low enough to assure the ash, which is produced from the combustion of the fuel, is maintained in a state where the ash deposits can be easily removed. Additionally, heat flux to the furnace walls and convective pass heat exchangers must be maintained within material limits. For this reason recycled flue gas is supplied to the unit through a combination of new ducts and the existing air ducts. The modified system was designed to generate approximately $3.1x10^6$ lbm/hr of steam, which represents the Maximum Continuous Rating of the unit. Two of the key assumptions used in the development of the material and energy balance were an oxygen stream purity of 99% by weight, and an air infiltration rate equivalent to one % of the total oxygen required for the process.

Boiler efficiency for Concept B was 90.47%, as compared with 88.13% for the Base Case, due to the addition of the Oxygen Heater and Parallel Feedwater Heaters. The net plant heat rate also increased, significantly, to 14,802 Btu/kWh, equivalent to an overall plant thermal efficiency of about 23%**.** This is about 66% of the Base Case value. Total auxiliary power increased to 183,365 kW as a result of the added Air Separation Unit and the CO_2 Compression and Liquefaction System. Net plant output was reduced to 279,691 kW. Carbon dioxide emissions are 51,702 lbm/hr or about 0.185 lbm/kWh (about 9% of the base Case value).

Air Separation Unit. The Air Separation unit (ASU) includes a cryogenic plant for air separation. Economic considerations for this application favored the selection of oxygen stream purity of 99% by weight. Three trains were required to produce the required oxygen mass flow rate of about 8924 tons per day. This system consumes 95,943 kW of electric power or about 21% of the generator output. The plot plan for this equipment requires about 2.5 acres.

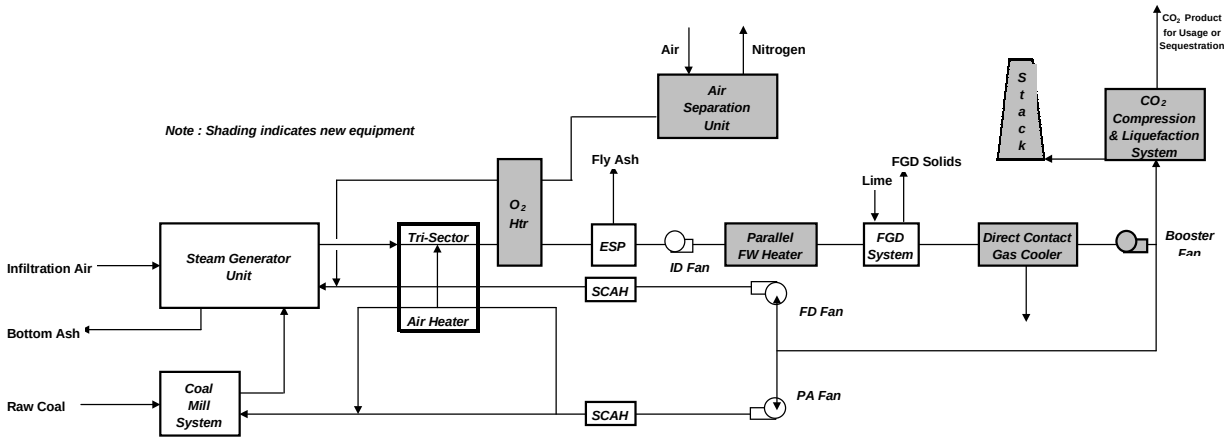

Figure 5: Simplified Gas Side Process Flow Diagram for CO_2 Separation with Oxygen Firing (Concept B)

Boiler Heat Transfer Analysis. The primary objective of the systems analysis task was to develop a system, which would produce high carbon dioxide content flue gas from an existing coal-fired boiler without requiring pressure part modifications to the boiler. In order to assess whether pressure part modifications would be necessary an accurate heat transfer analysis of the boiler was required. The first step was to set up a steady state performance model of the Conesville #5 steam generator unit. After the model was calibrated, as a part of the Base Case analysis, additional adjustments were required in order to obtain an accurate heat transfer analysis with the high carbon dioxide content flue gas of the Concept B system. The combustion process occurs in a non-conventional environment, which produces gases of different physical and thermal properties as compared to the gases with air firing. These gas property differences cause significant differences in the heat transfer processes, which occur within the steam generator unit. Analyses were made to determine the impact of the heat transfer differences on boiler behavior. The ALSTOM Power RHBP model accounts for three modes of heat transfer in the upper furnace and convective pass of the unit (direct radiation, non-luminous radiation and convection).

Heat transfer in the lower and upper furnace regions as calculated by the RHBP is compared in Figure 6. This figure compares heat fluxes (Btu/hr-ft^2) in the lower and upper furnace region between air firing and oxygen firing. Lower furnace results show firing zone heat flux to be about 11% higher with oxygen firing. Upper furnace region results show the reheat radiant wall is about 6% higher and the superheat panels are about 13% higher with oxygen firing. Similarly, the upper furnace waterwall region is about 10% higher.

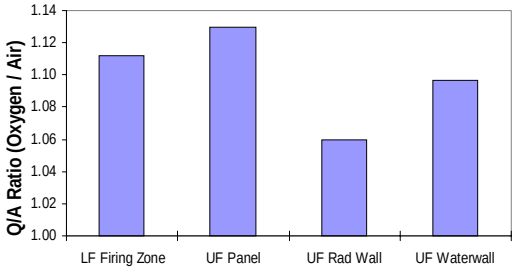

Figure 6: Furnace Region Heat Flux Comparison

Convection Pass Analysis**.** Convective heat transfer in utility steam generator units is dependent upon many of the transport properties of the flue gas (viscosity, thermal conductivity, density, specific heat and others). Additionally, convection depends strongly on gas velocity. With this system, there are significant changes in the flue gas analysis as compared with air firing. These gas analysis changes cause both transport property and gas velocity changes throughout the unit. Significant differences in non-luminous radiant heat transfer are also expected. Of the gases produced by the complete combustion of a fuel, only carbon dioxide, water vapor and sulfur dioxide emit radiation over a sufficiently wide band of wave lengths to warrant consideration. With this system the primary change in the flue gas as compared to air

firing is the large increase in the CO_2 content and decrease in N_2 content. The total heat transfer rates (convective + non-luminous radiation) for the convection pass are shown Figure 7. Increases are calculated to be in the range of 1 to 8% for oxygen firing over the values with air firing.

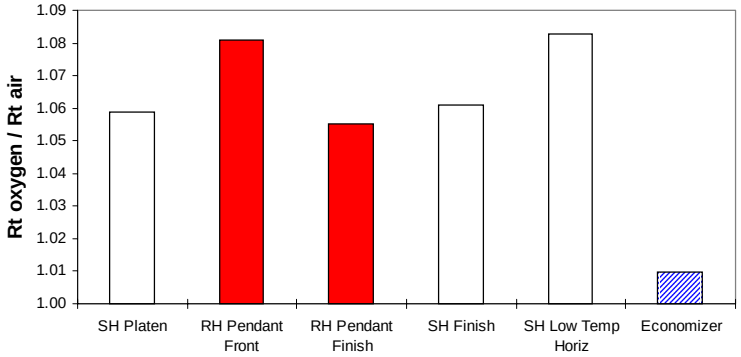

Figure 7: Convection Pass Total Heat Transfer Rate Comparison

Steam temperature control was achieved through the use of burner tilt and de-superheating spray. The performance analysis results indicated the reheater circuit required about 1.45% spray to maintain the reheat outlet temperature at the design value. The superheater circuit required about 0.34% spray to maintain the superheat outlet temperature at the design value. The burner tilt was set at –10 degrees, same as for the Base Case, the minimum value the customer uses.

With the increased heat transfer rates with oxygen firing and similar steam temperature profiles, there was concern regarding metal temperatures throughout the unit. A detailed analysis was, however, beyond the scope of this study. A very brief review of metal temperatures at only a few selected points was done in this study. In general, for the points investigated, the metal temperatures were found to be the same or slightly lower than with air firing. The primary reason for this result was that although the heat transfer rates were slightly higher and the steam temperature profile was similar, the gas temperatures were also lower. This combination yields similar heat flux conditions and ultimately similar metal temperatures.

Boiler System Modifications. It is recommended that the Boiler Island be inspected for potential air leaks into the system and should be sealed to minimize any infiltration. Special attention should be given to all penetrations including seal boxes for convective surfaces, sootblowers, wallblowers, expansion joints, ductwork, fuel piping, fans and windbox. Additionally, new recycle gas ductwork would have to be provided. A new oxygen heater, parallel feedwater heater, and booster fan would also be provided.

Steam Cycle System. The steam cycle system for Concept B was modified slightly with the addition of a low-pressure feedwater heater arrangement in parallel with two low pressure extraction feedwater heaters. The parallel feedwater heater was used to recover additional sensible heat in the flue gas as a result of reduced air heater performance with oxygen firing. The modified steam cycle system produces 463,056 kW with a steam turbine heat rate of 8089 Btu/kWh.

Carbon Dioxide Separation and Compression System. The flue gas stream leaving the flue gas desulfurization system is cooled to 100^{o}F in a direct contact gas cooler. The flue gas stream leaving the cooler is split into two streams with about two thirds recycled back to the boiler and the remaining one third feeding the CO_2 compression and liquifaction system. Because of the oxygen firing of the boiler, the flue gas stream has high enough CO_2 content that simple compression, refrigeration, and rectification can produce a suitable CO_2 product. The system recovers about 94% of the CO_2 with separation occurring between –21 and -48 ^{o}F and 346 psig. Auxiliary power requirements for the system are 57764 kW. The plot plan required is about 3 acres for the CO_2 liquefaction and compression, and direct contact cooling systems. The ultimate CO_2 liquid product for this study concept was found to have the following characteristics: CO_2 = 97.8 vol. %; N_2 = 1.2 vol.%; SO_2 = 215 vppm; O_2 = 9300 vppm; temperature = 82 ^{o}F; and pressure = 2000 psig. The concentration of oxygen in this product is too high for current pipeline operating practices, due to the corrosive nature of the oxygen. Hence, design of the transport pipe to an EOR site for example would have to take this characteristic under consideration.

Concept C: CO_2 Separation by MEA/MDEA Absorption

In Concept C, coal is burned conventionally in air. An ABB designed process comprising an optimized mixture of monoethanolamine (MEA) and methydiethanolamine (MDEA), installed downstream of the flue gas desulfurization unit, is integrated into the power plant to strip CO_2 from the effluent gas stream (containing about 15% CO_2 by volume). The mixture of MEA and MDEA cannot be made to be oxygen-resistant. Therefore, while this process potentially offers an improved system from the standpoint of solvent regeneration energy requirement, it is necessary that the excess oxygen in the flue gas be converted to CO_2 by combustion with natural gas over a De-Oxy catalyst upstream of the solvent contactor.

Overall System Description. A simplified process flow diagram for the modified unit is shown in Figure 8. The operation and performance of the existing Boiler, ESP, and FGD systems are identical to the Base Case and are not affected by the addition of the MEA/MDEA based CO_2 removal system. Heat recovery is provided in the De-Oxy system by generation of high pressure superheated steam, which is expanded through a new steam turbine for additional power generation. The exhaust from this turbine provides part of the feed for the reboilers of the MEA/MDEA system. The de-oxygenated flue gas leaving the De-Oxy system is supplied to the MEA/MDEA system where about 91% of the CO_2 is removed, compressed, liquefied, and is available for usage or sequestration. The remaining flue gases leaving the new MEA/MDEA system absorber, consisting of primarily, nitrogen, water vapor, carbon dioxide, and relatively small amounts of sulfur dioxide and methane, is discharged to the atmosphere through stacks above the absorbers.

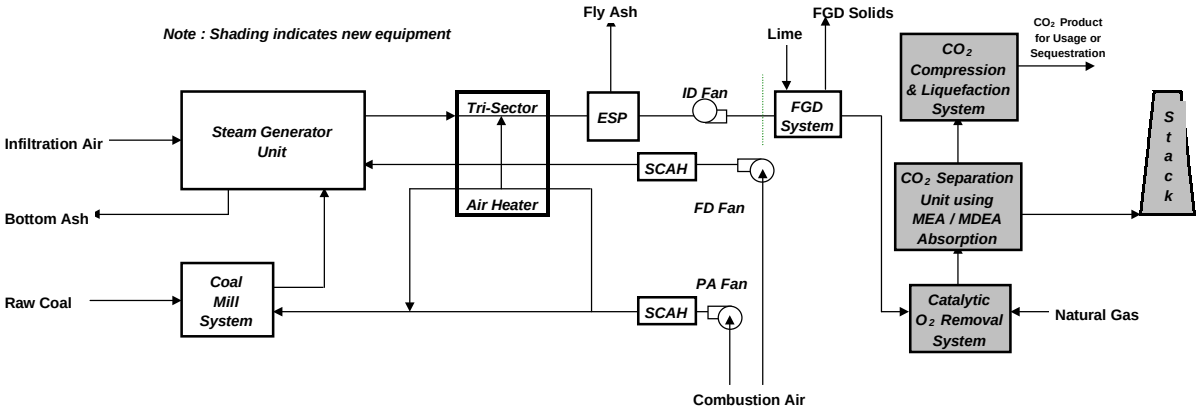

Figure 8: Simplified Gas Side Process Flow Diagram for CO_2 Separation by MEA/MDEA Absorption (Concept C)

Boiler performance for this case was identical to the Base Case. Boiler efficiency was 88.13%. The net plant heat rate increased significantly to 14,916 Btu/kWh due to steam cycle changes and increased auxiliary power, which is equivalent to an overall plant thermal efficiency of about 22.9% or about 65% of the Base Case. The total auxiliary power is increased to 89,738 kW and the net plant output was reduced to 341,551 kW. Fuel heat input to the overall system is increased by about 20% as compared to the Base Case. The fuel heat input to the boiler is the same as in the Base Case and Concept A; however, the De-Oxy system consumes a significant quantity of natural gas. Carbon dioxide emission was 89,915 lbm/hr, or about 0.263 lbm/kWh (about 13% of the Base Case).

Steam Cycle Modifications and Performance. The steam cycle system for Concept C is modified as described below. About 45% of the IP turbine exhaust is extracted from the IP/LP crossover pipe. This steam is expanded to about 65 psia through a new letdown steam turbine generating 36,343 kW. The exhaust from the letdown turbine, at about 478 ^{o}F, is de-superheated and then provides most of the heat requirement for the reboilers of the MEA/MDEA CO_2 capture system. High temperature heat recovery is provided in the De-Oxy system between two catalytic combustors by the generation of high pressure

superheated steam. This steam is then expanded through a second new steam turbine for additional power generation. This turbine generates 37,751 kW. The exhaust from this turbine provides about 20% of the feed for the reboilers of the MEA/MDEA system. Low temperature heat recovery is provided in the De-Oxy system with a low pressure feedwater heater which is located in a feedwater stream which is in parallel with the three existing low pressure extraction feedwater heaters. The modified existing steam cycle system produces 357,196 kW. The total output from the modified steam cycle is 431,290 kW. This represents a gross output reduction of 32,188 kW, which is about 7% of the Base Case output.

Carbon Dioxide Separation and Compression System. CO_2 recovery from the flue gas is accomplished by using a combination of primary and tertiary amines. They are specifically chosen to be more energy efficient to remove the absorbed CO_2. Another difference between the amines used in this concept and in Concept A is that the amines need not be oxygen resistant. The need for oxygen resistance is no longer necessary because the oxygen is converted to CO_2 by combustion with natural gas over a De-Oxy catalyst upstream of the amine contactor. After the carbon dioxide is extracted, it is liquefied by compression and refrigeration. The system recovers about 91% of the CO_2. Auxiliary power requirements for the system are 61,898 kW. The plot plan required for this equipment is about 7 acres. The ultimate CO_2 liquid product in this study was found to have the following characteristics: CO_2 = 99. 97 vol. %; N_2 = 0.03 vol.%; temperature = 82 ^oF; and pressure = 2000 psig. This product would meet the specifications for current pipeline practices.

COMPARISON WITH PRIOR WORK

Table 1 summarizes the pertinent technical results determined in this study. Figures 9 and 10 compare net plant heat rates and CO_2 emissions for this study with selected results from the literature (3,4). This study shows a significantly greater impact on net plant heat rate, for the MEA process, than David and Herzog show. A partial explanation for this difference can be seen in Figure 10. The present work shows higher CO_2 removal (kg/kWh) than David and Herzog show. With respect to oxy-fuel firing, it is seen that producing the oxygen in a ceramic membrane system leads to an improvement in net plant heat rate of more than 20% over the cases whereby the cryogenic method is used to produce oxygen (e.g., 10501 vs. 13796 Btu/kWh).

Table 1
Summary of Performance for Existing and CO_2 Capture Study Cases

Quantity	(Units)	Original Plant (Base Case)	Concept 3A MEA	Concept 3B O2 Fired	Concept 3C MEA/MDEA
Boiler Paramaters					
Coal Heat Input (HHV)	(10^6 Btu/hr)	4228.7	4228.7	4140.0	4228.7
Natural Gas Heat Input (HHV; De-Oxy System)	(10^6 Btu/hr)	---	---	---	866.0
Total Fuel Heat Input (HHV)	(10^6 Btu/hr)	4228.7	4228.7	4140.0	5094.7
Boiler Efficiency	(percent)	88.13	88.13	90.47	88.13
Steam Cycle Paramaters					
Existing Steam Turbine Generator Output	(kW)	463478	269341	463056	357196
CO_2 Removal System Turbine Generator Output	(kW)	---	62081	---	36343
De-Oxy System Turbine Generator Output (Concept C)	(kW)	---	---	---	37751
Total Turbine Generator Output	(kW)	463478	331422	463056	431290
Total Auxiliary Power	(kW)	29700	70665	183365	89738
Net Plant Output	(kW)	433778	260757	279691	341551
Overall Plant Performance Paramaters					
Net Plant Efficiency (HHV)	(fraction)	0.350	0.210	0.231	0.229
Normalized Efficiency (HHV; Relative to Base Case)	(fraction)	1.000	0.601	0.659	0.654
Net Plant Efficiency (LHV)	(fraction)	0.367	0.220	0.241	0.242
Net Plant Heat Rate (HHV)	(Btu/kWh)	9749	16217	14802	14916
Net Plant Heat Rate (LHV)	(Btu/kWh)	9309	15485	14134	14107
Overall Plant Emissions					
Carbon Dioxide Emissions	(lbm/h)	866102	31049	51702	89915
Specific Carbon Dioxide Emissions	(lbm/kWh)	1.997	0.119	0.185	0.263
Normalized CO2 Emissions (Relative to Base Case)	(fraction)	1.000	0.060	0.093	0.132
Avoided Carbon Dioxide Emissions (as compared to Base)	(lbm/kWh)	---	1.878	1.812	1.733
Specific Carbon Dioxide Emissions	(kg/kWh)	0.906	0.054	0.084	0.120
Avoided Carbon Dioxide Emissions (as compared to Base)	(kg/kWh)	---	0.852	0.823	0.787

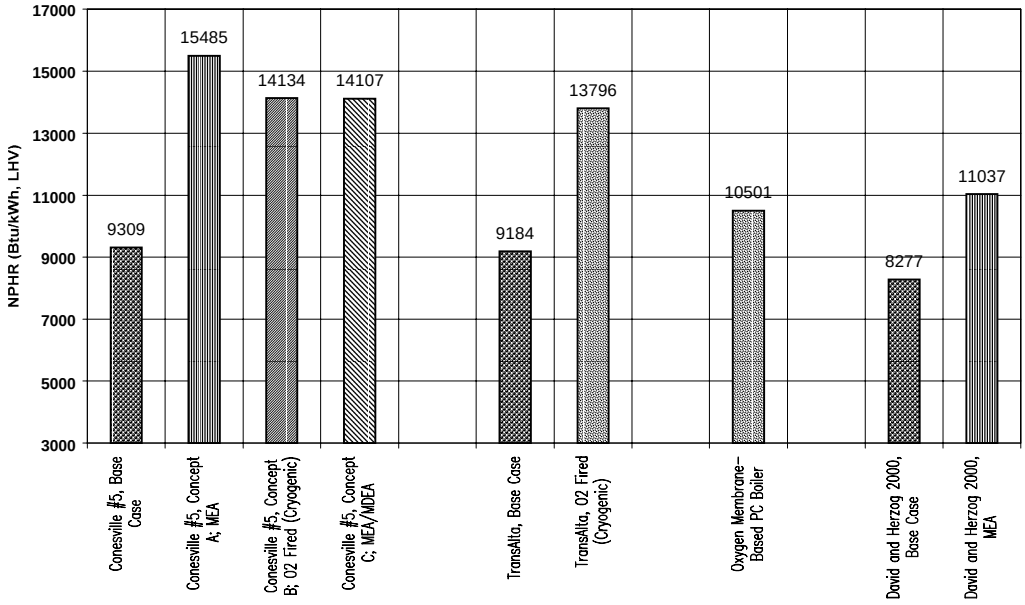

Figure 9: Comparative Coal Power Net Plant Heat Rate Results

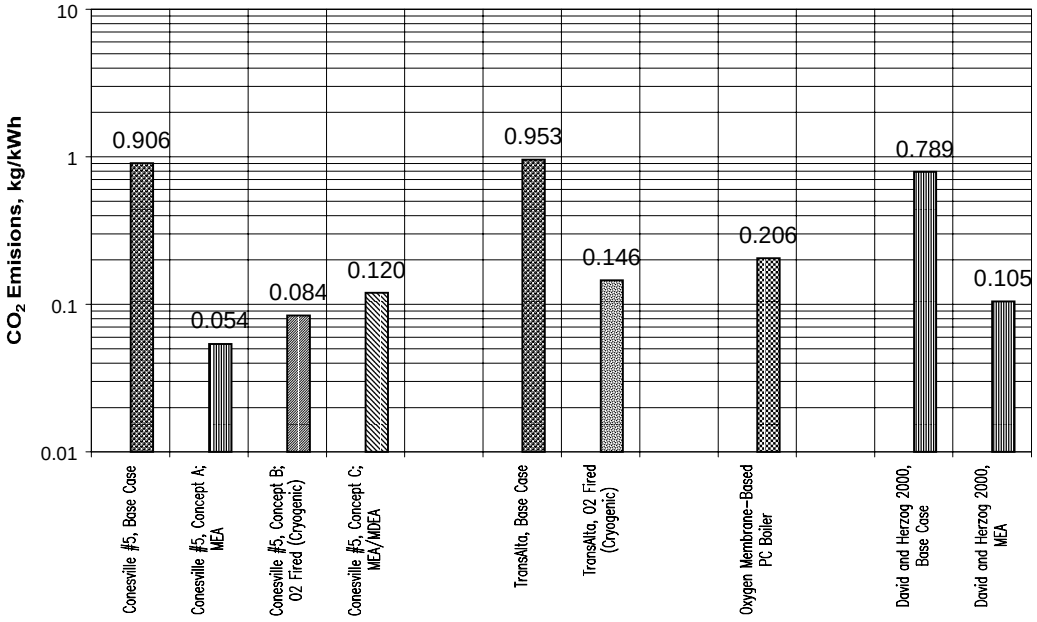

Figure 10: Comparative Coal Power CO_2 Emissions

SUMMARY AND CONCLUSIONS

- No major technical barriers exist for retrofitting AEP's Conesville Unit #5 to capture CO_2 for any of the three concepts considered under this study
- Nominally, 5-7 acres of new equipment space is needed and is approximately 1500 feet from the Unit #5 stack on the existing ~200 acre power plant site.
- Energy requirements and power consumption are high, resulting in significant decrease in overall power plant efficiencies (HHV basis), ranging from 21 to 24% as compared to 35% for the Base Case.
- Specific carbon dioxide emissions were reduced from about 2 lbm/kWh for the Base Case to 0.12 – 0.26 lbm/kWh for the study cases. Recovery of CO_2 ranged from 91 to 96%.

ACKNOWLEDGMENTS

The authors appreciatively acknowledge the following people for their contributions to the successful performance of the work presented herein: Mark Borman and Tom Ross of AEP Conesville Plant for providing field unit information; Michelle Fugate, Lorraine Miemiec, and Roland Tetreault of ALSTOM Power's Boilers and Environment Segment for providing FGD performance prediction, boiler performance prediction, and design graphics, respectively. The financial support of this project by OCDO (Contract No CDO/D-98-8), DOE National Energy Technology Laboratory (Contract No DE-FC26-99FT40576), ALSTOM Power Inc. and ABB Lummus Global Inc. is also appreciated. The in-kind financial support of the project by American Electric Power is greatly appreciated.

REFERENCES

1. Barchas, R. and Davis, R., "The Kerr-McGee/Lummus Crest Technology for the Recovery of CO_2 from Stack Gases," Presented at the First International Conference on Carbon Dioxide Removal, Amsterdam, The Netherlands, March 4-6, 1992

2. Dakota Gasification Company, "Carbon Dioxide Specifications," http://www.dakotagas.com/specs/co2spec.htm

3. Davis, J. and Herzog, H., "The Cost of Carbon Capture," Presented at the MIT Sequestration Forum, Cambridge, MA, October 31 – November 1, 2000

4. Palkes, M., Liljedahl, G., Nsakala, N., McDonald, M., and Gupta, J.C., "Preliminary Design of a CO_2/O_2 Combustion Retrofit To an Existing Coal-Fired Boiler for CO_2 Extraction,' Presented at Electric Power Gen '99 Conference, Baltimore, MD, April 20-22, 1999

EXPERIMENTAL AND COMPUTATIONAL STUDIES OF FLUID FLOW PHENOMENA IN CARBON DIOXIDE SEQUESTRATION IN BRINE AND OIL FIELDS

Chuang Ji (chuang.ji@netl.doe.gov)
National Energy Technology Laboratory
Department of Energy, Morgantown, WV 26507-0880
BOX 5725 Clarkson University
Potsdam, NY 13699

Goodarz Ahmadi (ahmadi@clarkson.edu)
BOX 5725 Clarkson University
Potsdam, NY 13699

Duane H. Smith (duane.smith@netl.doe.gov)
National Energy Technology Laboratory
Department of Energy, Morgantown, WV 26507-0880

INTRODUCTION

Sequestration of CO_2 by injection into deep geological formations is a method to reduce CO_2 emissions into the atmosphere. However, when CO_2 is injected underground, it forms fingers extending into the rock pores saturated with brine or petroleum. This flow instability phenomenon, known as viscous fingering, is significant for CO_2 sequestration because it will govern the available volume for CO_2 storage in the deep formation. Thus a greater understanding of viscous fingering could ultimately lead to increased capacities for CO_2 sequestration.

In our study, an experimental method is developed for providing a fundamental understanding of geological sequestration (Ogunsola, et al., 2000). In this experiment, a flow cell, which is an artificial porous medium made by etching channels of random width into glass plates, is used to simulate the CO_2 displacement of brine inside the opaque rock pores. Since the flow cell is transparent, the viscous fingering can be observed during the gas displacement of water through the flowcell. Images of the flow can be recorded and used to analyze the flow patterns and calculate saturations of water and gas. The pressure drop through the flow cell can also be measured and the relative permeability can be calculated.

To provide predictions and an explanation of the experimental results, a numerical simulation of this experiment is also conducted with FLUENT^{TM} (a computer code for fluid flow). Here a "flow cell" with square-lattice grids of square cross-section flow channels is studied numerically. The geometry of the "flow cell" and the width of the channels are close to those of the physical flow cell. The boundary conditions, such as the inlet flow rate and the outlet pressure are chosen to be similar to the experimental conditions. The VOF free surface model of FLUENT^{TM} Code is used in the analysis. This model is appropriate for studying two or more immiscible fluids with or without surface tension (Fluent User Guide, 1994). In this study, the simulations are performed for different fluid viscosity ratios with zero surface tension. Therefore the analysis is applicable to miscible fluids and/or the cases that the surface tension between the two immiscible fluids is very small.

The advantage of the computational model is that it provides the magnitudes of pressure, velocity, saturation and other properties of the fluid phases at each grid of the "flowcell." The data may then be used for evaluating the relative permeability of different phases in the flow cell. The study shows that the relative permeability is a strong function of saturation. Furthermore, the relative permeability also varies with the flow pattern and the viscosity ratio of the fluid phases.

OBJECTIVE

The objective of this project is to improve the efficiency of CO_2 geological sequestration in oil fields and brine saturated fields, to provide a more accurate description of two-phase flow in sequestration, and to develop a better understanding of the displacement of oil or brine by CO_2.

APPROACH

In this project, first a laboratory experiment is conducted. A flow cell, which is an artificial transparent porous medium, is used in the experiment. Pressure and flow rate of injected gas and displaced water are measured. The images of viscous fingering in the flow cell are recorded and analyzed to obtain residual saturations of gas and relative permeabilities of water and gas. Variations of flow pattern and relative permeability with the fluid properties, such as viscosity and density, and injection conditions, such as gas flow rate, are studied.

A numerical simulation of the experiment is also conducted with the FLUENT™ computational code. The multiphase flow model for two immiscible fluids is used to simulate the experimental conditions in the flow cell. The numerical results are to be compared with the experimental results and those obtained from other numerical models, such as pore-level model of CO_2 sequestration in oil fields and brine fields (Bromhal, et al., 2001; Ferer, et al., 2001).

PROJECT DESCRIPTION

EXPERIMENTAL SECTION

The experimental flow system, which is shown in Figure 1, consists of a flow cell, which simulates the porous medium, a syringe pump, which provides a constant-volume-rate injection of gas into the flow cell, a pressure transducer for measuring the pressure drop across the flow cell, and a balance for measuring the mass of displaced liquid.

The flow cell is made by etching channels of random width into a glass plate and fusing a second, flat plate to it, thereby creating a network of enclosed channels connected to inlet and outlet manifolds. Two flow cells having different channel widths were used in this study: Cell #1, with channel width uniformly distributed from 175-575 m, and Cell #2, with channel widths from 260-1305 m.

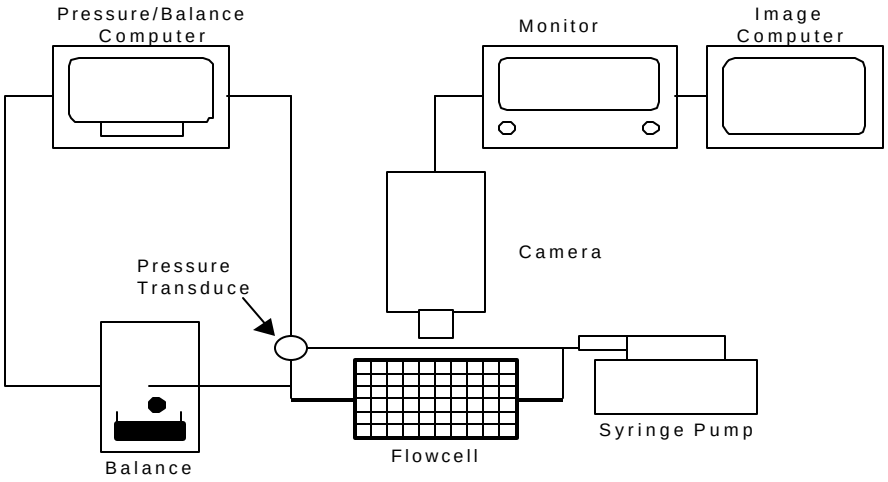

Figure 1. Experimental flow system

COMPUTATIONAL SECTION

A computational model for the "flow cell" is developed, where a total of 3 206 206 grids were used. The square-lattice channels with an average width of 200 microns are distributed uniformly in the computational cell, with the top and bottom layers being "sealed" as boundaries. At the initial time the "flow cell" is flooded with fluid 1. Then fluid 2 is injected from

the inlet on the left side into the flow cell with a constant flow rate and the fluid 1 is displaced out of the flow cell from the outlet on the right hand side.

RESULTS

This section presents results from experiments and numerical simulations with FLUENT^{TM} . Pictures of the flow patterns in experimental and numerical simulations are shown, the phase permeabilities of fluid 1 and 2 are computed, and the relation between phase permeabilities and saturation is presented.

Figure 2 shows the flow pattern formed by injection of gas into a water-saturated cell. The flow cell is horizontal; and the cell inlet is on the left and the outlet is on the right. The air injection rate is roughly 0.5ml/min and the picture is taken at 10s after gas began to flow into the cell. In this figure, the bright area is occupied by gas and the water is in the dark area. It is seen that the gas penetrated into the flow cell and forms an irregular fractal interface with water.

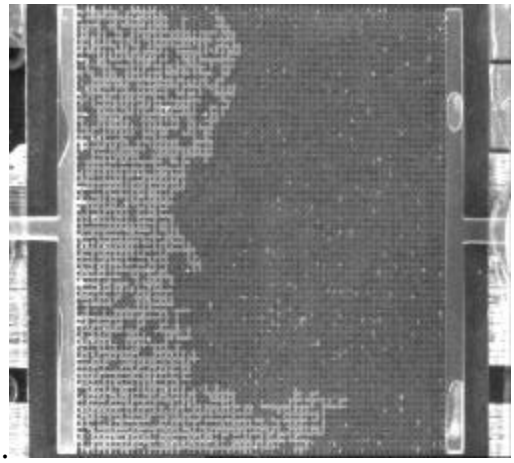

Figure 2. Picture of flow pattern in flow cell for a gas injection rate of 0.5ml/min at 10s.

Figure 3 shows a sample simulation result of the saturation condition in the “flow cell” after fluid 2 is injected into the “flow cell” for 10.5s. Here the viscosity ratio of fluid 1 to 2 is 58, the density ratio is 1000, and the surface tension is zero. The injection rate of fluid 2 is 0.5ml/min. In this figure, saturation of fluid 2 increases form 0 to 1 as the color of the channel

varies from dark blue to red. It is also seen that fluid 2 percolates into the "flow cell" with several "fingers", some of which have penetrated across the "flow cell".

It is also observed that an irregular interface between fluids 1 and 2 forms in the cell. The pattern shown in Figures 2 and 3 clearly illustrates the "viscous fingering" phenomenon that is observed in CO_2 sequestration.

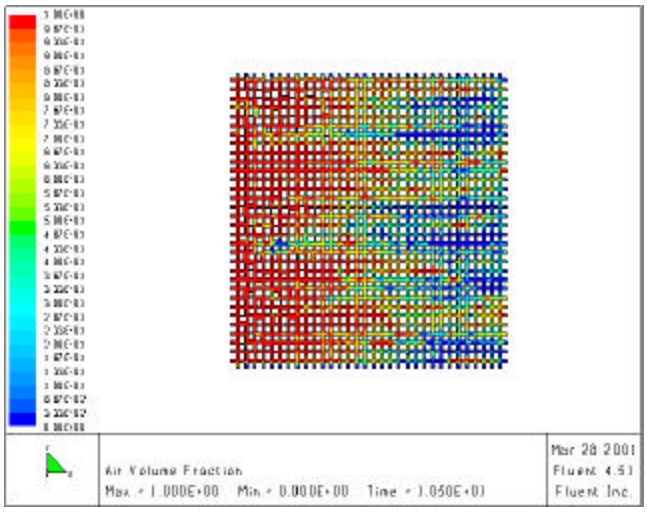

Figure 3. Variations of volume fraction of fluid 2 in the simulated flow cell.

To analyze the simulation data, a "moving average" method is used. Here a moving "window" of 206 16 grids is considered and moving averages across the "flow cell" are evaluated. Average saturation, pressure drop across the window, and velocities of fluid 1 and 2 in each block are computed. In Figure 4, the average saturation of fluid 1 and fluid 2 are shown for each block. Here the average saturation is evaluated using

$$S_n = \frac{\sum_{i=1}^{16}\sum_{j=1}^{206} s_{nij} l_{ij} w_{ij}}{\sum_{i=1}^{16}\sum_{j=1}^{206} l_{ij} w_{ij}} \qquad (1)$$

where l_{ij} and w_{ij} are, respectively, the length and width of each grid, and S_n refers to the average saturation of fluid 1 or 2 at each block. In Equation (1) and in the subsequent analysis subscript n = 1 or 2 corresponds to fluids or 2, respectively.

Figure 4 shows that the average saturation of fluid 2 decreases gradually from the left side to the right side of the "flow cell," while the saturation of fluid 1 increases

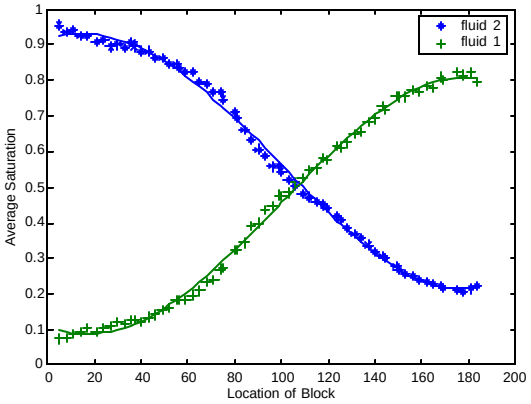

Figure 4. Average saturation of fluid 1 and 2 at each block.

with an opposite trend. Variations of computed saturation in Figure 4 are similar to those seen in Figure 3.

Similarly, the average velocities of fluid 1 and 2 across the cell are evaluated by a moving averaged defined as

$$V_n = \frac{\sum_{i=1}^{16} \frac{\sum_{j=1}^{206} f_{nij} s_{nij}}{\sum_{j=1}^{206} l_{ij}}}{16} \qquad (2)$$

where V_n refers to the average superficial velocity of fluid 1 or 2, and f_{nij} is the flow flux in the major flow direction of fluid 1 or 2 at each grid.

Figure 5 shows variations of the average superficial velocity across the cell. It is seen that average velocity of fluid 2 decreases from the inlet side toward the outlet, while the average velocity of fluid 1 increases as the outlet is approached.

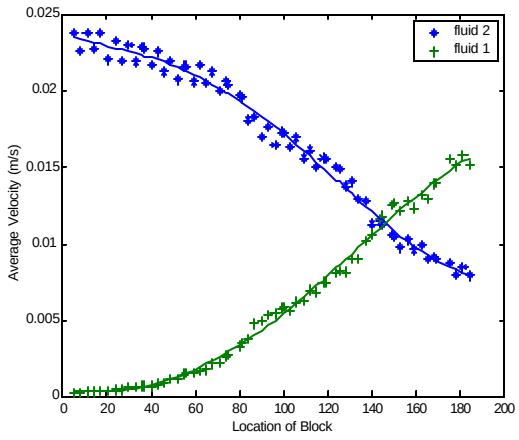

Figure 5. Average velocity of fluid 1 and 2 at each block.

To compute the pressure drop variations across the cell, first the average pressure at the inlet and outlet of each block are evaluated. That is

$$P_{im} = \frac{\sum_{j=1}^{206} p_{mj} l_{mj}}{\sum_{j=1}^{206} l_{mj}} \qquad (3)$$

The pressure drop of each block is given by

$$P_i = P_{iI} \quad P_{iO} \qquad (4)$$

where P_m refers to the average pressure at inlet or outlet of each block. Here m = I denotes inlet and m = O corresponds to outlet, and p_{im} is the pressure at each grid of inlet or outlet section of the moving average block. P_i is the pressure drop across each (moving average) block,

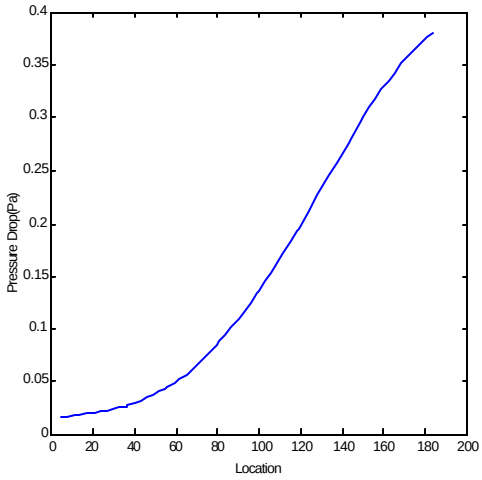

Figure 6. Pressure drop at each block.

Figure 6 presents the pressure drop across each moving averge block. It is seen that the pressure difference between the inlet and outlet of each block increases gradually across the "flow cell."

According to Darcy's law, the phase permeabilities of fluid 1 and 2 are defined as

$$k_{ni} = \frac{V_i m_n}{P_i / L_i} \tag{5}$$

where k_n is the phase permeability, $_n$ is the viscosity and L_i is the width of each block. Plots of phase permeability of fluid 1 and 2 versus saturation of fluid 1 are presented in Figure 7. It is observed that the phase permeability of fluid 2 decreases sharply as the saturation of fluid 1 increases. This implies that in the parts of the cell that are mostly occupied by fluid 2, the relative permeability of fluid 1 is quite low. In contrast, the phase permeability of fluid 1 increases sharply its saturation increases.

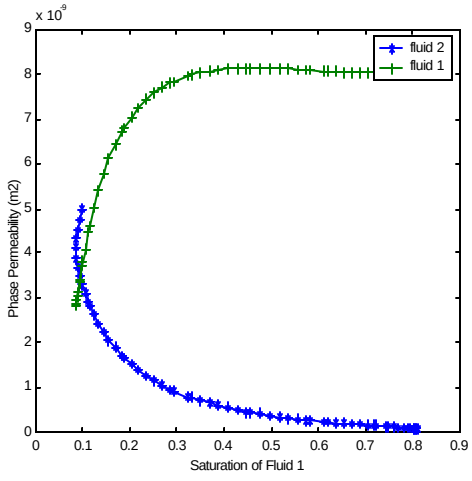

Figure 7. Permeabilities of fluid 1 and 2 for different saturation of fluid 1.

BENEFITS

The present experimental approach provides a visible image of the flow pattern during the displacement of one fluid by another. The process can be observed and recorded to provide detailed information of the nature of multiphase flows in porous media. The laboratory data can then be used to test a variety of different computational models. The computational model also solves the exact dynamical equations for a viscous flow in small channels. Therefore, the model can accurately account for the viscous effects of the multiphase fluids flows in porous media. Extensions of the present study could also be used for assessing the limitations of the Darcy flow model for sequestration of CO_2 in formations saturated with oil and/or brine.

FUTURE ACTIVITIES

The future experimental study includes the further development of experimental methods to improve the accuracy of measurement of pressure and flow rate. Another important aspect is to conduct the experiment with different orientations of the flow cell. The plan is to repeat the experiment with the flow cell set horizontally or vertically to measure the effect of gravity on the flow pattern.

Development of more detailed computer simulations is also an important part of the future study. We plan to study effects of the flow cell geometry and properties of different fluid phases, as well as injection conditions. We also plan to use the FLUENT^{TM} code to develop a refined computational model of the flow cell and account for the surface tension and capillary effects as well as contact angle in addition to the viscous effects. The goal is to provide a better understanding of the effects flow patterns and residual saturation on the relative permeability under various conditions.

REFERENCE

1. Bromhal, G.S., Ferer, M. and Smith, D.H., (2001) "Pore-Level Modeling of Carbon Dioxide Sequestration in Oil Fields: A Study of viscous and Buoyancy Force", Proceedings of 1st National Conference on Carbon Sequestration, Washington, DC, May 14-17, 2001.
2. Ferer M., Bromhal, G.S. and Smith, D.H., (2001) "Pore-Level Modeling of Carbon Dioxide Sequestration in Brine Fields," Proceedings of 1st National Conference on Carbon Sequestration, Washington, DC, May 14-17, 2001.
3. Fluent Users Guide, Version 4.52, Fluent Corp., Letanon, NH (1994)
4. Ogunsola, O., Ramer, E. and Smith, D.H., (2000) "Analysis of Viscous Fingering in Two-Dimensional Flow Cell by Fractral Dimension," Fuel Division preprint, Washington, DC, August 20-24,2000.

Pore-Level Modeling of Carbon Dioxide Infiltrating the Ocean Floor

Grant S. Bromhal, Duane H. Smith, US DOE, National Energy Technology Laboratory, Morgantown, WV 26507-0880; M. Ferer, Department of Physics, West Virginia University, Morgantown, WV 26506-6315

Ocean sequestration of carbon dioxide is considered to be a potentially important method of reducing greenhouse gas emissions (US DOE, 1999). Oceans are currently the largest atmospheric carbon dioxide sink; and certainly, enough storage capacity exists in the oceans to hold all of the CO_2 that we can emit for many years. Additionally, technologies exist that allow us to pump liquid CO_2 into the oceans at depths between one and two kilometers for extended periods of time and five times that deep for shorter durations.

The biggest unknown in the ocean sequestration process, however, is the fate and transport of the carbon dioxide once it is released. It could sink or float, depending on its density and the formation of hydrate, or it could react with sediments on the ocean floor. Over geologic time, any carbon dioxide anthropogenically introduced into the oceans will probably diffuse in the ocean water and cause a very small percent change in the total dissolved carbon concentration; however, the near-term local effects of releasing highly-concentrated CO_2 in the ocean are not well-understood.

Deep ocean storage is a widely-discussed potential method of carbon dioxide sequestration. In this scenario, one pumps liquid CO_2 at depths below which pure carbon dioxide is denser than water. Because the CO_2 is heavier, it would not return to the surface due to buoyancy forces. Unfortunately, such a system would require a very deep injection, on the order of 3km below sea level. It has been posited that such an injection will create the existence of a carbon dioxide “lake” on the ocean floor (US DOE, 1999). Although such a lake would not rise due to buoyancy forces, it could be translated horizontally by deep ocean currents over hundreds of years.

However, the carbon dioxide plume is not likely to stop at the ocean floor, but may continue downward through the porous sediment. It has long been known that when a connate fluid is vertically displaced by a denser, less-viscous fluid, significant fingering will occur in the invading front, and the CO_2 might penetrate the sea sediments to a much more significant distance than one would initially expect. A better understanding of the fluid displacement process in sea water-saturated porous media may aid in future modeling of the fate of liquid CO_2 beneath the ocean floor.

Introduction

Two-phase flow in porous media has long been a topic of interest in the scientific and engineering community, particularly in the environmental and petroleum fields. Generally, flow on a large scale is modeled by using a form of Darcy’s law to describe the movement of each phase through the medium. However, recent studies have shown

that in certain well-defined limits, the compact flow assumptions of Darcy's law are not accurate, at least on a small scale. A number of pore-level analytical and computer models, such as diffusion-limited aggregation and invasion percolation, have been developed to describe the fractal growth patterns known to occur in special flow situations (Feder, 1988; Ferer and Smith, 1994; Ewing and Berkowitz, 1998).

We have developed a rule-based, pore-level network model (similar to diffusion-limited aggregation and invasion percolation) to describe the processes of two-phase, immiscible, incompressible, non-wetting fluid invasion into porous media (Bromhal, 2000). This model generates random distributions of pore radii to simulate porous medium properties and incorporates fluid viscosities, fluid densities, and interfacial tension between the fluids into the flow calculations.

Objective

One objective of this work is to predict the proportion of CO_2 deposited in a "lake" on the ocean floor that will be trapped in the sediments beneath the ocean bottom. Additionally, we compare the rate of infiltration into the porous medium to that of dissolution into seawater. These relationships rely heavily on the type of soil and the height of the "lake" above the ocean floor. Of course, many others factors may affect the infiltration, including the formation of hydrates. A more complete discussion may be found in the next section.

Approach

Using the rule-based model, we simulate the infiltration of a liquid CO_2 plume into the sediments on the deep sea floor. Since carbon dioxide becomes denser than water only at depths approximating 3km and deeper, the depths being considered are from 3km to 6km below sea level. At these depths, the ambient pressure is greater than 300atm; additionally, a large percentage of the deep ocean floor falls within this range.

For this work, we consider a plume of pure liquid CO_2 sitting on the ocean floor, as shown in Figure 1. The carbon dioxide on the sea floor will be under a greater pressure than the surrounding ocean water because of the pressure head from the plume. If the pressure head is great enough, it will overcome the capillary pressure in the sediment and the CO_2 will infiltrate the ocean bottom. For all of the simulations in this work, an average throat radius of 50μm is assumed. This corresponds to a fine sand or a silty sand soil type. While some ocean sediments are smaller than this (fine silt or clay), a reduction in pore size would require a proportional increase in overburden pressure, and the size of a CO_2 plume required to penetrate the soil under such conditions is considered unrealistic. Experimental values of viscosity, density, and interfacial tension for carbon dioxide and the carbon dioxide-water mixture are presented in Table 1.

Other concerns are the formation of hydrates and chemical reactions between CO_2 and sediment. Depths below 3km are well within the hydrate formation region (Teng et al, 1997), so CO_2 hydrate will form relatively quickly in the bulk. However, it will not form as quickly in the sediment pores, and recent studies suggest that a thin fluid layer exists between the hydrate shell and solid surface (Tabe et al, 2000) so that the hydrate

will not block flow in the throats under such pressure differences. If ocean sediment reacts with the CO_2, it should aid in sequestration by binding the carbon dioxide in carbonates or other substances (Harrison et al., 1995). To be conservative, we do not include such reactions in our simulations.

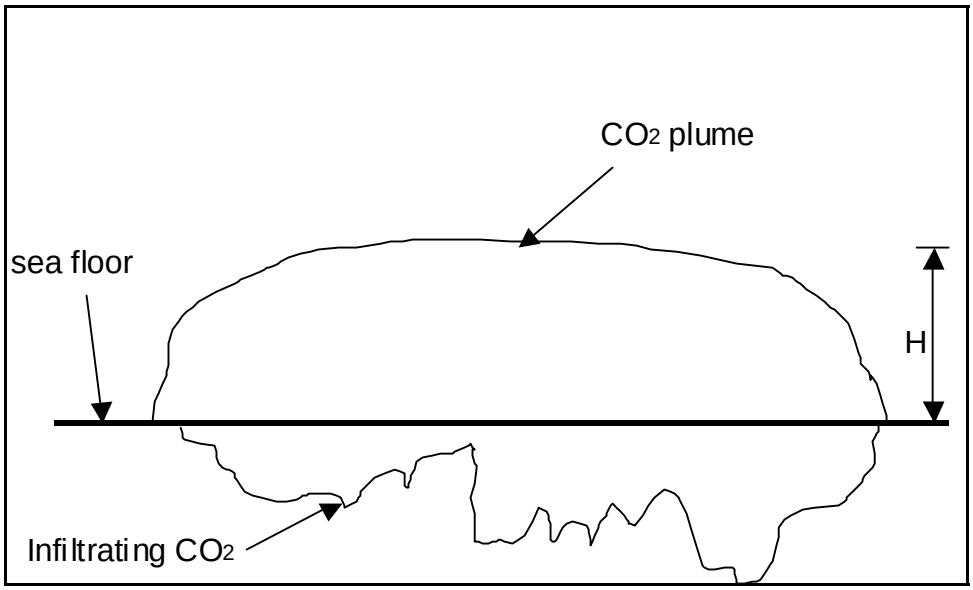

Figure 1. Diagram of a CO_2 plume on the ocean floor.

A 100x100 square network is simulated for the ranges of parameters shown in Table 1 at depths of 3km and 6km. An average surface tension of 22 mN/m is used, as the difference between 21 and 23 mN/m is small. For each depth, the head of the carbon dioxide plume, H, is varied up to 10m thick.

Table 1. Physical properties of CO_2 and CO_2-water interface at high pressure, low temp.

	Surface tension[1] (mN/m)	**Density[2,3] (g/cm3)**	**Viscosity[3] (g/cm-s)**
3km	21-23	1.05	0.0014
6km	21-23	1.11	0.0018

[1]Chun and Wilkinson (1995) [2]Angus et al. (1976) [3]Michels et al. (1957)

Model Description

The model that we have developed is a pore-level network model, akin to cellular automata, that simulates non-wetting fluid invasion in porous media. A set of simple rules, based on the physics of the flow through each throat, defines how the invading fluid moves through the matrix. Modifications to the local rules have been made in an attempt to capture the global behavior of the system.

Because of its power and flexibility, such a model has great potential for describing the behavior of two-phase fluid flow across the entire range of important dimensionless parameters (Lenormand et al, 1988; Held and Illangasakare, 1995). It is fast enough that a typical 100x100 network simulation goes to breakthrough in minutes. However, this significant time savings comes at the cost of an imperfect representation of

the physics of the two-phase flow (in the form of an inexact pressure field). The velocity used in the model is only an estimation of the velocity than can be calculated in a mechanistic model. However, over a large number of simulations on multiple randomly-generated porous media realizations, the approximations used in the program should be adequate.

The porous pore structure is modeled as an *M x N* square matrix of pores (nodes) and a similar matrix of both vertical and horizontal throats (connections) as shown in Figure 1. A similar network has been used by many others (Lenormand et al., 1988; Blunt et al., 1992; Dullien, 1992; Ferer and Smith, 1994; Aker et al., 1998). Throats have radii but not volume, and pores have both. Variability in the soil structure is introduced through a random sampling of throat sizes. The radii of the horizontal and vertical throats (RH and RV in Figure 2) can be generated randomly from any closed-form probability distribution, though only uniform(0,1) distributions have been used in the simulations for this work.

To increase computational efficiency, the flow parameters (e.g., viscosity ratio and surface tension) have been transformed into variables that have been nondimensionalized. Also, because of this transformation, no system of units is assumed *a priori*. In the rule-based model, the throat length, defending fluid density, defending fluid viscosity, and the gravitational acceleration constant are set to unity. From these assumptions, values that correspond to other parameters are calculated. Equations 1a-d show how to transform the parameters into the model variables:

$$H' = \frac{H\rho_d}{\ell\rho_i}, \tag{1a}$$

$$\rho' = \frac{\rho_i}{\rho_d}, \tag{1b}$$

$$\mu_i' = \frac{\mu_i}{\mu_d}, \tag{1c}$$

$$\sigma' = \frac{\sigma}{g\rho_d\ell^2}, \tag{1d}$$

where H is the head, ρ is the density, μ is the viscosity, σ is the surface tension, g is the acceleration due to gravity, and ℓ is the unit length. Subscripts *i* and *d* correspond to invading and displaced fluids, respectively.

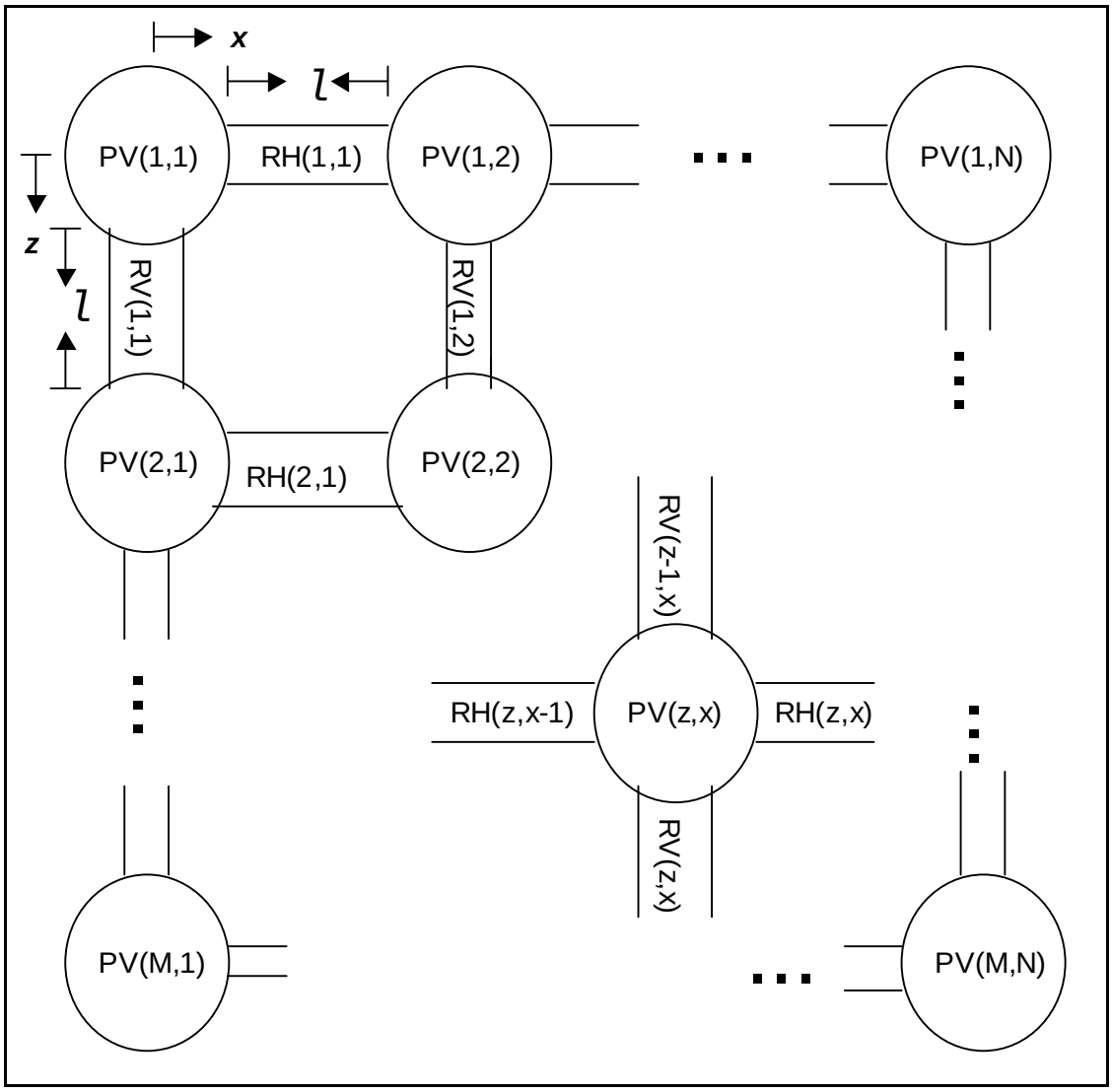

Figure 2. Schematic of *M* x *N* network of pores and throats. PV is pore volume; RH and RV are radii of horizontal and vertical throats, respectively; distance between nodes is l.

The model invokes an iterative process; during each time step, pores are scanned from the bottom of the flow domain to the top (the source):

1) Each pore is checked to determine if it is on the interface between the two fluids (i.e., if it is filled with defending fluid and a pore beside or above it is filled with invading fluid)
2) Each interfacial throat (a throat that connects an interfacial pore with a pore filled with invading fluid) is checked to see if the threshold pressure is reached.
3) If threshold is reached, then the pore is filled to a level that depends on the velocity of fluid in the throat; if threshold is not reached, then the pore does not fill.

4) If the pore is completely filled in that time step, then the surrounding pores are on the interface for the next step; if not, the value of the proportion filled is stored and added to in the next step, again at a rate depending on the velocity.
5) If the pore is overfilled, the surrounding pores are checked to determine if they can receive defending fluid; if so, the pores are filled according to step 3; if not, the time step is reduced and the pores are checked again, beginning at the bottom of the infiltration.

This procedure is similar to some modified invasion percolation procedures (Frette et al., 1992; Ewing and Berkowitz, 1998). The main differences between the models are that this procedure calls for filling (or partially filling) more than one pore in a time step, it uses different rules to decide if a pore should be filled, and the pore volumes and throat radii decide how quickly a pore is filled. The rule-based model process is also different from that of a mechanistic model because it does not link the pressures in all of the pores through a system of equations; instead, it estimates velocities in throats on the fluid-fluid interface to speed up the computational process. This simplifies the model so that it can run much faster than any mechanistic model; but of course, these simplifications are paid for by introducing some heuristic corrections.

In step 2 above, a threshold value is calculated using the modified Washburn equation (Dullien, 1992) expressed in terms of the variables used in the program code:

$$\rho' g' H' + (\rho' - 1) g' k - \frac{2\sigma'}{r'} > 0 \Rightarrow \begin{cases} \text{Yes : Fill the pore} \\ \text{No : Do not fill the pore} \end{cases}, \qquad (2)$$

where $k = z / \mathrm{l}$ (depth) and $r' = r / \mathrm{l}$ (radius).

Once the threshold for a particular throat has been exceeded, the modified Washburn equation is used to estimate the velocity of the fluid through the throat:

$$\hat{u} = \frac{R^2}{8(\mu' L_i' + (N - k)} \left[\rho' H + (\rho' - 1) - 2\sigma' \big/ r' \right], \qquad (3)$$

where $\hat{u}$ is the dimensionless velocity, R is average radius of the tube in units, N is the number of vertical pores in the network, and L'_i is stream length, found by assuming that the pores filled with invading fluid are equivalent to a single tube of pores connected in series (Bromhal, 2000).

As mentioned above, the velocity calculated using the modified Washburn equation is an approximation of the actual velocity through an interfacial throat. First, the stream paths in porous media are not as simple as the one described above; they may split and rejoin multiple times. Second, the idealized stream path is still just an approximation of a single stream path that does not include pores or the friction losses at locations where the radius changes. Finally, the flow through the entire tube is assumed to be steady state (similar to the assumptions made in mechanistic models for each throat).

In an attempt to correct for these approximations, a heuristic correction has been made to the calculation of velocity in each interfacial throat. Because one of the main objectives of this work is to study unstable fronts, the correction is based on the Saffman-Taylor (1958) stability analysis, derived from the Laplace equation and Darcy's law. The velocity at a point on the interface between two fluids in a Hele-Shaw cell can be connected to a parameter, γ, which relates the rate of growth of an (unstable) finger and the length of the finger.

For this correction, a total velocity for a throat is taken to be a linear combination of a velocity correction, $\hat{u}_c$, and the value of velocity, $\hat{u}$, from the modified Washburn equation. The method of redistributing the velocity is as follows. First, a value of γ' is determined for the throat on the interface:

$$\gamma' = \frac{(\mu' - 1)r'^2\hat{v} + (\rho' - 1)g'}{(\mu' + 1)r'^2} n, \tag{4}$$

where $\hat{v}$ is the averaged value of the velocities through throats on the frontal interface calculated from the modified Washburn equation for the previous time step and *n* is the wavelength of the infiltration front. A value of $\hat{u}_c = \gamma' x$ is then calculated (where *x* is the fingerlength). Since the component of velocity from the Saffman-Taylor analysis is added to the average velocity at all points on the interface so that these corrections sum to zero, the velocity corrections ($\hat{u}_c$) are therefore normalized. The total velocity for a throat is calculated by:

$$\hat{u}_t = \hat{u} + \beta\hat{u}_c, \tag{5}$$

where β is a weighing factor for the velocity correction.

Thus, the total velocity through a throat for a time step used in the program is taken from Equation 5. Since the throats are assumed to have no volume, the amount of invading fluid that reaches the pore in each time step is calculated using the total velocity times the area of the throat (to reach a flow rate). This flow rate is then multiplied by a dimensionless time parameter, giving a value that is compared to the volume of the pore. If this value exceeds the value of the pore volume, the pore is filled, and the remaining fluid begins to fill a connecting pore through the largest throat using the same procedure as above. If the volume of fluid does not exceed the volume of the pore, it is stored for the next iteration; then, the volume of invading fluid in the pore adds up over successive iterations until the pore is completely invaded, and the pore is designated as filled. Then, its connecting throats are assumed to be on the interface. If there are no surrounding pores that can accept invading fluid (i.e., they are already filled with invading fluid or the threshold is too high) or if the amount of "excess" fluid would fill more than half of a pore, then the time step is reduced, all of the values for all of the pores are reset, and the iteration is begun again.

Once all of these steps are completed, the program moves on to the next pore to decide if it should be filled. This process is repeated until the invading fluid reaches the lowest layer of pores in the model, at a chosen depth from the ocean floor. A more complete description of this model and its simulation process can be found in Bromhal (2000).

Results

In this section, we present results from simulations for different heads of the CO_2 plume at two different depths, as discussed above. Tables 2a-b show the velocity (flow rate per unit area), saturation, and fractal dimensions of the infiltration patterns at breakthrough. For each combination of input parameters, the random network (of throat sizes) was generated thirty times. The results from these realizations were averaged to get the numbers seen in Tables 2a-b. Standard deviations are within about 10% of the mean for all results but the fractal dimension, which was typically within ±0.02 of the mean.

Because of the capillary pressure between the fluids in the pores, a significant pressure head was required to propagate the fluid into the sediment. At a depth of 3km, the density difference between the fluids was so small that a head of 9.7m was required to cause movement. For the 6km depth, the density difference was much more significant, and a head of only 1.4m was required. No one to our knowledge has predicted a realistic height of a CO_2 "lake" on the sea floor, but our model could help predict the plume height if a steady state occurs.

We can estimate fluxes of carbon dioxide into the sediments by simply multiplying the velocity by the saturation. These values are also shown in Tables 2a-2b. Diffusive flux can be estimated in the bulk using simple Fickian diffusion. Assuming no hydrate formation (a very conservative assumption) and a diffusivity coefficient of $1.39 m^2/s$ (Inoue et al., 1996), we have estimated the vertical (upward) flux of carbon dioxide into the ocean water. The vertical volume flux is on the order of 4mm/s, in contrast to the fluxes in the ocean sediment.

Table 2a. Velocity, saturation, and fractal dimension for 3 different heads at a depth of 3km

Head	1m	5m	10m
Vel (μm/s)	0	0	34.73
Saturation	0	0	36.42
Fractal dim.	0	0	1.843
Flux (mm/s)	0	0	0.0126

Table 2b. Velocity, saturation, and fractal dimension for 3 different heads at a depth of 6km.

Head	1m	2m	5m	10m
Vel (μm/s)	0	31.76	113.9	245.9
Saturation	0	38.34	37.09	34.84
Fractal dim.	0	1.783	1.772	1.764
Flux (mm/s)	0	0.0122	0.0422	0.0857

Conclusion & Future Work

The most notable conclusion is the high heads required to facilitate penetration of the ocean floor, ~10m at 3km deep and ~1.5m at 6km deep. Since the average pore size was 50μm, which is at the upper end of what we would find on the ocean floor, it is likely that heads of 20-100m would be required to move the plume for clays and other common sediment types with an average pore size of 5μm or less. Such high plumes seem unlikely, so we conclude that infiltration is improbable for fine soils.

In contrast, flow most likely will occur in the sandy and silty soils. In the cases presented here, the flux into the soil appears to be between 5 and 15 times smaller than the diffusive flux, with the most favorable being the 6km deep, 10m high plume and the least favorable being the 3km deep, 10m high plume. In these cases, flow into the sediment is not insignificant, but it much less a factor than diffusion.

However, hydrate formation was not taken into consideration in the bulk phase. Inoue et al (1996) have shown that the presence of hydrate in such a CO_2 lake will significantly slow the diffusion, by at least an order of magnitude. In this case, the fluxes are about equal (or the downward flux is greater), and so flow into the sediment appears to be as much or more important than diffusion.

Thus, infiltration into sediment on the ocean floor should not be overlooked when one considers deep ocean sequestration options near high permeability sediments. Such trapped CO_2 would be more stable than that in liquid or hydrate form. Future work should consider the nature of hydrates that form in the ocean sediment. This is a significant unknown in the process, and it is possible that the presence of hydrate in the pores will slow the downward flux as much or more than hydrate in the bulk. Modeling of hydrate formation in porous media and its effects on flow would be very useful to this analysis.

References

Aker, E., K.J. Maloy, and A. Hansen. "Simulating temporal evolution of pressure in two-phase flow in porous media." *Physical Review A.* Vol. 58, No. 2, p. 2217-2226, 1998.

Angus, S. B. Armstrong, and K.M.deReuck (eds). International Thermodynamic Tables of the Fluid State: Carbon Dioxide. Pergamon Press. Oxford, England. 1976.

Blunt, M., M.J. King, and H. Scher. "Simulation of two-phase flow in porous media." *Physical Review A.* Vol. 46, No. 12, p. 7680-7699, 1992.

Bromhal, Grant S. Stochastic simulation of two-phase flow in porous media: Immiscible non-wetting fluid invasion in groundwater. Doctoral Thesis. Carnegie Mellon University. August 2000.

Chun, Byung-Soo and Gordon T. Wilkinson. "Interfacial tension in high pressure carbon dioxide mixtures." *Industrial Engineering Chemical Res*. Vol. 34, p. 4371-4377, 1995.

Dullien, F.A.L. Porous Media: Fluid Transport and Pore Structure. 2nd ed., Academic Press, NY, 1992.

Ewing, R. and B. Berkowitz. "A generalized growth model for simulating initial migration of dense non-aqueous phase liquids." *Water Resources Research*. Vol. 34, No. 4, p. 611-622, April 1998.

Feder, J. Fractals. Plenum Press, New York, NY, 1988.

Ferer, M. and D.H. Smith. "Dynamics of growing interfaces from the simulation of unstable flow in random media." *Physical Review E*. Vol. 49, No. 5-A, p. 4114-4120, 1994.

Frette, Vidar, Jens Feder, Torstein Jossang, and Paul Meakin. "Buoyancy-driven fluid migration in porous media." *Physical Review Letters*. Vol. 68, No. 21, May 1992.

Harrison, Wendy J., Richard F. Wendlandt, and E. Dendy Sloan. "Geochemical interactions resulting from carbon dioxide disposal on the seafloor." *Applied Geochemistry*. Vol. 10, p. 461-475, 1995.

Held, R. and T. Illangasekare. "Fingering of dense nonaqueous phase liguids in porous media: Analysis and classification." *Water Resources Research*. Vol. 31, No. 5, p. 1223-1231, May 1995.

Inoue, Yoshiro, Kazunari Ohgakl, Yushi Hirata, and Eiichi Kunugita. "Numerical study on effects of hydrate formation on deep sea CO_2 storage." *Journal of Chemical Engineering of Japan*. Vol. 29, No. 4, p. 648-655, 1996.

Lenormand, R., E. Touboul, and C. Zarcone. "Numerical models and experiments on immiscible displacements in porous media." *Journal of Fluid Mechanics*. Vol. 189, p. 165-187, 1988.

Michels, A., A. Botzen, and W. Schuurman. "The viscosity of carbon dioxide between 0^oC and 75^oC at pressures up to 2000 atmospheres." *Physica* Vol. 23, p. 95-102, 1957.

Saffman, P.G. and G. Taylor. "The penetration of a fluid into a porous medium or Hele-Shaw cell containing a more viscous liquid." *Proc. of the Royal Society of London Sec. A.* Vol. 245, p. 312-329, 1958.

Tabe, Yutaka, Shuichiro Hirai, and Ken Okazaki. "Massive CO_2 clathrate hydrate growth at a high-polar-energy surface." *Journal of Crystal Growth*. Vol. 220, p. 180-184, 2000.

Teng, H., A. Yamasaki, M.-K. Chun, and H. Lee. "Why does CO_2 hydrate disposed of in the ocean in the hydrate-formation region dissolve in seawater?" *Energy*. Vol. 22, No. 12, p. 1111-1117, 1997.

U.S. Dept. of Energy, Office of Science, Office of Fossil Energy. Carbon Sequestration: Research and development. Technical Report. December, 1999.

Pore-Level Modeling of Carbon Dioxide Sequestration in Brine Fields

M. Ferer, (mferer@wvu.edu) Department of Physics, West Virginia University, Morgantown, WV 26506-6315, Grant S. Bromhal, (bromhal@netl.doe.gov) US DOE, National Energy Technology Laboratory, Morgantown, WV 26507-0880; and Duane H. Smith, (dsmith@netl.doe.gov) US DOE, National Energy Technology Laboratory, Morgantown, WV 26507-0880 & Department of Physics, West Virginia University.

Underground injection of gas is a common practice in the oil and gas industry. Injection into deep, brine-saturated formations is a commercially proven method of sequestering CO_2 . However, it has long been known that displacement of a connate fluid by a less viscous fluid produces unstable displacement fronts with significant fingering. This fingering allows only a small fraction of the pore volume of a brine-saturated formation to be available for sequestration, while providing a large interfacial region between the carbon dioxide and the brine. A better understanding of the fluid displacement process should lead to reduced capital and operating costs for CO_2 sequestration in brine fields. The interfacial length will provide information to study the extent of dissolution of CO_2 in the brine as well as the extent of possible hydrate formation. By studying the flow for several viscosity ratios, the effect of polymeric viscosifiers can be evaluated.

We have developed a pore-level model of the immiscible injection of CO_2 (a non-wetting fluid) into a porous medium saturated with brine (a wetting fluid). This model incorporates a distribution of different 'pore-throat' radii , the wettability of the formation (i.e. the gas-liquid-solid contact angle, the interfacial tension between the fluids, the fluid viscosities, and all other parameters that appear in the capillary number. The computer code for the model maintains a constant injection to within a few per cent.

The model has been used with experimental values of interfacial tensions and a range of possible viscosities, to study the injection of carbon dioxide into brine-saturated porous media, at high pressures. Results are presented for saturations and fingering patterns for a range of capillary numbers and viscosities.

I. Introduction

Flow in porous media is a subject of scientific and engineering interest for a number of reasons. For half a century, it has been believed that flow in porous media is a compact (i.e. Euclidean) process whereby the interface advances linearly with the total amount of the fluid as predicted by a Darcy's law treatment using saturation-dependent relative permeabilities.[1]-[5] In the last fifteen years, it has been appreciated that flow in porous media is fractal in certain well-defined limits.[6]-[9] The flow is known to be described by self-similar diffusion-limited-aggregation (DLA) fractals in the limit of zero viscosity ratio, $M = \mu_I / \mu_D = 0$ (i.e. where the injected fluid has zero viscosity and the displaced fluid has finite viscosity). [6]-[8],[10]-[12] The flow is known to be described by self-similar invasion percolation fractals in the limit of zero capillary number, $N_C = \mu_D V / \sigma \cos\theta = 0$, where viscous drag forces

(viscosity of the displaced fluid times average fluid velocity) are zero, while the capillary forces (proportional to interfacial tension, σ, times sine of the contact angle θ) are finite.

Diffusion Limited Aggregation (DLA) was originally introduced to describe colloidal aggregation.[13] Soon, it was appreciated that because the continuum versions of both DLA and viscous fingering are both governed by Laplace's Equation, both should provide equivalent displacement patterns in the limit of zero viscosity ratio.[14] Indeed, evidence from both experiment and modeling showed that not only were the DLA and viscous fingering patterns visually similar but they also had the same fractal character.[6]-[9] ,[11],[12],[15]-[19]

Invasion Percolation was proposed as a model of immiscible drainage (where a non-wetting fluid is injected into a medium saturated with a wetting fluid), in the limit of zero injection velocity, i.e. at zero capillary number. [7]-[9],[20] In Invasion Percolation, only the largest throat (with the smallest capillary pressure) on the interface is invaded by the injected, non-wetting fluid. In this Invasion Percolation rule, it is assumed that wetting fluid will be displaced towards the outlet. However, in two dimensions, one may need to include trapping effects where a blob of the wetting fluid cannot reach the outlet because it is surrounded by non-wetting fluid. The patterns of injected fluid from Invasion Percolation with trapping (IPwt) have been observed to have a fractal character with a fractal dimension $D \approx 1.82$.[7]-[9],[20] Experiments have shown that patterns of drainage at small capillary number ($N_{Ca} = 10^{-5}$) are visually similar to patterns from IPwt and that they have the same fractal dimension, $D \approx 1.84$, as IPwt.[21]

Recently, we have shown that our model produces results which agree with both DLA (in the limit of very large viscosity ratio) and with IPwt (in the limit of very small capillary number).[22] Having demonstrated the validity of our model in these two very different limits, coupled with the physicality of the model and the excellent consistency with fluid conservation, we are be confident in extending our studies to the physically relevant intermediate regime, where the limiting models (DLA and IPwt) are not valid.

II. Objectives

We have used our computer model, as described in Section III, to study the injection of carbon dioxide into a brine saturated reservoir. In our modeling, we used typical experimental values of surface tension and viscosity for carbon dioxide at high pressures , $\sigma = 21$ dynes/cm, $\mu \approx 0.05$ cp (viscosity ratio M=0.05) and larger.[23],[24] We assumed a water-wet porous medium, i.e. a contact angle $\theta = 0^o$. We assumed a size scale for the porous medium where the typical pores are 100μm apart (i.e. the length scales in our model is $\ell =$ 100μm). For our model, this would give a smallest capillary pressure of 7500 dynes/cm^2 . Although this size scale would significantly affect the pressure necessary to inject the carbon dioxide, the saturations should be more directly affected by variations in capillary number than by the size scale of the porous medium.

In section IV, we present results for the saturation profiles and fingering patterns from a range of capillary numbers for model systems with 2700 pore bodies. Surprisingly for these systems, the saturation's are nearly independent of capillary number. The fingering patterns

show that the saturation's are consistent with IPwt at small capillary numbers; for this small viscosity ratio, the fingering changes from IPwt-like to DLA-like as the capillary number increases. Both fingering models (IPwt and DLA) yield small CO_2 saturations. For larger viscosity ratios, we show that the saturations increase with capillary number as expected.

III. Approach - Description of the Model

The pore-level model is intended to incorporate, as realistically as possible, both the capillary pressure that tends to block the invasion of narrow throats and the viscous pressure drop in a flowing fluid. The two-dimensional model porous medium is a diamond lattice, Fig.1, which consists of pore bodies of volume, ℓ^3, at the lattice sites and throats connecting the pore bodies which are of length, ℓ, and have a randomly chosen cross-sectional area between 0 and ℓ^2. Compared to several models reported in the recent literature, we believe that our model should be both more general and more flexible, in part because both the throats and the pore bodies have finite volume in comparison with i) refs. [6] and [25], where the throats contain zero volume of fluid, and ii) refs. [26]-[28], where the pore bodies have zero volume. Furthermore, in our model, the volumes of both the pore bodies and throats can be set as desired. In this sense the work of Periera is closer to our model, but this work focuses on three-phase flows at constant pressure.[29] Of course all of these models include the essential features of random capillary pressures blocking the narrowest throats and a random conductivity depending on a given viscosity ratio.

III.A. Capillary Pressure

When the interface has entered one of the pore throats, the radius of curvature, R, of the meniscus is fixed by contact angle, θ, and the radius of the pore throat, r ;

$$R = r/\cos\theta \quad . \tag{1}$$

Therefore, the pressure drop across the meniscus is fixed at the capillary pressure

$$P_{cap}(R) = \frac{2\ \sigma\ \cos\theta}{r} \quad , \tag{2}$$

where σ is the surface tension. Thus the flow velocity is given by the throat conductance times the total pressure drop across the throat; see Fig. (2),

$$q = g_{throat}\ (P_{nw} - P_w - P_{cap}). \tag{3a}$$

In the model the transmissibility (conductance) of the throat is given by

$$g_{throat} = g^* \frac{(A_{throat}^2/\ell^4)}{(x + (1-x)\ M)} \tag{3b}$$

where A_{throat} is the cross-sectional area of the throat, x is the fraction of the throat of length ℓ which is filled with defending fluid, and M is the ratio of the non-wetting, invading fluid's (CO_2) viscosity to that of the wetting, defending fluid (brine), $M = \mu_{nw} / \mu_w$. (Note: this definition

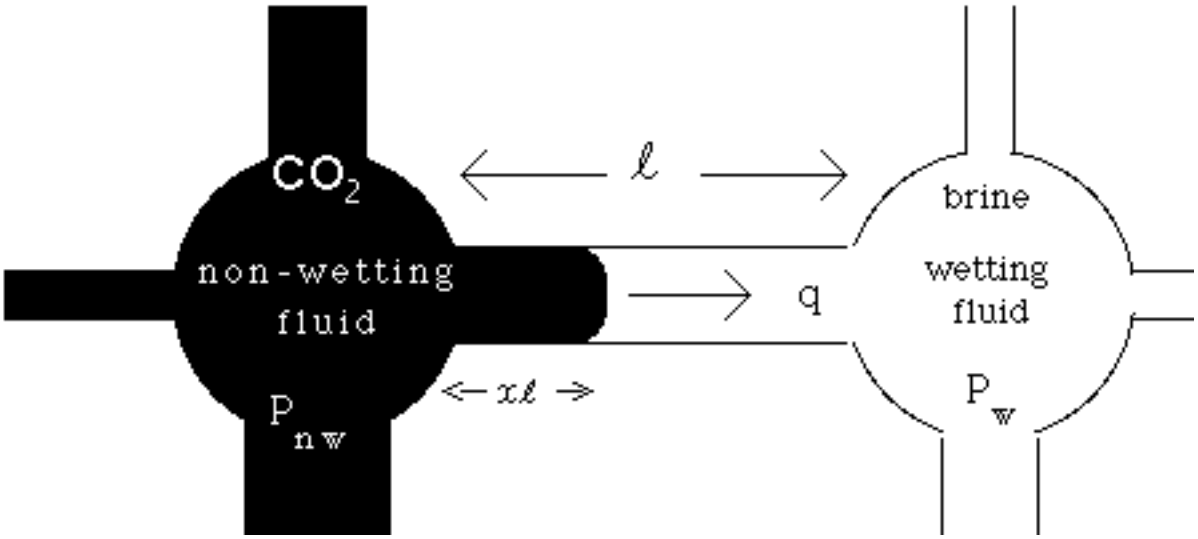

Figure 1
shows the CO_2 displacing the brine with volume flow velocity $q_{throat} = g_{throat} (P_{nw} - P_w - P_{cap})$. of course if $P_{nw} - P_w < P_{cap}$ the CO_2 retreats and the brine re-occupies the throat.

of M agrees with the convention of Lenormand [6], but it is the inverse of the convention used in our earlier papers on miscible, unstable flow [15]-[18].) The quantity, g*, carries all the dimensionality of g_{throat}

$$g^* = \ell^3 / (8 \pi \mu_w) \qquad (4)$$

Many of our results for the flow velocity will presented in terms of $q^* = q/g^*$, which is independent of the particular value of the viscosity of the wetting fluid. From Eq. (3a), the non-wetting fluid advances if the pressure difference between the pore filled with CO_2 (non-wetting fluid) and the pore filled with brine (wetting fluid) exceeds the capillary pressure. Otherwise the CO_2 will retreat.

Naive use of Eq. 2 causes a number of complications in the programming. These complications arise because of the blocking that occurs if the CO_2 fluid is at the entrance to a throat, Fig. 3; if the sign of the pressure drop ($P_{nw} - P_w$) is such that it would advance the non-brine but the magnitude of the pressure drop does not exceed the capillary pressure ($P_{nw} - P_w < P_{cap}$) , the interface remains stationary at the inlet of the throat. This will lead to very small time steps. If the CO_2 is close to the entrance of a narrow throat, which will likely be blocked to this invading fluid, a very small time step may be needed to advance the fluid to the entrance of the throat, but not into the throat. This makes a reliable control on the velocity difficult; as the inlet pressure is changed to maintain a constant flow the throat blockages will change requiring a complicated feedback loop connecting inlet pressure, flow velocity and throat blockages. A clever solution to these problems was suggested in refs. [26]-[28]; they argued that real throats would have a gradual decrease in cross-sectional area accompanied by a gradual increase in capillary pressure. Consistent with this work, we assume that the capillary pressure increases

from zero at the inlet to a throat of radius r and length ℓ to the value in Eq. 2 at the center of the throat. This dependence is given by the equation

$$P_{cap} = \frac{2\ \sigma\ \cos\theta}{r} \sin\left(\frac{\pi x}{\ell}\right), \qquad (5)$$

where x is still the distance along the throat from 0 to ℓ. Eq. (5) solves the problem of trying to advance a fluid into a blocked throat, because the inlet of a throat will never be blocked since it has zero capillary pressure. Furthermore, the feedback between blockage and the inlet pressure is removed, so that the constant velocity condition is easier to satisfy.

Implicit in this model, is the assumption that the pressure within a pore body is uniform. Assuming otherwise would require doing full fluid dynamics using the Navier-Stokes equation. This is inconsistent with the pore-level model approach and would severely limit the size of the model porous medium, given finite computer resources. Although, these idealizations (Eq. (5), etc.) may seem unphysical on a real microscopic scale, the model has a random distribution of conductances and correlated capillary pressures. Significantly, the pressure must exceed the randomly-distributed capillary pressures in Eq. 2 to pass through the throat; and the flow velocity (Eq. 3) has the correct dependence upon throat radius.

III.B. Finding the Pressure Field

Volume conservation of the incompressible fluid, dictates that the net volume flow q out of any pore body must be zero. Let us consider use of the above rules for the situation in Fig 2. In Fig. 2, the flow velocities, as directed out of the (i,j) pore body through the throats are

$$q_{i-2,i-1} = g_{i-2,i-1}\,(P_{i,j} - P_{i-2,i-2}) \qquad q_{i,j+1} = g_{i,j+1}\,(P_{i,j} - P_{i+2,j+2} - P_{cap,i,j+1})$$

$$q_{i-1,j} = g_{i-1,j}\,(P_{i,j} - P_{i-2,j} - P_{cap,i-1,j}) \qquad q_{i+1,j} = g_{i+1,j}\,(P_{i,j} - P_{i+2,j} - P_{cap,i+1,j}). \qquad (6a)$$

Requiring that the net flow out of pore body (i,j) be zero leads to the following equation for $P_{i,j}$:

$$(g_{i-2,i-1} + g_{i,j+1} + g_{i-1,j} + g_{i+1,j})P_{i,j} =$$
$$(g_{i-2,i-1}\,P_{i-2,i-2} + g_{i,j+1}\,P_{i+2,j+2} + g_{i-1,j}\,P_{i-2,j} + g_{i+1,j}\,P_{i+2,j}) + \qquad (6b)$$
$$(g_{i,j+1}\,P_{cap,i,j+1} + g_{i-1,j}\,P_{cap,i-1,j} + g_{i+1,j}\,P_{cap,i+1,j})$$

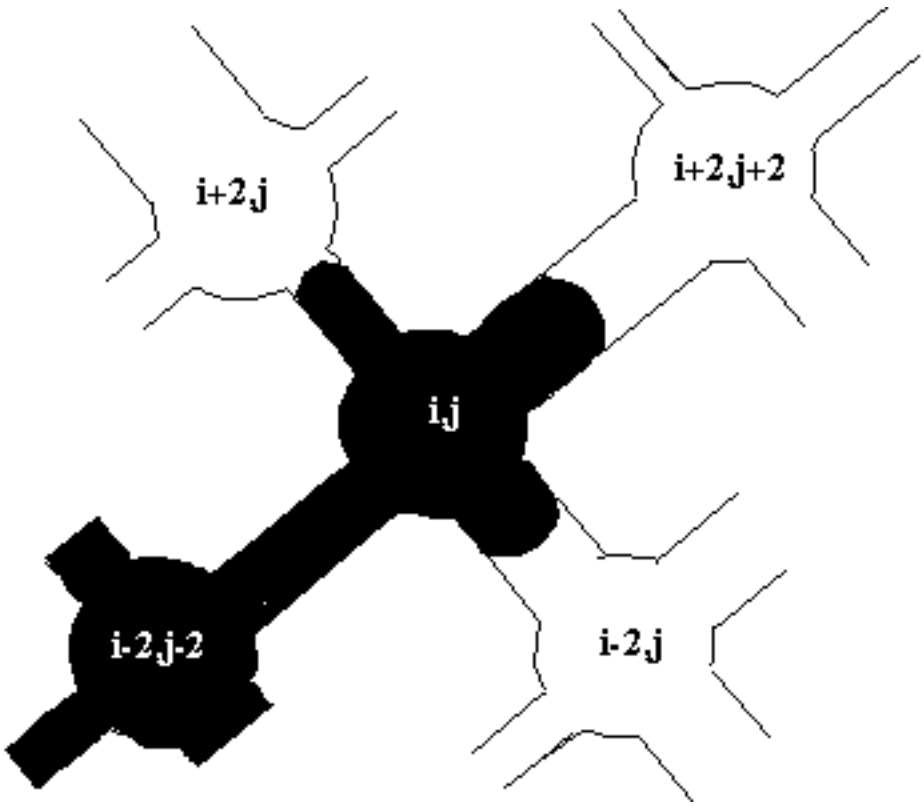

Figure 2
shows a possible occupation of adjacent pore-bodies. For this occupation, the flow velocities are given by Eq. (6a) and the pressure in the (i,j) pore body is given by Eq. (6b) (a specific realization of Eq. (7)).

Eq. (6b) is of the form

$$(\sum g)\, P_{i,j} = (\sum g\, P) + (\sum f\, g\, P_{cap}) \qquad (7)$$

where i) the factor f is zero if there is no meniscus in the throat; ii) the factor f is +1 if the pore body (i,j) is filled with non-wetting fluid (CO_2) and the connecting pore body is filled with wetting fluid (brine); iii) the factor f is -1 if the pore body (i,j) is filled with brine and the connecting pore body is filled with CO_2.

Once the location of the interface is known, the numerical value of the capillary pressure in each throat is known (zero, if the interface is neither in the throat nor at either inlet to the throat). Furthermore, for each pore body at (i,j), the values of the sums $(\sum g)$ and $(\sum f\, g\, P_{cap})$ can be calculated and stored; note that these sums are independent of the values of the pressures in the pore bodies. Then the program iterates (Eq. 7), determining the pressure field until stability is achieved where the residual is less than some small value; i.e. until

$$R = \sum (P_{new} - P_{old})^2 < \varepsilon, \qquad (8)$$

where ε is chosen to be small, e.g. $\varepsilon = 10^{-3}$. This value of ε is chosen to minimize run-time without seriously sacrificing mass-conservation. For example, in one of the typical sets of five runs presented in this paper, after an average of 77,000 time steps there was an average difference of less than 1% between the total volume of fluid injected into the medium and the total volume of fluid expelled from the medium.

To maintain a constant volume flow q_o, the flow velocity was determined for two estimates of the inlet pressure. Assuming a linear relationship between flow velocity and inlet pressure (consistent with Eq. 6a), the linear relationship would then predict an inlet pressure, P_o, to produce the desired volume flow, q_o.[28] If the two estimates of the inlet pressure are too close together, the prediction of P_o will be unreliable; on the other-hand, if the estimates of the inlet pressure are too far apart computer time will be wasted iterating Eq.7 to determine the different pressure fields for each. In practice, the difference between the two initial estimates needs to increase with capillary number. With a good choice of initial estimates, this procedure is very accurate; for a typical set of runs, the standard deviation from the average outlet flow velocity, q=50.4, represented an scatter of 0.007%.

III.C. Flow Rules

Once the pressure field has been determined, we can determine the interface advance through a time interval Δt. A throat is on the interface, if the pore body at one end contains some wetting fluid (it may be filled with wetting fluid) and if the pore body at the other end is fully invaded by non-wetting fluid (or was fully invaded and is not yet fully re-invaded by wetting fluid due to backflow). As discussed earlier, a time interval, Δt, needs to be chosen which is small enough that

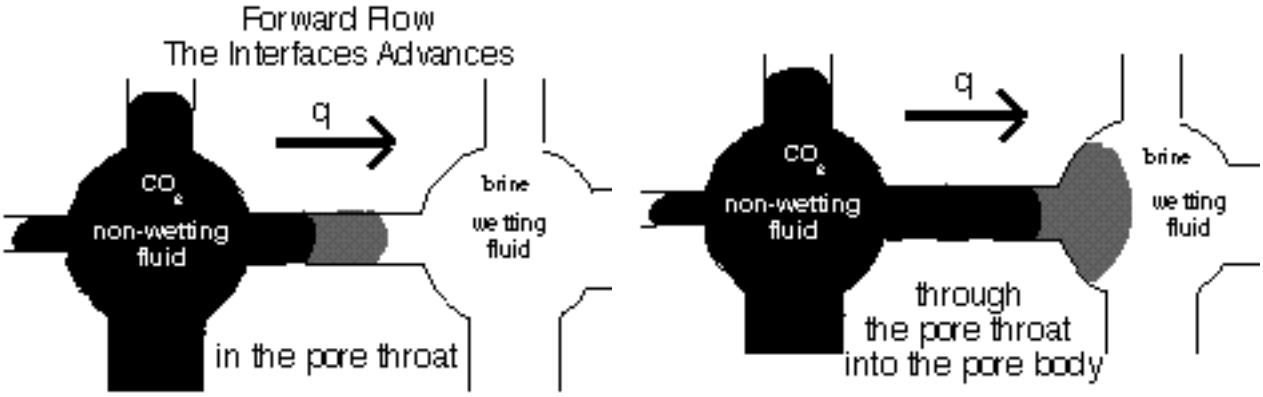

Figure 3 the CO_2 can advance within the pore throat (left-hand figure) or through the pore throat into the pore body (right-hand figure).

spurious local oscillations in the flow are avoided but not so small that the program run-time is unnecessarily long. For the cases discussed here, with large surface tension, the following prescription seems adequate. For all interfacial throats where the non-wetting fluid has yet to reach the midpoint of that throat, so that the capillary pressure is still increasing, the time interval is chosen so that the non-wetting fluid advances no more than 3.5% into any such throat. For all throats where the non-wetting fluid has advanced past the midpoint, so that the capillary pressure

is decreasing, the time step allows the interface to advance no further than 33% into any such throat. Having determined the interface and chosen the time step, we have attempted to make the flow rules as non-restrictive as possible.

Flow can increase the amount CO_2 within the pore throat (Fig. 3a), or through the pore throat into the pore body (Fig. 3b). Similarly, backflow can cause the interface to retreat within the pore throat (Fig. 4a) or through the pore throat into the pore body (Fig. 4b). If, during a time step, either type fluid over-fills a pore body, the excess is shared by the outflow throats. For these flow-rules, the throats are taken to be cylindrical with cross-sectional area A and length ℓ, consistent with refs. [26]-[28],[30] . The variation in the capillary pressure, Eq. (5), can be assumed to results from variations in contact angle. Again, this aspect of dubious microscopic physicality does not affect the basic feature of the model that the pressure drop across any throat must exceed the capillary pressure of that cylindrical throat, Eq. (2), for the non-wetting fluid to advance through the throat.

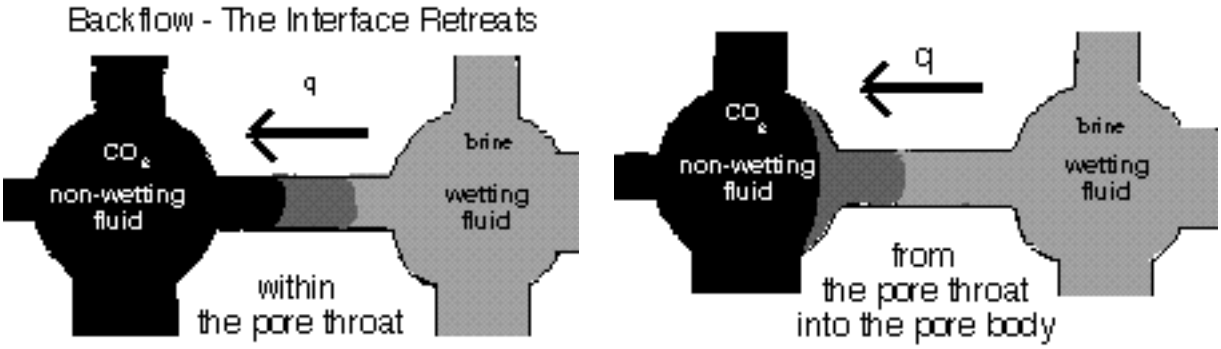

Figure 4 the CO_2 can retreat within the pore throat (left-hand figure) or through the pore throat into the pore body (right-hand figure).

We have attempted to make the flow-rules as non-restrictive and physical as possible.

i) All parts of the porous medium, pore-throats and pore-bodies have a volume which can be occupied by either type of fluid.

ii) Locally, back-flow as well as forward flow are allowed if they are ordained by the local pressure drops.

iii) Complications, such as over-filled pore bodies or plugs of fluid trapped in the pore throats are treated as physically as possible.

iv) Unphysical aspects, such as isolated 'blobs' of wetting fluids residing in pore-bodies, are tracked by the program and found to be insignificant.

v) Most importantly, the flow rules accurately account for all of the non-wetting fluid injected into the porous medium. For the smallest capillary number, there is a 0.25% difference between flow-rule

determination of the volume of injected fluid occupying the medium and the volume of fluid injected into or displaced out of the medium. For the larger capillary number, this difference is less than 0.01%.

IV. Results - Dependence of Saturations and Fingering Patterns upon N_c and M

In this section, we present results from running our computer code on systems which are 90 pores wide by 30 long (in the direction of average flow) using typical experimental values for surface tension and viscosity of CO_2 and brine as discussed in section II. We chose to model our flow on short wide systems, since long narrow geometries are known to mis-represent the fingering because of coarsening.[7]-[9] Figure 5 shows some typical, near-breakthrough fingering patterns where the CO_2 is injected along the lower edge.

Figure 6 shows near-breakthrough CO_2 saturation profiles for a wide range of capillary numbers with viscosity ratio M=0.05. The data points show averages over 5 different realizations of the porous medium (i.e. for each realization a different seed was used in the random number generator to determine the cross-sectional area of each throat); the error bars show the standard errors from the set of five realizations. Over this wide-range of capillary numbers there is little difference between the saturation profiles or between the total breakthrough saturations of CO_2 which are all around 20% or less.

Although the effect of capillary number on CO_2 saturation is small, if not negligible, capillary number has a significant effect upon the geometry of the fingering. For M=0.05, Figure 5a shows that the fingering for a low capillary number, $N_c = 6.25 \times 10^{-6}$, is identical to the fingering for IPwt (Invasion Percolation with trapping). Using the same model porous medium, the CO_2 occupation from our model for this low capillary number is shown by the open circles, while the CO_2 occupation from the IPwt is given by the small filled circles. That is, when the pore body location is marked by an open circle with a small filled circle inside, that same pore body was occupied by CO_2 using our model and independently by CO_2 using IPwt. For the five model porous media on which we've run the model, the agreement between IPwt and the model was excellent. In the worst case, the occupation of seven pore bodies was different between our model and IPwt. For the model porous medium shown in Fig. 5, the CO_2 occupation from the model and IPwt are identical. Figure 5b shows the CO_2 occupation at a larger capillary number for this same porous medium. Of course, since this is the same porous medium as that shown in Fig. (5a), the IPwt occupation, shown by the small filled circles, is the same for both. However, the fingering from the model at this large capillary number is very different from the IPwt fingering in Fig.5a. Indeed, at large capillary number the fingering from the model (open circles) is visually similar to DLA fingering.[7]-[9],[22] Since both DLA and IPwt have low breakthrough saturations, both of these fingering patterns are consistent with the CO_2 saturation profiles in figure 6.

These low CO_2 saturations for M=0.05 are to be contrasted with the saturations that can be achieved at larger viscosity ratios. For the same capillary numbers (i.e. the same surface tension and volume flows), we have performed the simulations with viscosity ratio, M=1. The

Figure 5 shows the occupation of a particular realization of a model porous medium.

The small solid circles show the CO_2 occupation as predicted by Invasion Percolation with trapping (IPwt).

The open circles show the CO_2 occupation as predicted by our pore-level model for M=0.05 and M=1 at two different Capillary numbers

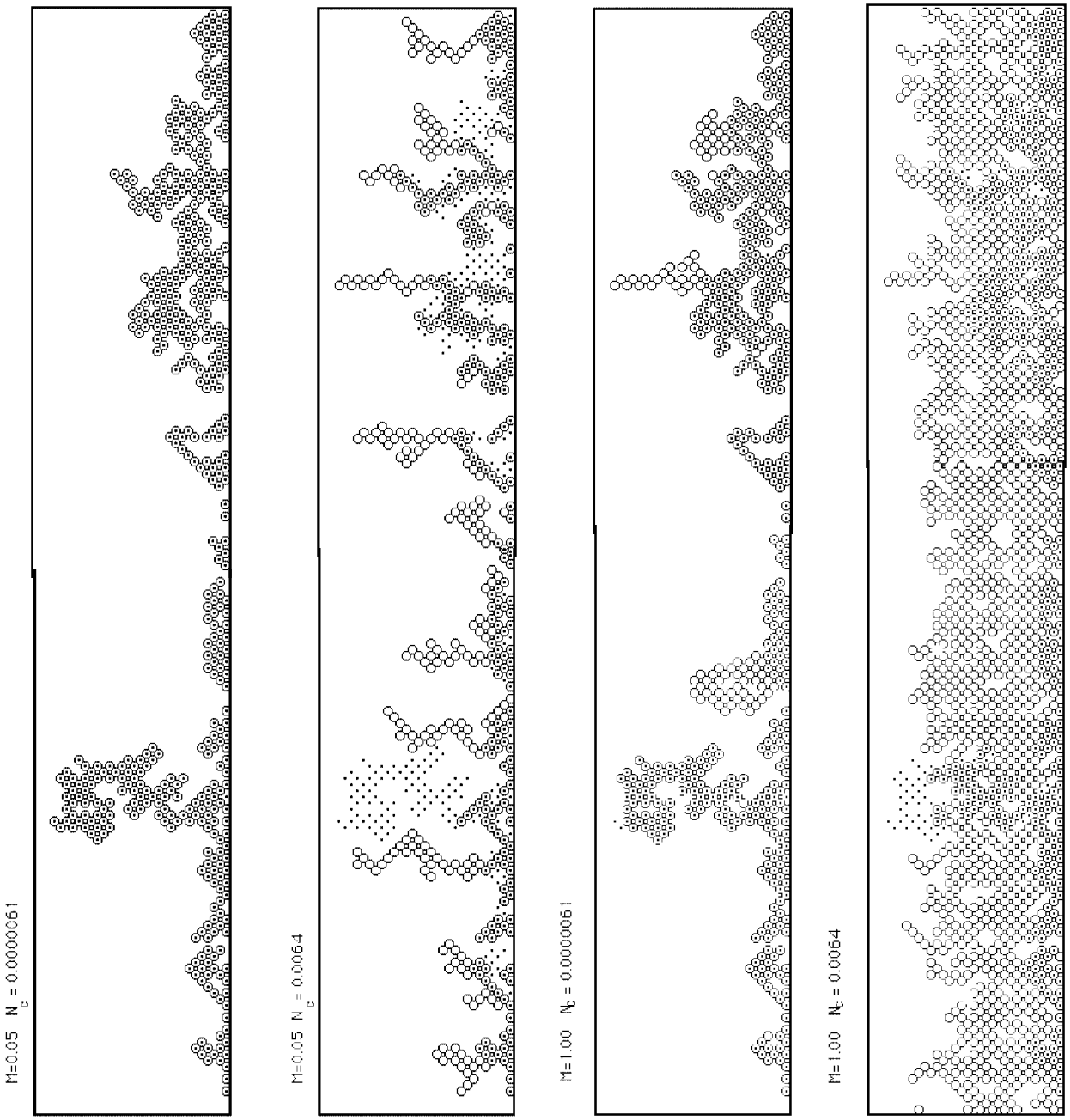

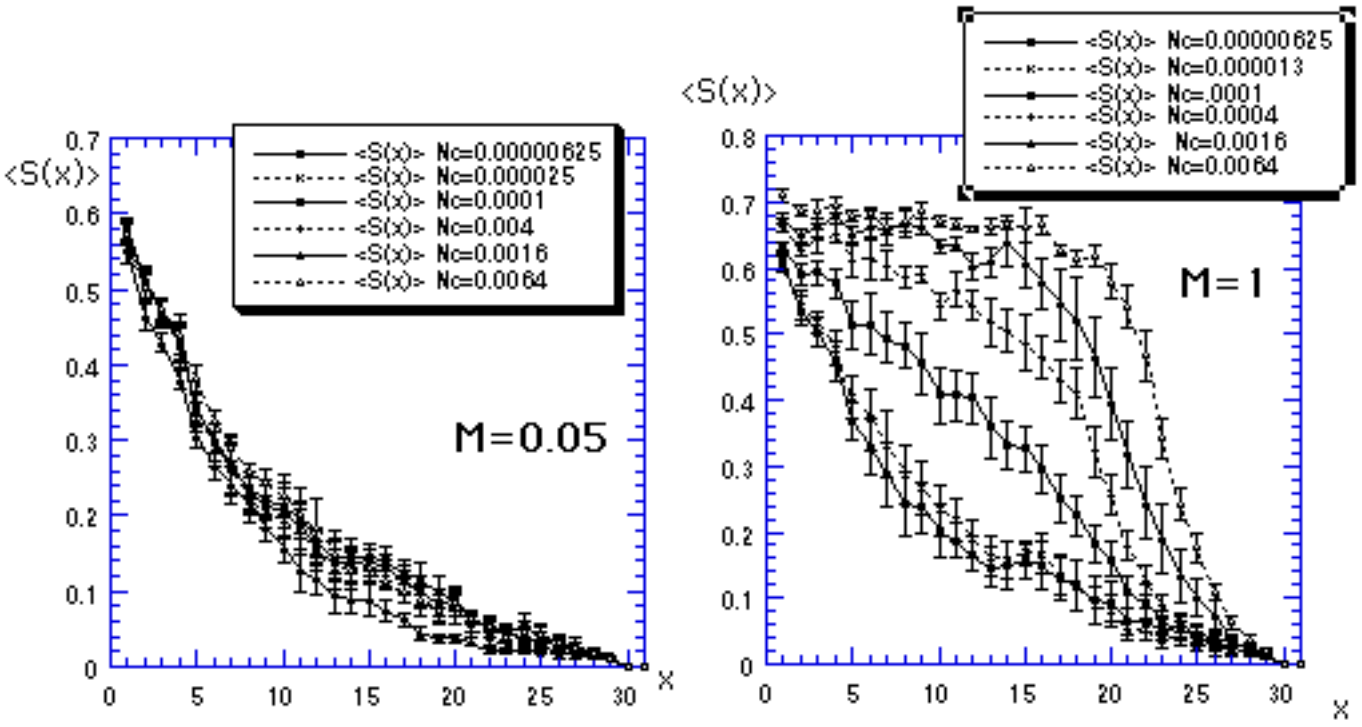

Figure 6 shows the near-breakthrough CO_2 saturation profiles of for viscosity ratios M=0.05 (left-hand figure) and M=1.00 (right hand figure) for a range of N_c from 6.25×10^{-6} to 6.4×10^{-3} .

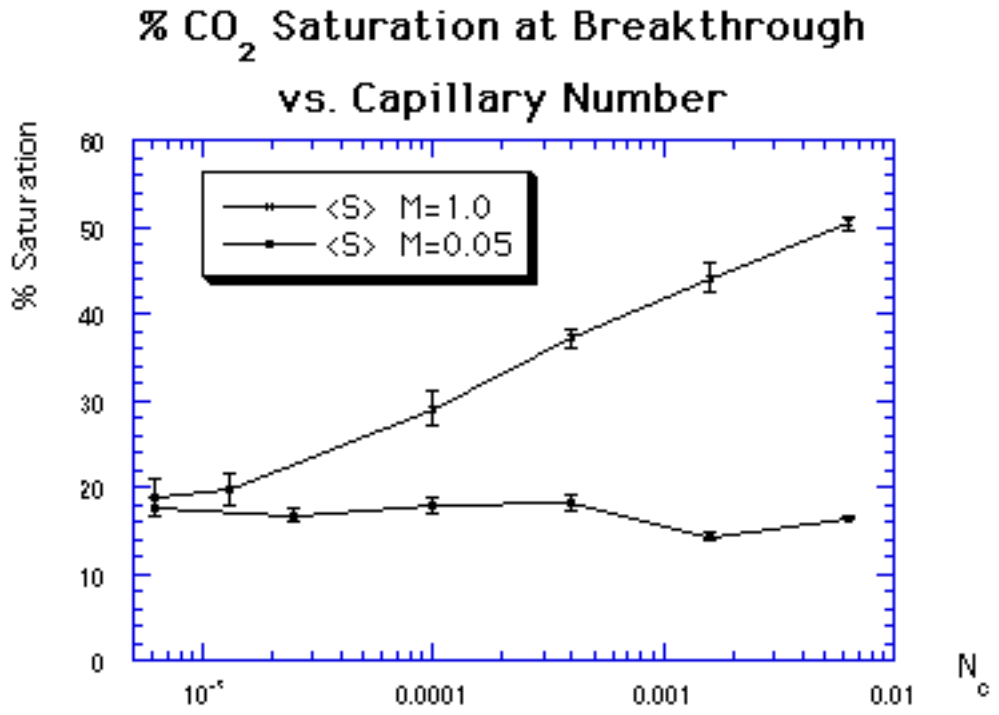

Figure 7 shows the breakthrough saturations of CO_2 in the 30x90 porous media with viscosity ratios M=0.05 (filled circles) and M=1 (x).

results are very different. At small capillary number, the M=1 saturations and fingering are similar to IPwt as they should be (see fig. 5c), but for M=1, even at this low capillary number deviations from IPwt are setting in. However, as capillary number increases, the flows become compact with negligible fingering (Fig. 5d) and the saturations increase dramatically (Fig. 6). Figure 7 shows the variation in CO_2 saturations at breakthrough vs. capillary number for both M=0.05 and M=1.00. As we've seen above, the breakthrough CO_2 saturations are nearly constant for M=0.05, whereas they increase significantly for the larger viscosity ratio M=1.0 .

V. Conclusions and Future Work

Our results from simulations show that injection of low viscosity CO_2 into the two-dimensional porous medium leads to small fractional saturations at breakthrough yielding the sequestration of only a small amount of carbon dioxide. If the viscosity of the carbon dioxide could be increased sufficiently, these results suggest that the efficiency of carbon dioxide sequestration could be doubled. Since this work has been done on small systems with only two viscosity ratios, it is important to ascertain how these effects change when one scales-up to realistically sized systems. However, it is interesting that the viscosity ratio M=0.05 produces DLA-like fingering on the size scale in Fig. 5, since our earlier work on miscible systems showed that flows for even smaller viscosity ratios were compact (negligible fingering) at even smaller size scales. It is also important to determine how this effect depends upon viscosity ratio throughout the range of physical interest.

References

1. Blackwell, R. J., J. R. Rayne and W. M. Terry, Trans. AIME, **216**, 1-8, (1959).
2. Collins, R. E., "Flow of Fluids through Porous Materials," 1961 Reinhold Publishing Corporation, New York.
3. Bear, J., "Hydraulics of Ground Water," 1979 McGraw-Hill Publ. Co., New York.
4. Dullien, F. A. L. "Porous Media: Fluid Transport and Pore Structure" 1979 Academic Press, New York.
5. Rhee, H.-K., R. Aris and N. R. Amundson, "1st-Order Partial Differential Equations: Vol. I (Theory and Applications of Single Equations," 1986 Prentice Hall, Englewood Cliffs, New Jersey.
6. Lenormand, R., E. Touboul and C. Zarcone, J. Fluid Mech., **189**, 165-187, (1988).
7. Feder, J., "Fractals," 1988 Plenum Press, New York.
8. Vicsek, T., "Fractal Growth Phenomena," 1989 World Scientific, Singapore.
9. Meakin, P., "Fractals, scaling, and growth far from equilibrium," 1998 Cambridge University Press, Cambridge.
10. Chen, J.-D. and D. Wilkinson, Phys. Rev. Lett., **55**, 1892-1895, (1985).
11. Nittmann, J., G. Daccord and H. E. Stanley, Nature, **314**, 141-144, (1985).
12. Daccord, G., J. Nittmann and H. E. Stanley, Phys. Rev. Lett., **56**, 336, (1986).
13. Witten, T. A. J. and L. M. Sander, Phys. Rev. Lett., **47**, 1400-1403, (1981).
14. Paterson, L., Phys. Rev. Lett., **52**, 1621-1624, (1984).

15. (Note the viscosity ration used in refs. 15-18 is the inverse of the one used in this paper.) Ferer, M. and D. H. Smith, Phys. Rev. E, **49**, 4114, (1994).
16. Ferer, M., R. A. Geisbrecht, W. N. Sams and D. Smith, Phys. Rev. A, **45**, 6973, (1992).
17. Ferer, M., W. N. Sams, R. A. Geisbrecht and D. H. Smith, AIChE J., **49**, 749, (1995).
18. Ferer, M., J. Gump and D. H. Smith, Phys. Rev. E, **53**, 2502-2508, (1996).
19. Halsey, T. C., P.Today DLA: A Model for Pattern formation, November, 36-41 (2000).
20. Wilkinson, D. and J. F. Willemsen, J. Phys. A, **16**, 3365, (1983).
21. Maloy, K., F. Boger, F. J and T. Jossang,Dynamics and Structure of Viscous Fingers in Porous Media,111-138,"Time Dependent Effects in Disordered Materials" , edited by Pynn and Riste (ed. 1987, Plenum Press, New York).
22. Ferer, M., G. S. Bromhal and D. H. Smith, Groundwater, to be sumbitted, (2001).
23. Vesovic, V. and e. al., J. Phys. Chem. Ref. Data, **19**, 763-808, (1990).
24. Chun, B.-S. and G. T. Wilkinson, Ind. Eng. Chem. Res., **34**, 4371-4377, (1995).
25. van der Marck, S. C., T. Matsuura and J. Glas, Phys. Rev. E, **56**, 5675-5687, (1997).
26. Aker, E. V K. Jorgen-Maloy ,A. Hansen and GT. Batrouni, Transport in Porous Media, **32**, 163-186, (1998).
27. Aker, E., K. Jorgen-Maloy and A. Hansen, Phys. Rev. E, **58**, 2217-2226, (1998).
28. Aker, E., K. Jorgen-Maloy and A. Hansen, Phys. Rev. E, **61**, 2936-2946, (2000).
29. Pereira, G., Phys. Rev. E, **59**, 4229-4242, (1999).
30. Akers, E., A Simulation for Two-Phase Flow in Porous Media, (1996).

Pore-Level Modeling of Carbon Dioxide Sequestration in Oil Fields: A study of viscous and buoyancy forces

Grant S. Bromhal, U.S. Department of Energy, National Energy Technology Laboratory, Morgantown, WV 26507-0880, gbromhal@netl.doe.gov, M. Ferer, Department of Physics, West Virginia University, and Duane H. Smith, U.S. Department of Energy, National Energy Technology Laboratory, Morgantown, WV 26507-0880

Underground injection of carbon dioxide for enhanced oil recovery (EOR) is a common practice in the oil and gas industry and has often been cited as a proven method of sequestering CO_2 (US DOE, 1999). Of all sequestration methods, this is probably the best understood, as carbon dioxide has been used in the oil industry for many years. Additionally, most oil fields have been relatively well characterized geologically, and often have impermeable layers above them, which will act as traps for sequestered CO_2. Miscible CO_2 flooding is particularly favorable for both EOR and sequestration because the absence of capillary forces increases the efficiency of the displacement. Of course, the goals of enhanced oil recovery and CO_2 sequestration are not the same, so a flooding process optimized for sequestration will be somewhat different than one for oil recovery.

There are still some difficulties with CO_2 sequestration in oil fields. For example, it has long been known that displacing connate oil by a less-dense, less-viscous fluid produces flow stratification and unstable fingering patterns in the displacement fronts. These phenomena reduce the oil production of the reservoir, as well as the available space for sequestration. Gravity override and viscous fingering are still not well understood, even in the oil recovery industry. A better understanding of these processes could lead to reduced capital and operating costs for CO_2 sequestration in oil fields and for enhanced oil recovery.

We have developed a pore-level numerical model of the miscible injection of one fluid (CO_2) into a porous medium saturated with another fluid (oil). The model incorporates a distribution of "pore-throat" radii, fluid viscosities, and fluid densities to mechanistically represent the physical flow situation. This model has been used, with experimental values of viscosities and densities, to study the high-pressure injection of liquid carbon dioxide into oil-saturated porous media. Results are presented for a number of viscosity and density ratios.

Introduction

Two-phase flow in porous media has long been important to scientists and engineers in the environmental and petroleum industries. Most modeling of two-phase flow is done on large reservoir simulators meant to predict general flow properties, such as saturation and total recovery (Blunt et al., 1992). These simulators typically rely on a form of Darcy's law to describe the movement of each phase through the medium. However, for nearly twenty years, it has been known that in certain well-defined limits, the compact flow assumptions of the Buckley-Leverett equations are not accurate.

The physical processes that contribute to the inaccuracies in Darcy's law and the Buckley-Leverett equations manifest themselves on a pore-level. These are the same processes that cause flow phenomena such as viscous fingering. We believe that the best way to understand this type of flow behavior is to create pore-level models that capture these flow phenomena. The models may then be used to scale up flow properties to field size and inform modifications in reservoir simulators. A number of pore-level analytical and computer models, such as diffusion-limited aggregation and invasion percolation, have been developed to describe the fractal growth patterns known to occur in special two-phase flow situations (Feder, 1988; Ferer and Smith, 1994).

We have developed a mechanistic pore-level network model to describe miscible and immiscible, incompressible, non-wetting fluid invasion into porous media. This model generates random distributions of pore radii to simulate porous medium properties and incorporates fluid viscosities and fluid densities. This is an extension of previous models (Ferer and Smith, 1994; Ferer et al., 2001) that did not include buoyancy forces.

Objective

The main objective of this work is to use the mechanistic model to simulate miscible displacement of oil by carbon dioxide. The displacement is horizontal, so gravity forces are considered to be in the transverse direction, as opposed to being in the direction of flow. We study the relationship between viscosity and density differences and CO_2 displacement efficiency for the case of miscible displacement of oil. The viscosity ratio ($M=\mu_1/\mu_2$) and the density ratio ($D=\rho_1/\rho_2$) are common dimensionless numbers that we relate to saturation and fractal dimension.

Approach

Using the mechanistic model, we simulate the horizontal infiltration of liquid carbon dioxide into a porous medium saturated with oil. Since oil fields exist under a variety of temperatures and pressures, ranges of density and viscosity are taken from experimental values and used as input parameters for the model. At all relevant depths, carbon dioxide is significantly less viscous and less dense than oil. In some cases, the carbon dioxide will be a supercritical fluid and therefore compressible. Nevertheless, we assume fluid incompressibility in our model, which is a conservative assumption for CO_2 sequestration.

All simulations have been run on a 50x50 diamond lattice of pores and throats. Simulations were run for a range of viscosities and densities that would correspond to liquid and supercritical CO_2. The values used in the simulations are shown in Table 1. Experimental values for density and viscosity of oil were also used to calculate the input parameters. Physical properties of the oil may vary almost as much as those of carbon dioxide. However, to simplify, only average values of oil viscosity and density were used: μ=50cP and ρ=1.1g/cm^3 (Lake, 1989).

Table 1. Physical properties of oil under low, average, and high pressure.

Pressure	Density[1,2] (g/cm3)	Viscosity[2] (cP)
low	0.15	0.01
average	0.50	0.05
high	0.90	0.09

[1]Angus et al. (1976) [2]Chun and Wilkinson (1995)

Model Description

The model described here is essentially an extension of the model by Ferer and Smith (1994). Capillary forces are included in the model, but they are not used in this work because the displacement is miscible. The model is a diamond lattice of pores and throats as shown in Figure 1. Flow through each throat is determined by the conductance of the throat (depending on throat radius) and the pressure gradient between the pores (depending on the pressure in each pore, the capillary pressure, and the gravitational gradient). An excellent description of the model without gravity can be found in Ferer et al. (2001), so we will be concentrating on a description of how buoyancy forces are added here.

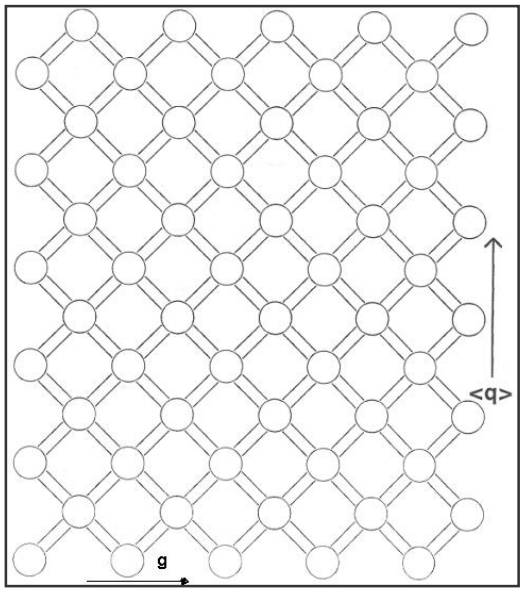

Figure 1. Diamond lattice of pores and throats; cross-current gravity.

To determine the flow in each throat, the value of the pressure gradient must be calculated for each time step. One component of the pressure gradient comes from the pressure differential between the pores on each side of the throat. Absent capillarity, the only other component is due to gravity. When a single fluid is in a pore and throat, the calculation is fairly simple:

$$P_G = \rho g x \sin\psi \,, \qquad (1)$$

where PG is the pressure gradient due to gravity, is the density, g is the acceleration due to gravity, x is the distance from the center of one pore to the other, and is the angle that the throat makes with respect to the horizontal. The direction of this pressure gradient is always in the same direction (downward in the transverse direction to the flow).

When two fluids are in the pores and throats, however, the situation becomes more complex. Basically, the pore-throat system can be split up into two sections, the section filled with invading fluid and the section filled with displaced fluid. Once you find the length of each section, you can use Equation 1 for each distinct part and sum

them to get the total pressure gradient. If two fluids are in the throat, then the pressure gradient in the throat is:

$$P_G = \rho_1 g a x \sin\psi + \rho_2 g (1-a) x \sin\psi , \qquad (2)$$

where a is the volume fraction of the invading fluid (fluid 1) in the throat.

For each pore, the invading fluid is assumed to be in the center of the spherical pore in a ball, while the defending (wetting) fluid surrounds it and stays next to the pore wall. Spheres in the model have a unit volume of 1, so the pressure gradient along the pore would be:

$$P_G = \rho_1 g \left(\frac{3a}{4\pi}\right)^{1/3} \sin\psi + \rho_2 g \left[\left(\frac{3}{4\pi}\right)^{1/3} - \left(\frac{3a}{4\pi}\right)^{1/3}\right] \sin\psi , \qquad (3)$$

where *a* is the volume fraction of invading fluid in the pore.

Including gravitational forces in the model also requires a distinct pressure distribution around the boundary of the modeled flow cell. Figure 3 shows what that pressure distribution would look like for the cell. Notice that this is the pressure distribution that would envelope the cell if it were surrounded by oil in hydrostatic equilibrium moving from left to right.

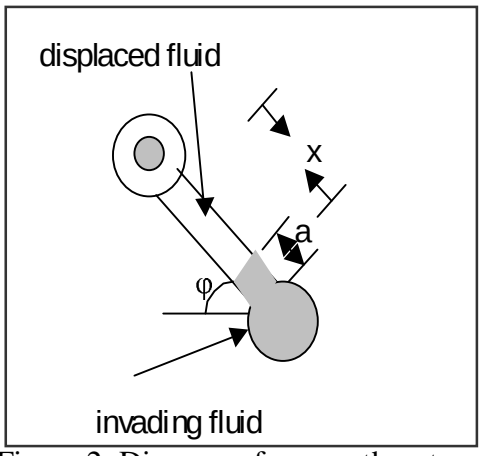

Figure 2. Diagram of a pore-throat system; invading fluid is gray.

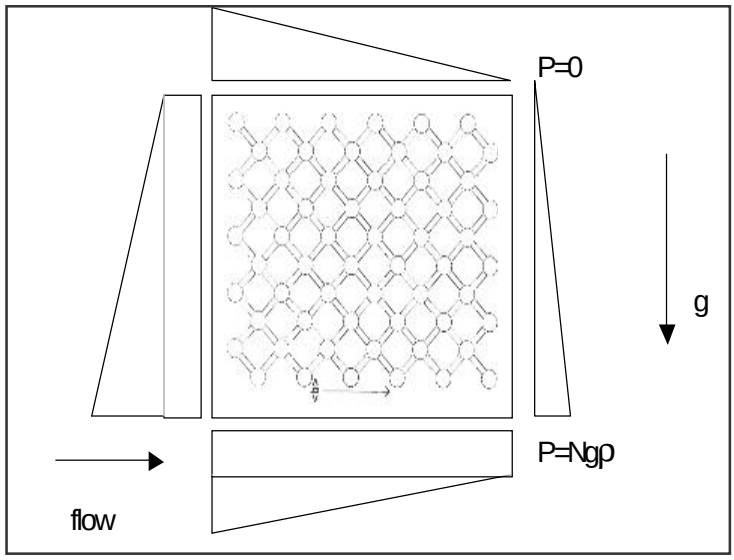

Figure 3. Diagram of pressure field around cell.

Results

In this section, results from simulations of size 50x50 pores are presented. Table 2 shows the saturations and fractal dimensions for the simulations that were run and how they relate to the viscosity and density ratios. The general relationship between these variables is fairly clear and is consistent with what is known about the effects of gravitational and viscous forces on two-phase miscible displacement. Saturation and fractal dimension both decrease with decreasing viscosity ratio and decreasing density ratio. Notice also that a difference in density causes a greater change in saturation than an equivalent change in viscosity, at least for the ranges tested here. Whereas saturation varies by about 25% for about an 85% change in density, it changes by only about 10% for a similar change in viscosity.

Table 2. Saturation and fractal dimension as related to viscosity and density ratios.

	D=0.1		**D=0.4**		**D=0.7**	
	Sat	**D_f**	**Sat**	**D_f**	**Sat**	**D_f**
M=0.0003	15.7	1.69	18.8	1.73	20.5	1.74
M=0.0010	16.3	1.70	19.1	1.73	21.3	1.74
M=0.0018	17.2	1.70	19.8	1.75	23.1	1.76

It is important to place these results in context. While the values of the density ratio are within one order of magnitude from unity, the values of viscosity ratio are much less. Other studies have suggested that the further from unity the viscosity ratio is, the less relative difference is found in the corresponding saturations (Lenormand et al, 1988). This means that the viscosity ratio is probably as significant a factor in determining the saturation as the density ratio, only not as important for this range of values. Nonetheless, these results are only preliminary, and a final determination of the relative importance of viscosity and density must wait for more information.

Conclusion & Application

Practically, these results tell us two things. First, within the range of temperatures and pressures that one would find in oil fields, the saturation can vary significantly. This suggests that some fields will be better suited for sequestration than others, i.e., the ones that correspond to higher CO_2 viscosities and densities. This, of course, does not necessarily mean the lowest depths, as in some of these cases, the CO_2 is in a supercritical state, wherein the viscosity can vary widely.

A second practical consideration is that the viscosity seems to be significantly less important than the density within this region of the M-D parameter space. Thus, adding viscosifiers to the CO_2 to make it “thicker” would not be very useful. More important would be the addition of some substance that would increase the CO_2 density without significantly increasing the mass. This would not necessarily be true, however, for other CO2 sequestration situations, such as in brinefields, where chances in the viscosity ratio may have much more significant effects.

Of course, the results presented here are fairly preliminary, and it is difficult to make any final practical conclusions until these simulations are run on larger systems to determine what kind of scaling effects we can observe. Because of the sizes of the systems, it is not clear how well the flow will scale up with these parameter values. Preliminary fractal dimension calculations are consistent, but better estimates should come with larger systems.

Future Activities

The first area of future work is to generate more random fields of pores and run the simulations with the same parameters to help determine how robust the system is. Following this, of course, we would like to simulate using larger pore networks (70x70 and 100x100) for the same range of parameters. This would give us some idea of the scaling properties of the system (Ferer and Smith, 1994).

Ideally, we would vary the values of viscosity and density outside the range of those practical in oil field sequestration to better understand the relationship between these variables and determine if the viscosity ratio becomes more significant as is increases. Then, we could creating a parameter space for viscous and buoyancy forces similar to the one suggested by Lenormand et al. (1988) for capillary number and viscosity ratio. Such a diagram would allow us to place the relative importance of viscosity and density into some larger context.

Another plan for the future is to expand this model to allow flow in three dimensions. Two dimensional models can be good at determining the relative importance of viscous and density forces, but to truly scale up to large three-dimensional systems requires at least some testing on 3-D networks.

References

Angus, S. B. Armstrong, and K.M.deReuck (eds). International Thermodynamic Tables of the Fluid State: Carbon Dioxide. Pergamon Press. Oxford, England. 1976.

Blunt, M., M.J. King, and H. Scher. "Simulation of two-phase flow in porous media." *Physical Review A.* Vol. 46, No. 12, p. 7680-7699, 1992.

Chun, Byung-Soo and Gordon T. Wilkinson. "Interfacial tension in high pressure carbon dioxide mixtures." *Industrial Engineering Chemical Res.* Vol. 34, p. 4371-4377, 1995.

Feder, J. Fractals. Plenum Press, New York, NY, 1988.

Ferer, M., Grant S. Bromhal, and Duane H. Smith. "Pore-level modeling of carbon dioxide sequestration in brine fields." *Proceedings of the First National Conference on Carbon Sequestration*. Washington, DC May 15-17, 2001.

Ferer, M. and D.H. Smith. "Dynamics of growing interfaces from the simulation of unstable flow in random media." *Physical Review E*. Vol. 49, No. 5-A, p. 4114-4120, 1994.

Lake, Larry W. Enhanced Oil Recovery. Prentice Hall, NJ. 1989.

Lenormand, R., E. Touboul, and C. Zarcone. "Numerical models and experiments on immiscible displacements in porous media." *Journal of Fluid Mechanics*. Vol. 189, p. 165-187, 1988.

U.S. Dept. of Energy, Office of Science, Office of Fossil Energy. Carbon Sequestration: Research and development. Technical Report. December, 1999.

Formation of Hydrates from Single-Phase Aqueous Solutions and Implications for Oceanic Sequestration of CO_2.

G. Holder (holder@engrng.pitt.edu) 412-624-9809
L. Mokka (lakshmi.mokka@netl.doe.gov) 412-386-6019
Department of Chemical and Petroleum Engineering
University of Pittsburgh
Pittsburgh, PA 15261

R. Warzinski* (robert.warzinski@netl.doe.gov) 412-386-5863
U.S. Department of Energy
National Energy Technology Laboratory
P.O. Box 10940
Pittsburgh, PA 15236-0940

Introduction[a]

Gas hydrates are crystalline solids formed from mixtures of water and low molecular weight compounds, referred to as hydrate formers, that typically are gases at ambient conditions (1). Generally, hydrates are formed in the laboratory from two-phase systems by contacting a hydrate former or formers in the gas or liquid phase with liquid water and increasing the pressure until crystalline hydrate forms. However, the formation of hydrate from a single-phase aqueous system using only the hydrate former dissolved in the aqueous phase has been demonstrated in prior work at the National Energy Technology Laboratory (NETL) (2) and more recently by others (3).

The prior work at NETL focused on the impact of CO_2 hydrate on oceanic sequestration of CO_2 and showed that the initial effective density of a hydrate cluster depends on the number of phases present when the hydrates form (2). If the hydrate was formed from a two-phase system of either gaseous or liquid CO_2 and water, the hydrate clusters were initially less dense than the water-rich phase because of the presence of free CO_2 that adheres to or is occluded in the hydrate clusters without actually being incorporated in the lattice of the hydrate. However, if the hydrate was formed from a single-phase system consisting of CO_2 dissolved in water or seawater, the hydrate that formed was initially more dense than the aqueous phase. This would have implications in some processes being considered to inject CO_2 into the deep ocean (>500 m) for the purposes of non-atmospheric sequestration. Forming a sinking hydrate particle could facilitate such a process by transporting the CO_2 to depths greater than that used for injection. On the other hand, a rising hydrate particle would have the opposite impact.

This preprint summarizes a general thermodynamic model and experimental results that demonstrate the formation of hydrates from single-phase aqueous systems. A complete description has been accepted for publication (4)

[a] This manuscript has recently been published by the American Chemical Society Division of Fuel Chemistry in the Preprints of the Spring 2001 National Meeting in San Diego, California.

Results and Discussion

Models for Hydrate Equilibrium

For calculation of hydrate formation from a single-phase water-rich liquid containing dissolved hydrate former, the conditions where the hydrate phase is in equilibrium with the water-rich liquid are needed. At these conditions, the chemical potentials of the species in various phases must be equal. The following equations describe the chemical potential difference of water in the hydrate phase ($\Delta\mu_H$) and the chemical potential difference of water in the water phase ($\Delta\mu_L$) (4).

$$\Delta\mu_H = -RT \sum_{j,cavities} \nu_j \ln\left(1 - \sum_i \theta_{ji}\right) \qquad (1)$$

$$\frac{\Delta\mu_L}{RT} = \frac{\Delta\mu^0}{RT_o} - \int_{T_o}^{T_F} \frac{\Delta h}{RT^2} dT + \int_0^P \frac{\Delta v}{RT} dP - \ln X_w \qquad (2)$$

In these equations, $\Delta\mu_H$ is the difference in the chemical potential between an empty hydrate water lattice and one occupied by a guest molecule (5), $\Delta\mu_L$, Δh, and Δv are the chemical potential, enthalpy, and volumetric differences, respectively, between water in an empty hydrate lattice and pure water, and $\Delta\mu^0$ is a reference chemical potential treated as a constant whose value can change according to the gas species present. Also in these equations, ν_j is the ratio of j type cavities present to the number of water molecules present in the hydrate phase, θ_{ji} is the fraction of j-type cavities occupied by i-type guest molecules, and X_w is the mole fraction of water in the water-rich liquid phase. θ_{ji} is related to P^{sat} which is the pressure required to obtain a given solubility of hydrate former in the water phase (4). At pressures lower than P^{sat}, the hydrate former will come out of solution as a gas bubble or liquid drop.

Using these two equations with different saturation pressures, the possibility of hydrate formation from a single-phase, water-rich system containing dissolved CO_2 can be determined (4). This is illustrated graphically in Figure 1 for a temperature of 275 K.

In this figure, point A represents the pressure at which hydrate would form if excess CO_2 were present (VLH equilibria). Point B represents the pressure at which hydrates would form from a water-rich single-phase system containing 0.016 mole fraction CO_2. At point A, the water rich liquid would contain more CO_2 ($\cong$ 0.0188) than at point B. At 275 K, all compositions less than that at Point A hydrates could form if the pressure was sufficiently high. This is shown in Figure 2, which gives the pressure required to form hydrates for various amounts of dissolved CO_2 at 275 K and at two other temperatures. As the mole fraction of CO_2 decreases, the pressure required to form hydrates will increase.

It is evident from Figure 1, that the formation of hydrates from a subsaturated water-rich liquid requires the slope of the chemical potential of liquid water vs. pressure from Equation 2 be less than the slope of the chemical potential of hydrate water vs. pressure from Equation 1. A similar analysis has been performed for other hydrate formers (4). Single-phase hydrate formation is predicted to be possible for methane and ethane; however, it may not be possible for propane. Experimental work is underway to verify these predictions.

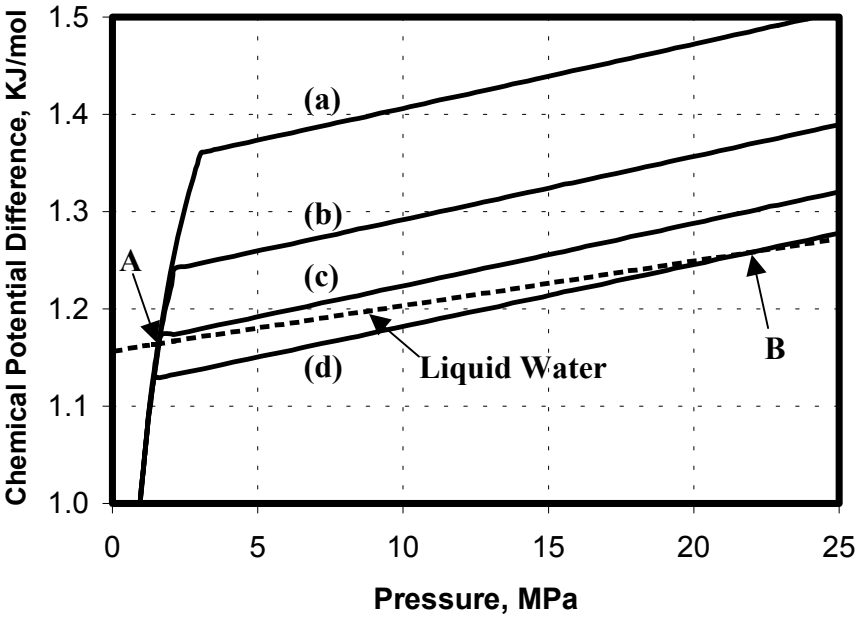

Figure 1. The chemical potential difference of water in the CO_2 hydrate and in the aqueous phases. Lines (a) through (d) represent calculations for water in the hydrate phase at a saturation pressure P^{sat} and mole fraction of dissolved CO_2, respectively, of: (a) 3.0 MPa, 0.026; (b) 2.0 MPa, 0.020; (c) 1.6 MPa, 0.019; (d) 1.4 MPa, 0.016. The points of intersection A and B are equilibrium points for VLH and LH equilibria respectively. T=275 K.

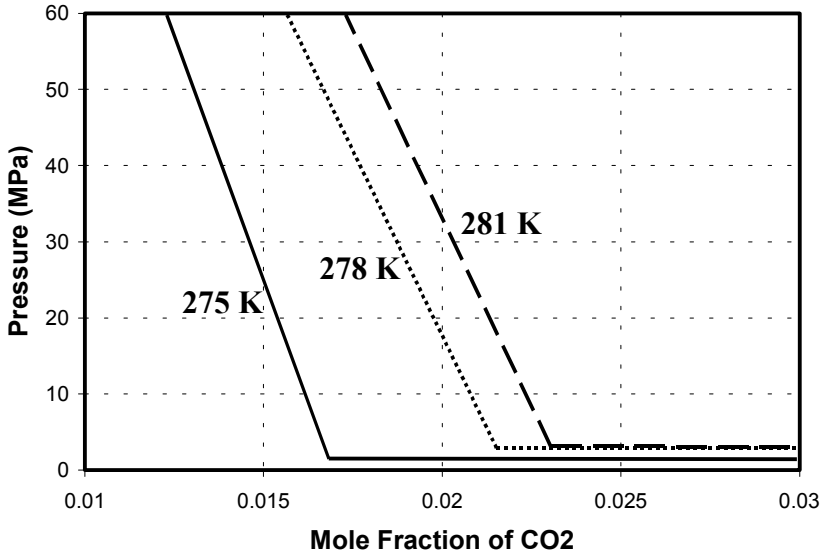

Figure 2. Pressure required to form hydrates as a function of the overall mole fraction of CO_2 in a CO_2 water system at three different temperatures. Hydrates are predicted to form in the region of the line.

Experimental Observations of Hydrate Formation from Dissolved CO_2

Experimental observations of hydrate formation have been made at NETL in a high-pressure, variable-volume viewcell that demonstrated the formation of CO_2 hydrate from single-phase aqueous systems (2, 4). As previously mentioned, formation under these conditions always resulted in a CO_2 hydrate that was more dense than the aqueous phase that it formed in.

Experiments are continuing at NETL to better understand and define the single-phase hydrate formation process. A new viewcell system is being used that permits improved control of the experimental parameters and better data collection capabilities. Figure 3 contains the pressure/temperature history of a recent experiment in which a single-phase solution of water (prepared by reverse osmosis and vacuum degassing) and CO_2 (0.018 mole fraction) was subjected to hydrate forming conditions. The rate of cooling and heating was 0.3 K/h. The pressure drop observed upon cooling at 276.7 K and 17.5 MPa indicates the formation of hydrate. As the system was warmed the hydrate gradually decomposed with complete decomposition occurring near 278.1 K and 18.3 MPa.

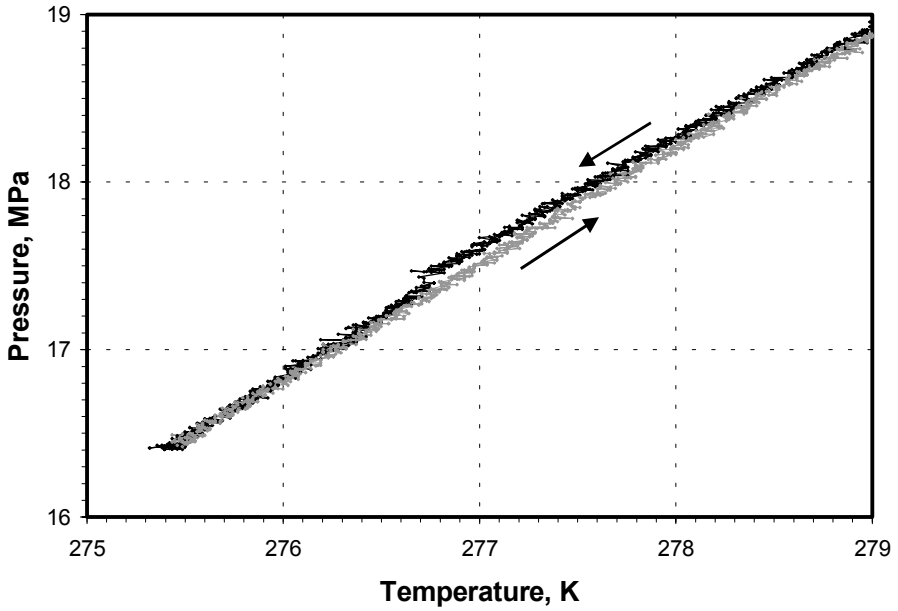

Figure 3. Experimental pressure and temperature data showing evidence for hydrate formation from a single phase solution containing CO_2 dissolved in water.

Conclusions

It is clear from both theoretical and experimental evidence that hydrates can form from dissolved gas in the absence of a free-gas phase. Experiments show that CO_2 hydrate will form when no gas phase is present when the solution contains dissolved CO_2. Conventional models can be modified to predict the hydrate formation pressure as a function of the amount of dissolved CO_2 allowing for the design of experiments or processes utilizing this phenomena.

References

(1) Sloan, Jr., E.D. *Clathrate hydrates of natural gas (2nd ed.*). New York: Marcel Dekker. 1998
(2) Warzinski, R.P., Cugini, A.C., & Holder, G.D. *Coal Science*, J.A. Pajaras & J.M.D. Tascòn, Eds; Elsevier, 1995; pp. 1931-1934.
(3) Buffett, B.A., & Zatsepina, O.Y. *Marine Geology*, **2000**, *164*, 69-77.
(4) Holder, G.D, Mokka, L.P., & Warzinski, R.P. *Chemical Engineering Science* – accepted for publication, **2001**.
(5) Holder, G.D., Zetts, S.P. & Pradhan, N. (1988). Phase behavior in systems containing clathrate hydrates, a review. *Reviews in Chemical Engineering, 5*(1-4), 1 – 70.